Order Number 9130315

Linear interfacial stability of a core-annular flow with application to liquid-liquid displacements in small pores

Georgiou, Evangelos, Ph.D.

City University of New York, 1991

U·M·I
300 N. Zeeb Rd.
Ann Arbor, MI 48106

A

LINEAR INTERFACIAL STABILITY OF A CORE-ANNULAR FLOW WITH APPLICATION TO LIQUID-LIQUID DISPLACEMENTS IN SMALL PORES

by

EVANGELOS GEORGIOU

A dissertation submitted to the Graduate Faculty in Engineering in partial fulfillment of the requirements for the degree of Doctor of Philosophy, *The City University of New York*

1991

This manuscript has been read and accepted for the Graduate Faculty in Engineering in satisfaction of the dissertation requirement for the degree of Doctor of Philosophy.

3/25/91
Date

David S. Rumschitzki
Professor David S. Rumschitzki
Chair of Examining Committee

3/29/91
Date

Gerard G. Lowen
Professor Gerard G. Lowen
Executive Officer

Prof. David S. Rumschitzki

Prof. Charles Maldarelli

Prof. Andreas Acrivos

Prof. Joel Koplik

Prof. Daniel D. Joseph
(*University of Minnesota*)

Prof. Demetrios T. Papageorgiou
(*New Jersey Institute of Technology*)

Supervisory Committee

The City University of New York

Abstract

LINEAR INTERFACIAL STABILITY OF A CORE-ANNULAR FLOW WITH APPLICATION TO LIQUID-LIQUID DISPLACEMENTS IN SMALL PORES

by

EVANGELOS GEORGIOU

Advisors: **Professor David S. Rumschitzki** (Mentor)
Professor Charles Maldarelli (Co-Mentor)

This work focuses on the problem of the interfacial stability of perfectly co-axial, core-annular flow with particular attention to the conditions of liquid-liquid displacement in small rock pores. Such situations occur when flushing rocks with water or an aqueous solution in order to recover crude oil trapped there. Ideally, one would like to encourage a flow of the less wetting fluid remaining for long stretches in the core and riding on an annular film of the more wetting fluid. This work concentrates on two possible sources of stability of such a flow arrangement.

In the first problem we examine the linear stability of an annular film surrounding a dielectric-fluid core in a tube in the presence of double layers of charges at the film-core and at the film-tube interfaces, when the fluid-fluid interface is of low tension. In the absence of electrostatic forces, the surface tension force arising from the circumferential curvature destabilizes and that from the axial curvature stabilizes the system. The competition is such that waves larger than the unperturbed interface circumference are unstable and those shorter are stable. For charged layers in the film, two cases are examined: (i) double layer repulsion where the volume charge density is everywhere of the same sign and (ii) double layer attraction where the diffuse layers next to the film interfaces are of opposite signs.

In the first case, double layer repulsion and surface tension lowering stabilize the destabilizing action of the circumferential component of the surface tension force, and a window of stability can exist. In the case of double layers of opposite signs, double layer

attraction destabilizes the system, and growth rates larger than those caused by pure capillarity can arise. Finally, for the case of a core bounded by an infinite electrolyte, surface tension lowering stabilizes the destabilizing action of the circumferential component of the surface tension force and destabilizes the longitudinal one, although the magnitudes of these effects may differ. As a result the thread can become unstable to waves even shorter than the undisturbed interface circumference.

In the second problem we study the linear stability of a gravity and possibly pressure-driven perfect core-annular flow in the limit of small film thickness in the presence of viscosity and density stratification and gravity in addition to tension. Asymptotic expansions (in terms of the ratio of the film thickness to the undisturbed core radius) lead to analytical expressions that asymptotically govern the linear stability of the system. A glance at the resulting expression shows how to asymptotically order the parameters to bring out different effects. For a moderate flow at least three canonical regimes merit study: (i) large surface tension in the presence of viscosity and density stratification and moderate or low surface tension with density stratification in the (ii) presence or (iii) absence of viscosity stratification. In the first regime the stabilizing action of the viscosity stratification (with the less viscous fluid in the film) can overcome the destabilizing action of the circumferential component of surface tension while the density difference is merely a second order effect. These results confirm those found numerically by Joseph *et al.*. In the case of moderate surface tension and in the absence of viscosity stratification, the density difference alone is able to stabilize capillarity. Finally, when the less viscous fluid is in the core, viscosity stratification has a purely destabilizing effect and as a result the system becomes unstable to waves even shorter than the undisturbed interface circumference. The calculated growth rates in this case bear on the maximum length of linearly stable slugs in small pores.

Acknowledgments

I wish to thank Professor David S. Rumschitzki and Professor Charles Maldarelli for their continuous guidance and many contributions in directing this research. Professor D. T. Papageorgiou is thanked for numerous discussions and contributions regarding numerical technics involved in this research. I also wish to thank all members of the supervisory committee for their help and encouragement. Finally I would like to thank my wife, Evanthia, for her help and encouragement during the preparation of this manuscript.

This work was supported in part by grants from the National Science Foundation to Professor David S. Rumschitzki (Grants CBT 8505654 and CBT 8658147) and the Department of Chemical Engineering at *CCNY*. Their support is gratefully acknowledged.

Table of Contents

List of Figures

I Introduction

Perfect core-annular flows (abbreviated here as "PCAF's") are parallel flows of immiscible liquids in a cylindrical tube in which one liquid moves through the tube core, and the other liquid flows in an annular region that surrounds the core fluid. When caused to flow by a pressure gradient either in the absence of gravity or in the presence of gravity (with the tube arranged vertically), an exact laminar solution of the Navier-Stokes equations exists for the simple two-phase PCAF in which the liquid-liquid interface is circular and strictly concentric with the tube wall. The interfacial stability of this laminar solution, i.e., the stability to disturbances in the cylindrical interface, is an important question: The solution serves as a simple model for many technologically important two-phase tube flows (e.g., lubricated pipelining, concurrent flows in packed beds, coating processes and liquid-liquid displacements in the presence of a wall wetting layer in porous media), and the understanding of its stability allows for the prediction of whether the core-annulus geometry will be realized, or whether this structure will break down into another flow regime such as a slug or emulsion flow.

The general aim of this work is to understand the factors affecting the stability of the core-annular fluid arrangement and to determine the ranges of parameters that can stabilize it to small perturbations of the fluid-fluid interface. In this study we use linear stability theory to treat axisymmetric disturbances of the interface exclusively, in the belief, as shared by many other authors, e.g., Goren (1962), Preziosi Chen & Joseph (1989), Tomotika (1935) etc., that they are the most unstable modes for these types of problems.

This work examines two problems concerning the interfacial stability of a PCAF. Both are applied to liquid-liquid displacements in rock pores and each investigates a

potential mechanism for stabilizing long slugs of the non-wetting fluid surrounded by a film of the more wetting one. In our first problem we study the electrohydrodynamic stability of an annular electrolyte film surrounding a dielectric core in a tube in the absence of base flow and gravity. The fluid-fluid interface is of low tension and there are double layers of charge at the film-core and film-tube interfaces. We concentrate on the case of zero base flow in order to isolate the effects of the double layers of charge and to examine the way they couple with those of capillarity. The general surface tension lowering of the double layers as well the double layer repulsion will contribute to determining the cylindrical interface stability. However, the interfacial stability in this situation presents several interacting effects because the slightly perturbed cylindrical interface has two relevant curvatures of different stability character and the double layers of charge will affect each differently.

In our second problem we study the linear stability of two fluids of different viscosities and densities in a gravity and possibly pressure driven core-annular base flow in a vertical pipe with no double layers present. The viscosity difference causes a jump in the slope of the base state velocity profile and the density difference a jump in the curvature of the base state velocity profile at the interface; these facts can profoundly affect the interface's stability. In contrast to our first problem, we concentrate on the thin film limit and develop an analytic, asymptotic theory in powers of the ratio of the annular thickness to the undisturbed core radius. Our central aim is to use this theory to analytically describe the interfacial stability and to order and assess the magnitudes of the competing effects in the thin film limit. This is, of course the practical situation in the case of liquid-liquid displacements in rock pores.

Section *II* presents a detailed review of the literature pertaining to our two problems. In order to mention a few highlights of Sections *III* and *IV*, we first note that in the

absence of flow and electrostatic forces, the surface tension force arising from the circumferential curvature destabilizes and that from the transverse curvature stabilizes the system. The competition is such that waves larger than the unperturbed interface circumference are unstable and those shorter are stable. Section *III* of this proposal begins with a detailed motivation, sets up a mathematical framework for analysis, and solves the case of the electrolyte film. The analysis examines two sub-cases : (i) double layer repulsion where the volume charge density is everywhere of the same sign and (ii) double layer attraction where the diffuse layers next to the film interfaces are of opposite signs. In the first sub-case, double layer repulsion and surface tension lowering stabilize the destabilizing action of the circumferential component of the surface tension force, and a window of stability can exist. In the case of double layers of opposite signs, double layer attraction destabilizes the system, and growth rates larger than those caused by pure capillarity can arise. Moreover, for the case of a core bounded by an infinite electrolyte, surface tension lowering stabilizes the destabilizing action of the circumferential component of the surface tension force and destabilizes the longitudinal one, although the magnitudes of these effects may differ. As a result the thread can become unstable to waves shorter than the interface circumference.

The analysis of the vertical flow arrangement constitutes Section *IV*. As in Section *III*, we motivate and set the mathematical framework for analysis of this problem. With the tube arranged vertically (in the direction of gravity) two cases are examined: (a) free-fall under gravity and (b) forced-flow under a constant pressure gradient. Long wave theory motivates asymptotic expansions (in terms of the ratio of the film thickness to the undisturbed core radius) which lead to analytical expressions that asymptotically govern the linear stability of the system for all but the shortest waves. The analysis studies two canonical regimes for moderate flow: (i) large surface tension in the presence of viscosity

stratification and (ii) moderate surface tension in the absence of viscosity stratification. In the first regime the stabilizing action of the viscosity stratification (with the less viscous fluid in the film) can overcome the destabilizing action of the circumferential component of surface tension and the density difference is merely a second order effect. In the case of moderate surface tension and in the absence of viscosity stratification, the density difference alone is able to stabilize capillarity. Finally, when the less viscous fluid is in the core, viscosity stratification has a purely destabilizing effect and as a result the system becomes unstable to waves even shorter than the undisturbed interface circumference.

II Literature Review

The linear interfacial stability of the laminar solution for the simple, axisymmetric two-phase PCAF has motivated much research. It is clear from this literature that capillary forces and viscosity and density differences principally determine the stability.

1 STABILITY OF THE STATIC CORE-FILM GEOMETRY

(a) Capillarity

The interfacial stability of the static case and in the absence of electrostatic forces is governed by capillarity. Plateau and then Rayleigh (1879 and 1892) first studied the problem of the stability of an inviscid cylindrical thread, neglecting the effect of a surrounding fluid. Tomotika (1935) extended these studies to include the effects of thread viscosity and an infinite outer viscous fluid, and Goren (1962) studied an annular film (with a gas interface) located on the outside or the inside surface of a tube. All of these studies indicate that for axisymmetric disturbances of the fluid interface, the circumferential component of the interfacial tension force has a destabilizing effect (large waves growing the fastest) and the axial component has a stabilizing effect (short waves damped the most). The competition is such that waves larger than the interface circumference are unstable and those smaller are stable and that a wavelength of maximum growth rate exists and is of the order of the critical wavelength.

(b) Influence of Double Layers of Charge

When double layers of charge are present at the interface, the stability picture changes. Felderhof (1968) first studied the influence of double layers of charge

within the context of the stability of thin, inviscid, planar electrolyte films that were symmetric about their midplane. Felderhof identified two modes of vibration of such films, a squeezing mode in which the film thickness changes and a stretching mode in which the thickness is constant. For the stretching mode Felderhof found that for long waves the double layers of charge effectively reduce the interfacial tension, thereby destabilizing the system. For the squeezing mode, movement of the opposing interfaces towards each other brings charges of equal sign together, and Felderhof found that for long waves this double layer repulsion strongly stabilizes the system. Various studies extended Felderhof's results to include viscous lamella. They demonstrated that, as long as the base state is one of zero flow, viscosity affects the growth rates but not the criteria for stability (for reviews see Gallez & Coakly (1986) and Jain & Maldarelli (1988)).

Finally, Miller & Scriven (*I* and *II*) (1970) studied the case of single double layers of charge extending from a planar interface, and outward from a spherical interface. They found results similar to those for the stretching mode of Felderhof: For long waves, the presence of the double layer effectively lowers the surface tension and destabilizes the planar system. Miller & Scriven also showed that at shorter waves, the stabilizing effect of surface tension dominates the destabilizing action of the double layers. In the case of small spherical interfaces, they found that the repulsive interaction is important for all disturbances and the interface becomes unstable only when a small negative value of interfacial tension is reached.

2 STABILITY OF CORE-ANNULAR FLOWS

(a) Viscosity Stratification

The effect of viscosity differences on the stability of two-phase parallel flows was first established by Yih (1967) who studied the stability of plane Couette-Poiseuille flow between parallel plates with respect to long waves. Yih neglected the effects of gravity and density difference and focused his attention on the viscosity difference and the volume ratio. He was able to show analytically that disturbance waves with wavelengths much larger than the plate separation distance can become unstable when the fluid viscosities are different. However, he found that this long wave instability does not manifest itself when the less viscous fluid is in a thin layer on one of the plates.

There are three important facts associated with Yih's instability that deserve emphasis: First, the instability is realized for any value, however small, of the Reynolds number and it is therefore different from the high Reynolds number instability associated with plane Poiseuille flow. Second, the growth rate tends to zero with Reynolds number, so, unlike the capillary instability, flow is necessary to achieve the instability. Third, like the capillary instability, the deformation of the interface is necessary to obtain Yih's instability. If the interface remains planar then the instability is not realized.

Hooper (1985) extended Yih's results for Couette flow of a semiinfinite phase and a film resting on a moving plane. Hooper & Boyd (1983) studied the stability of Couette flow of two infinite fluids separated by a plane and found that short waves are unstable if surface tension is neglected. Renardy (1985) generalized Hooper & Boyd's results and showed numerically that short and intermediate

waves can become unstable even when long waves are stable. In the planar geometry surface tension has a pure stabilizing effect with the shorter waves damped the most. Yiantsios & Higgins (1988) extended these results including differences in density and thickness ratios, as well as the effects of interfacial tension and gravity. They showed that the flow is linearly unstable to a shear mode instability. The dependence of the critical Reynolds number for the shear mode on the viscosity ratio was reported and compared with available experimental data.

Joseph, Renardy & Renardy (1984) studied the stability of a core annular flow including viscosity in the absence of surface tension. They showed that all short waves are unstable and long waves are stable only when the more viscous fluid is in the core and the film is thin. Hickox (1971) was the first to combine viscosity difference and surface tension effects. Using Yih's long wave expansion he treated both axisymmetric and nonaxisymmetric disturbances for the case where the more viscous fluid is in the film. He found all such flows to be unstable. Preziosi, Chen & Joseph (1989) studied axisymmetric disturbances of all length scales with the less viscous fluid in the film by numerically solving the Orr-Sommerfeld equations. Their results show that viscosity stratified flow has a stabilizing effect at long waves for all Reynolds numbers and a destabilizing effect for short waves at high Reynolds numbers, effects as a function of wavelength that are opposite to those of capillarity. Thus they found a window in Reynolds number space where the simple two-phase PCAF is stable provided that: the film thickness is below a critical value and the film fluid is sufficiently less viscous than the core fluid. Finally, PCJ show that this window disappears as the viscosity of the film increases relative to that of the core.

(b) Density Difference

Kapitza (1948-1949) first studied the effect of density difference on the interface stability of parallel flows. He and others have observed wavy interfaces on a fluid film flowing down a vertical plane. Binnie (1957) sharpened such experiments by measuring the film Reynolds number R_e at which the instability appears as well as its speed and wavelength. Yih (1955), Benjamin (1957), Yih (1963) and later Benney (1966) studied the stability of liquid flow down an inclined plane, and found an instability due to density differences arising from the term in the tangential stress balance deriving from the perturbation of the interface. These authors explained the observation of a lower value of the Reynolds number below which no instability is seen as a result of vanishing slow growth rates for lower Reynolds numbers. Yih, using his long wave expansion technique in powers of the product af the wave number α and R_e, was able to improve Benjamin's analytical result and to give a more satisfactory explanation of this experimental observation he showed that the flow down an inclined plane is unstable for all Reynolds numbers larger than a critical value determined by the plane's angle of inclination and that for vertical flow this value is zero.). Yih (1963) also showed that a gravity driven flow at non-zero Reynolds number destabilizes the longest waves, and that surface tension which stabilizes the shortest waves can enter the first order growth rates if one assumes that the surface tension parameter is asymptotically large, i.e., $O(1/\alpha^2)$ as $\alpha \to 0$, where α is the wave number.

For the case of the simple two-phase PCAF, a density difference in the presence of gravity can also give rise to this instability. As in planar case, it is due to the jump in the curvature of the base velocity profile at the interface and arises from the interfacial perturbation's contribution to the tangential stress balance. It is con-

venient to examine this instability for vertical flow since this geometry yields an axisymmetric base flow. Smith (1989) studied the stability of long waves using the asymptotic technique of Yih, and found that the neutral curve is independent of the Reynolds number. He treated the case of equal viscosities and showed that when the density difference is small: (i) downward flows are *usually* stable when the lighter fluid is in the core and (ii) upward flows are *usually* stable when the heavier fluid is in the core.

Chen, Bai & Joseph (1990) examined the stability of a PCAF to axisymmetric disturbances in a vertical tube driven by both gravity and a pressure gradient by numerically solving the Orr-Summerfeld equations. They found as Smith suspected that in order to achieve a stable PCAF one should use a heavy lubricant for down-flow and a light one for up-flow. They also showed numerically that for all other parameters held fixed, there is an optimizing density ratio which gives the largest window in Reynolds number space where the system is stable.

III Electrohydrodynamic Stability of an Annular Electrolyte Film Surrounding a Dielectric Core in a Tube

1 INTRODUCTION

As noted in Section I, the goal of this study is to examine the influence of double layers of charge and capillarity on the linear interfacial stability of the static arrangement of an annular electrolyte film surrounding a dielectric core fluid in a tube, where the fluid-fluid interface is of low tension. The core-annular geometry is an excellent idealization of the flow geometries of many technologically important processes (e.g. lubricated pipelines (cf. Preziosi, Chen & Joseph (1989)), cocurrent flows in packed beds (cf. Saez *et al.* (1986)), coating processes and liquid-liquid displacements in the presence of a wall wetting layer in porous media as in tertiary oil recovery. The effects discussed below are probably most relevant for the latter case.). We concentrate on the static arrangement in order to isolate the effects and coupling of capillarity and double layers of charge. Flow introduces additional shear effects which can be stabilizing (Joseph, Renardy & Renardy (1984), Preziosi, Chen & Joseph (1989), Hu & Joseph (1989), Papageorgiou, Maldarelli & Rumschitzki (1990)) or destabilizing (Yih (1967), Hickox (1971)). A complete treatment of the stability of the core annular geometry will include all of these effects although the insight gained from the static case is essential (as it is in the study of pure capillarity (see references in Sec. I)).

The stability of a cylindrical interface surrounded by an electrolyte film presents several interacting effects because there are two curvatures and the double layers

of charge will affect each differently. The aim of this study is to establish the precise roles surface tension lowering and double layer repulsion play in determining the cylindrical interface stability. We shall consider only axisymmetric disturbances.

This study is divided into three major sections. Sec. 2 formulates the linear stability problem, and derives the dispersion equation. Sec. 3 presents and discusses neutral curves and growth rate curves, and the study ends with a summary and some conclusions in Sec. 4.

2 FORMULATION OF LINEAR STABILITY THEORY

2.1 Governing Equations and Boundary Conditions

Two immiscible, Newtonian, incompressible fluids of equal density are resting in a core-annular arrangement in a pipe of inner radius R_2. The interface is given by $r = R_1$. A dielectric fluid of viscosity μ_1 and density ρ occupies the core region $0 \le r \le R_1$. A second fluid which is a univalent electrolyte with viscosity μ_2 and density ρ occupies the film region $R_1 \le r \le R_2$. The film electrolyte is drawn from a neutral reservoir. Axisymmetric disturbances of the interface are defined by $r(z,t) = f(z,t)$ (see figure 1).

The equations of motion and continuity in the presence of electrostatic forces and with gravity neglected are

$$\rho \frac{d\mathbf{v}_i}{dt} = -\nabla \cdot (\mathbf{P}_i - \mathbf{T}_i) + \mu_i \nabla^2 \mathbf{v}_i, \tag{2.1.1}$$

and

$$\nabla \cdot \mathbf{v}_i = 0, \tag{2.1.2}$$

where $i = 1$ denotes the core fluid and $i = 2$ denotes the film fluid, d/dt is a convective derivative, $\mathbf{P}$ is the isotropic pressure tensor and $\mathbf{T}$ is the Maxwell stress

tensor from electrostatics ($\mathbf{T}_1 = \mathbf{0}$). The components of $\mathbf{P}$ are

$$\mathbf{P}_{ij} = p\,\delta_{ij}, \tag{2.1.3}$$

where p is the scalar pressure. The components of $\mathbf{T}$ are

$$\mathbf{T}_{ij} = \frac{\varepsilon_e}{4\pi}\mathbf{E}_i\mathbf{E}_j - \frac{(\varepsilon_e - \hat{\eta})}{8\pi}\mathbf{E}_k\mathbf{E}_k\delta_{ij}, \tag{2.1.4}$$

where ε_e is the dielectric constant, $\mathbf{E}$ the electric field, and $\hat{\eta}$ a material constant which depends on the way the force is separated into mechanical and electrical parts. Two frequently-used expressions for the force density are

$$\hat{\eta} = \varepsilon_e - 1 \quad \text{(Kelvin)} \qquad \text{and} \qquad \hat{\eta} = \rho\frac{\partial \varepsilon_e}{\partial \rho} \quad \text{(Helmholtz).} \tag{2.1.5}$$

It turns out that, due to the fluids' incompressibility, our final results are independent of $\hat{\eta}$ (see sec. 2.3).

To determine the electric field in the electrolyte film, we assume that the interfacial frequencies are slow enough so as to allow the ions to be in instantaneous thermal equilibrium for all interfacial positions. The absence of volume charge density in the core leads to a uniform potential and a zero electric field and Maxwell stress tensor there. In the film, assumed to have a uniform dielectric constant ε_e, the electrical potential $\hat{\Phi}$, relative to the potential λ of the reservoir from which the film is drawn, satisfies (cf. Melcher (1981)) for $[|\,\hat{\Phi} - \lambda\,| \ll K\,T\,/\,e]$,

$$\nabla^2(\hat{\Phi} - \lambda) - \frac{8\,\pi}{\varepsilon_e}\frac{e^2 n_0}{K\,T}(\hat{\Phi} - \lambda) = 0. \tag{2.1.6}$$

where

$$\nabla^2 \equiv \frac{\partial^2}{\partial r^2} + \frac{1}{r}\frac{\partial}{\partial r} + \frac{\partial^2}{\partial z^2}, \tag{2.1.7}$$

n_0 is the number density of univalent cations and anions, e is the elementary charge, K is the Boltzmann's constant and T is the absolute temperature. Let

$\Phi = \hat{\Phi} - \lambda$ be the potential defined relative to λ.

Certain boundary conditions for our system are clear: no slip at the wall $r = R_2$; the velocity field is bounded at the centerline; the velocity field is continues at the interface $r = f(z,t)$.

Stress balances at the fluid interface must account for pressure, electrostatic, interfacial phase tension and viscous forces as well as Marangoni stresses which may occur due to gradients of the adsorbed charged species. To account for these effects in a consistent manner, we make two principal assumptions: First we assume that sorptive kinetic processes between the bulk sublayer and the surface are fast enough so that the surface and subsurface remain in equilibrium with one another despite the surface movement. The second assumption is that the interfacial thickness is much smaller than the length scale of the diffuse layer. According to this view, adsorption from inside the diffuse layer onto the surface is purely chemically driven. Thus we take the phase tension σ to be divorced from electrostatic forces and to depend only on the sublayer concentration $n_s^{\mp}$ of cations or anions via the usual Gibbs' adsorption relation

$$\frac{\partial \sigma}{\partial \ln n_s^{\mp}} = -K\,T\,\Gamma^{\mp}, \tag{2.1.8}$$

where $\Gamma^{\mp}$ is the surface concentration of cations or anions.

The tangential Marangoni stress is

$$\nabla_s \sigma = \frac{\partial \sigma}{\partial \ln n_s^{+}} \nabla_s \ln n_s^{+} + \frac{\partial \sigma}{\partial \ln n_s^{-}} \nabla_s \ln n_s^{-}$$

where ∇_s denotes the surface gradient operator. This stress exactly cancels the electrostatic tangential force

$$\mathbf{n} \cdot (\mathbf{T}_2 - \mathbf{T}_1) \cdot \mathbf{t} = \sigma_e \mathbf{E} \cdot \mathbf{t} = -(e\Gamma^{+} - e\Gamma^{-}) \nabla_s \Phi_s,$$

where σ_e is the surface charge density and Φ_s the surface potential, since the bulk sublayer is in electrochemical equilibrium and therefore

$$\nabla_s(\ln(n_s^{\mp})) = \pm \frac{e}{K\,T} \quad \nabla_s \Phi_s.$$

Consequently the tangential and normal stress balances at the interface are

$$\mathbf{n} \cdot (\overline{\mathbf{T}}_2 - \overline{\mathbf{T}}_1) \cdot \mathbf{t} = 0 \qquad \text{at} \quad r = f(z,t), \tag{2.1.9}$$

and

$$\mathbf{n} \cdot (\hat{\mathbf{T}}_2 - \hat{\mathbf{T}}_1) \cdot \mathbf{n} = -2\,H\,\sigma \qquad \text{at} \quad r = f(z,t); \tag{2.1.10}$$

where (2.1.8), in principle determines the variations in the phase tension. The kinematic condition at the interface is

$$v = \frac{\partial f}{\partial t} + w\,\frac{\partial f}{\partial z} \qquad \text{at} \quad r = f(z,t), \tag{2.1.11}$$

where v and w are the r and z components of $\mathbf{v}$, respectively. In (2.1.9) and (2.1.10) $\mathbf{n}$ is the unit vector normal to the interface defined as positive when pointing from the core to the film and $\mathbf{t}$ is the tangential unit vector at the interface. In the boundary conditions $\hat{\mathbf{T}}_i$ is the total stress tensor

$$\hat{\mathbf{T}}_i = -\mathbf{P}_i + \overline{\mathbf{T}}_i + \mathbf{T}_i, \tag{2.1.12}$$

and $\overline{\mathbf{T}}_i$ is the fluid mechanical stress tensor

$$\overline{\mathbf{T}}_i = \mu_i\,[\nabla \mathbf{v}_i + (\nabla \mathbf{v}_i)^t]. \tag{2.1.13}$$

Finally, $2\,H$ is the sum of the principal curvatures

$$2\,H = -\frac{1}{f\,(1+f'^2)^{1/2}} + \frac{f''}{(1+f'^2)^{3/2}}. \tag{2.1.14}$$

In (2.1.14) f' and f'' are respectively the first and second derivative of the function f(z,t) with respect to z at a given time.

To close the problem requires setting the electrical boundary conditions. In general, when sorption equilibrium is assumed, specifying the adsorption isotherm relates the surface adsorption $\Gamma^{\mp}$ to the sublayer concentration of the charged species $n_s^{\mp}$ and thereby permits calculation of the surface's potentials. In dynamic events, we consider the limiting case of constant surface potential of both the wall and the interface

$$\Phi(r = R_2) = \Phi_W \quad \text{and} \quad \Phi(r = f(z,t)) = \Phi_I\,, \tag{2.1.15}$$

which requires of the isotherms that

$$\frac{\partial \Gamma^{\mp}}{\partial \Phi_s} = \pm \frac{e}{K\,T} \frac{\partial \Gamma^{\mp}}{\partial \ln(n_s^{\mp})}$$

be infinite. It is worth noting that in the case of constant surface potential, the zeroth and first order tangential electric fields are zero and thus the tangential electrical (and Marangoni) stresses are each individually zero. Moreover, since

$$d\sigma = \left(\frac{\partial \sigma}{\partial \ln(n_s^{+})} \frac{\partial \ln(n_s^{+})}{\partial \Phi_s} + \frac{\partial \sigma}{\partial \ln(n_s^{-})} \frac{\partial \ln(n_s^{-})}{\partial \Phi_s} \right) \nabla_s \Phi_s = e\ (\Gamma^{+} - \Gamma^{-})\, d\Phi_s,$$

constancy of Φ_s requires the phase tension σ in the interfacial boundary conditions to be constant as well.

We shall now make the hydrodynamic equations and boundary conditions dimensionless. We scale lengths with the inner radius R_1, velocities with $[\sigma/\mu_1]$, time with $[\mu_1 R_1/\sigma]$, pressure with $[\sigma/R_1]$, potential with $[KT/e]$ and the Maxwell stress tensor with $[(KT/eR_1)^2]$. We shall use the same symbols for dimensional and dimensionless variables.

The continuity equation is satisfied automatically by defining a stream function, Ψ, such that

$$u_i = \frac{1}{r}\frac{\partial \Psi_i}{\partial z} \quad \text{and} \quad w_i = -\frac{1}{r}\frac{\partial \Psi_i}{\partial r}. \tag{2.1.16}$$

Since the divergence of the Maxwell stress tensor is irrotational (cf. Felderhof (1968)) for this case in which the ions are distributed in thermal equilibrium , taking the curl of (2.1.1) eliminates the pressure and the Maxwell stress tensor. Substituting the above expressions for u_i and w_i gives the dimensionless differential equation for Ψ_i

$$\frac{J}{m_i}\left[\frac{\partial}{\partial t}(E^2\Psi_i) - \frac{1}{r}\left(\frac{\partial \Psi_i}{\partial r}\frac{\partial}{\partial z}(E^2\Psi_i) - \frac{\partial \Psi_i}{\partial z}\frac{\partial}{\partial r}(E^2\Psi_i)\right) - \frac{2}{r^2}\frac{\partial \Psi_i}{\partial z}E^2\Psi_i\right] = E^2(E^2\Psi_i), \tag{2.1.17}$$

where

$$E^2 \equiv \frac{\partial^2}{\partial r^2} - \frac{1}{r}\frac{\partial}{\partial r} + \frac{\partial^2}{\partial z^2}. \tag{2.1.18}$$

The dimensionless parameters

$$J \equiv \frac{\rho\sigma R_1}{\mu_1^2}, \quad m_1 = 1, \quad \text{and} \quad m_2 = m \equiv \frac{\mu_2}{\mu_1}, \tag{2.1.19}$$

appear in (2.1.17) as a result of the nondimensionalization proposed above. J is a surface-tension parameter introduced by Chandrasekhar (1961) in his study of the capillary instability of jets of a viscous liquid in air and m is the viscosity ratio of the two fluids. (The dimensionless boundary condition are given in section 2.3 in their linear form.)

2.2 Base State

We begin by examining the case where the interface is undisturbed. This base state velocity field is

$$u_i^0 = w_i^0 = 0 \qquad \text{for} \quad i = 1 \quad \text{and} \quad 2. \tag{2.2.1}$$

Equation (2.1.6) in dimensionless form is

$$\nabla^2\Phi - \kappa^2\Phi = 0, \tag{2.2.2}$$

where

$$\kappa^2 \equiv \frac{8\pi}{\varepsilon_e}\frac{e^2}{KT} n_0 R_1^2 \tag{2.2.3}$$

defines the nondimensional inverse debye length. Its base state potential solution is

$$\Phi^0(r) = a_1 I_0(\kappa r) + a_2 K_0(\kappa r), \tag{2.2.4}$$

where $I_0(x)$ and $K_0(x)$ are modified Bessel functions of order zero, and a_1 and a_2 are constants to be determined by the dimensionless boundary conditions

$$\Phi^0(r = a) = \Phi_W \quad \text{and} \quad \Phi^0(r = 1) = \Phi_I, \tag{2.2.5}$$

where

$$a \equiv \frac{R_2}{R_1}. \tag{2.2.6}$$

We apply the two boundary conditions to get the two constants a_1 and a_2

$$a_1 = \Phi_I \frac{K_0(\kappa a) - \left(1 - \frac{\Delta\Phi}{\Phi_I}\right) K_0(\kappa)}{I_0(\kappa)\, K_0(\kappa a) - I_0(\kappa a)\, K_0(\kappa)}, \tag{2.2.7}$$

$$a_2 = -\Phi_I \frac{I_0(\kappa a) - \left(1 - \frac{\Delta\Phi}{\Phi_I}\right) I_0(\kappa)}{I_0(\kappa)\, K_0(\kappa a) - I_0(\kappa a)\, K_0(\kappa)}, \tag{2.2.8}$$

where

$$\Delta\Phi = \Phi_I - \Phi_W. \tag{2.2.9}$$

2.3 Linear Stability

We now introduce a small disturbance to the interface

$$r(z,t) = 1 + \eta(z,t)\,\delta + O(\delta^2), \tag{2.3.1}$$

and thus to the base state

$$[\Psi(\mathbf{r}), P(\mathbf{r}), \Phi(\mathbf{r})] = [\Psi^1(\mathbf{r})\,\delta, P^0 + P^1(\mathbf{r})\,\delta, \Phi^0(\mathbf{r}) + \Phi^1(\mathbf{r})\,\delta] + O(\delta^2), \tag{2.3.2}$$

where δ is a ordering parameter. To determine the interface stability, we expand the first order variables in normal modes:

$$[\Psi^1(\mathbf{r}), P^1(\mathbf{r}), \Phi^1(\mathbf{r})] = [\psi(r), p(r), \phi(r)] \quad \exp[\mathbf{i}\,\alpha\,(z - c\,t)]. \tag{2.3.3}$$

We substitute (2.3.2) into (2.1.17) and (2.2.2), linearize with respect to δ and then substitute (2.3.3) to get

$$D\left(D\psi_i(r) + \frac{J\,\mathbf{i}\,\alpha\,c}{m_i}\psi_i(r)\right) = 0, \tag{2.3.4}$$

and

$$\frac{d^2\phi}{dr^2} + \frac{1}{r}\frac{d\phi}{dr} = \gamma^2\,\phi\,, \tag{2.3.5}$$

where

$$D \equiv \frac{d^2}{dr^2} - \frac{1}{r}\frac{d}{dr} - \alpha^2, \tag{2.3.6}$$

and

$$\gamma^2 = \kappa^2 + \alpha^2. \tag{2.3.7}$$

The boundary conditions in a linearized dimensionless form are

$$\psi_2 = 0 \quad \text{and} \quad \frac{d\psi_2}{dr} = 0 \quad \text{at} \quad r = a, \tag{2.3.8}$$

$$\psi_1 < \infty \quad \text{and} \quad \frac{d\psi_1}{dr} < \infty \quad \text{at} \quad r = 0, \tag{2.3.9}$$

$$\psi_1 = \psi_2 \quad \text{and} \quad \frac{d\psi_1}{dr} = \frac{d\psi_2}{dr} \quad \text{at} \quad r = 1, \tag{2.3.10}$$

$$m\,[D\psi_2 + 2\,\alpha^2\,\psi_2] - [D\psi_1 + 2\,\alpha^2\,\psi_1] = 0, \quad \text{at} \quad r = 1, \tag{2.3.11}$$

$$\frac{m}{\mathbf{i}\,\alpha\,r}\frac{d}{dr}[D\psi_2] + 2\,m\,\mathbf{i}\,\alpha\frac{d}{dr}\left[\frac{1}{r}\psi_2\right] - \frac{1}{\mathbf{i}\,\alpha\,r}\frac{d}{dr}[D\psi_1] - 2\,\mathbf{i}\,\alpha\frac{d}{dr}\left[\frac{1}{r}\psi_1\right]$$

$$+\frac{Q}{\Phi_i^2}\left[\frac{d\Phi^0}{dr}\frac{d\phi}{dr} - \phi\left(\frac{d^2\Phi^0}{dr^2} + \frac{1}{r}\frac{d\Phi^0}{dr}\right) - \left(\frac{d\Phi^0}{dr}\right)^2\eta\right] = [\alpha^2 - 1]\,\eta, \quad \text{at} \quad r = 1 \tag{2.3.12}$$

$$\eta = -\frac{1}{r}\frac{\psi_1}{c} \quad \text{at} \quad r = 1\,. \tag{2.3.13}$$

$$\phi = 0 \quad \text{at} \quad r = a \quad \text{and} \quad \phi + \eta \frac{d\Phi^0}{dr} = 0 \quad \text{at} \quad r = 1. \tag{2.3.14}$$

The dimensionless parameter Q appearing in (2.3.12) is the ratio of the electrostatic forces over the capillary forces

$$Q = \frac{\varepsilon_e}{4\pi} \frac{[\Phi_I K T / e]^2}{\sigma R_1}. \tag{2.3.15}$$

Note that the term in the square brackets in (2.3.15) is just the dimensional form of Φ_I. Also, observe that as in Felderhof (1968), $\hat{\eta}$ enters only the isotropic stress, which is substituted for and eliminated from the boundary conditions and the problem along with the pressure.

The solution to (2.3.4) is

$$\psi_i(r) = A_i\, r\, I_1(\alpha r) + B_i\, r\, K_1(\alpha r) + D_i\, r\, I_1(\beta_i r) + E_i\, r\, K_1(\beta_i r), \tag{2.3.16}$$

where $$\beta_i^2 = \alpha^2 - \frac{J \mathbf{i} \alpha c}{m_i}, \qquad \text{for} \quad i = 1 \quad \text{and} \quad 2. \tag{2.3.17}$$

The solution to (2.3.5) is

$$\phi(r) = a_3 I_0(\gamma r) + a_4 K_0(\gamma r). \tag{2.3.18}$$

We first apply the two electrostatic boundary conditions (2.3.14) to get the constants a_3 and a_4 in terms of η

$$a_3 = \frac{K_0(\gamma a)\, k[a_1 I_1(k) - a_2 K_1(k)]}{K_0(\gamma)\, I_0(\gamma a) - K_0(\gamma a)\, I_0(\gamma)} \eta, \tag{2.3.19}$$

$$a_4 = -\frac{I_0(\gamma a)\, k[a_1 I_1(k) - a_2 K_1(k)]}{K_0(\gamma)\, I_0(\gamma a) - K_0(\gamma a)\, I_0(\gamma)} \eta. \tag{2.3.20}$$

From (2.3.18), (2.3.19) and (2.3.20) we get $\phi(r)$ in terms of η.

Substituting (2.2.4), (2.2.7), (2.2.8), (2.3.13), (2.3.16), (2.3.18), (2.3.19) and (2.3.20) into (2.3.8) through (2.3.12) we get a (6X6) system of equations of the form

$$\mathbf{A}\,\mathbf{x} = \mathbf{0}. \tag{2.3.21}$$

The matrix **A**

$$\begin{bmatrix}
0 & 0 & I_1(\alpha a) & K_1(\alpha a) & I_1(\beta_2 a) & K_1(\beta_2 a) \\
0 & 0 & \alpha I_0(\alpha a) & -\alpha K_0(\alpha a) & \beta_2 I_0(\beta_2 a) & -\beta_2 K_0(\beta_2 a) \\
I_1(\alpha) & I_1(\beta_1) & -I_1(\alpha) & -K_1(\alpha) & -I_1(\beta_2) & -K_1(\beta_2) \\
\alpha I_0(\alpha) & \beta_1 I_0(\beta_1) & -\alpha I_0(\alpha) & \alpha K_0(\alpha) & -\beta_2 I_0(\beta_2) & \beta_2 K_0(\beta_2) \\
(m-1)2\alpha^2 I_1(\alpha) & (m-1)2\alpha^2 I_1(\beta_1) - \omega J I_1(\beta_1) & 0 & 0 & \omega J I_1(\beta_2) & \omega J K_1(\beta_2) \\
F_1 I_1(\alpha) - 2\alpha^2 I_0(\alpha) & F_1 I_1(\beta_1) + F_2 I_0(\beta_1) & 2m\alpha^2 I_0(\alpha) - 2m\alpha I_1(\alpha) & -2m\alpha^2 K_0(\alpha) - 2m\alpha K_1(\alpha) & -F_3 I_0(\beta_2) - 2m\alpha I_1(\beta_2) & F_3 K_0(\beta_2) - 2m\alpha K_1(\beta_2)
\end{bmatrix}$$

in (2.3.21) contains the coefficients of the constants of integration from the linearized boundary conditions. The constants appearing in **A** are

$$F_1 = \frac{1 - \alpha^2 + Q\,\mathcal{E}}{\omega}\alpha + 2\,\alpha, \tag{2.3.22}$$

$$F_2 = \left(J\frac{\omega}{\alpha} - 2\,\alpha\right)\beta_1, \tag{2.3.23}$$

$$F_3 = \left(J\frac{\omega}{\alpha} - 2\,m\,\alpha\right)\beta_2, \tag{2.3.24}$$

where ω is the growth rate

$$\omega = -\mathbf{i}\,\alpha\,c, \tag{2.3.25}$$

and where $\mathcal{E}$ reflects the electrostatic contribution to the stability of our system in the normal stress balance

$$\mathcal{E}=\frac{\Phi_r^0}{\Phi_I^2}\left(\frac{K_0(\gamma a)\,I_1(\gamma)+I_0(\gamma a)\,K_1(\gamma)}{I_0(\gamma a)\,K_0(\gamma)-I_0(\gamma)\,K_0(\gamma a)}\gamma\,\Phi_r^0+\Phi_{rr}^0\right). \tag{2.3.26}$$

In (2.3.26) Φ_r^0 and Φ_{rr}^0 are the first and second derivatives of the base state electrostatic potential Φ^0 at the interface, which are

$$\Phi_r^0=k(a_1\,I_1(k)-a_2\,K_1(k)), \tag{2.3.27}$$

$$\Phi_{rr}^0=k[a_1\,(\,kI_0(k)-I_1(k))+a_2\,(\,kK_0(k)+K_1(k))]. \tag{2.3.28}$$

Finally **x** is the vector of the constants of integration

$$\mathbf{x}=[A_1\quad D_1\quad A_2\quad B_2\quad D_2\quad E_2]^t. \tag{2.3.29}$$

The stability of the system is determined by the implicit equation for $\omega(\alpha)$ which we can write as

$$det(\mathbf{A})=0. \tag{2.3.30}$$

Below we solve (2.3.30) numerically to get a dispersion equation of the form

$$\omega=F\left(\alpha,a,J,m,Q,k,\frac{\Delta\Phi}{\Phi_I}\right). \tag{2.3.31}$$

We will choose to represent neutral curves as the electrostatic parameter Q versus the wave number α with the other dependences in (2.3.31) as parameters. Since the neutral states are non-flowing, these neutral curves, unlike the growth rates, will be independent of the fluid mechanical parameters J and m.

3 RESULTS

Using the LINPACK subroutines ZGECO and ZGEDE, we solve (2.3.30) numerically for the three cases that title the forthcoming subsections. In the results detailed here, the computed values of c are always purely imaginary (i.e. The calculated real parts are typically many orders of magnitude smaller than the calculated imaginary parts) and thus disturbances do not propagate. This is expected because the base state is one of zero flow. In the calculations given below, a new parameter ε given by

$$\varepsilon = \frac{R_2 - R_1}{R_2} \qquad \text{or} \qquad \varepsilon = 1 - \frac{1}{a}, \tag{3.0.1}$$

enters to replace a.

3.1 Pure Capillarity (Q = 0)

In this section we present the results in the absence of electrostatic effects which follow by setting Q equal to zero. The remaining parameters that determine the stability of the system are the surface-tension parameter J, the viscosity ratio m and the film thickness parameter ε. Figures 2(a-c) are typical growth rate versus wave number curves which illustrate the dependence of ω_r vs α on these groups. Each of these shows the universal and well known behavior that waves smaller than the interfacial circumference are stable while all others are unstable and that there is a fastest growing wave. These curves are new; they extend the results of Goren to include the influence of a core fluid.

As shown in Figure 2a increasing J retards the growth. The simplest way to understand Figure 2a is to note that since time is written in units of [$\mu_1 R_1/\sigma$] and the wave number in units of [$1/R_1$], increasing J in this figure can only be interpreted, in terms of physical variables, as increasing ρ. Since this increases the fluids' iner-

tia, the unstable growth rates should decrease, as Figure 2a demonstrates. Figure 2b shows that increasing m also has a retarding effect. This is due to the fact that, with μ_1 held fixed, increasing m corresponds to increasing the film fluid's viscosity and the additional fluid resistance slows the growth. On the other hand by increasing ε with R_1 fixed one increases the film's thickness. This decreases the viscous resistance in the film, allowing the instability to grow faster (see Figure 2c).

As a way of checking our numerical results we introduce the asymptotic expansion for long waves ($\alpha \to 0$) used by Yih (1967),

$$c = c^{(0)} + c^{(1)}\,\alpha + O\,(\alpha^2), \tag{3.1.1}$$

$$\psi = \psi^{(0)} + \psi^{(1)}\,\alpha + O\,(\alpha^2), \tag{3.1.2}$$

and

$$\phi = \phi^{(0)} + \phi^{(1)}\,\alpha + O(\alpha^2), \tag{3.1.3}$$

into the governing equations and solve for the leading order term in c. The first non vanishing term, $c^{(1)}$,in this expansion is found to be purely imaginary and is given by $c^{(1)} = c_h^{(1)}$ where

$$c_h^{(1)} = -\left[\frac{4\,(a^4 + m - 1)\log(a) + (m-4)\,a^4 + (8-4m)\,a^2 + 3m - 4}{16\,(m\,a^4 + m^2 - m)}\right]\mathbf{i}. \tag{3.1.4}$$

(We arrive at (3.1.4) as the leading order in α result in two ways. In the first we substitute the above expansions (3.1.1) to (3.1.3) into the Orr-Sommerfeld equation and solve the leading order problems sequentially. Alternately, we begin by separating the modified Bessel functions in the exact equation (2.3.21) into its logarithmic and power series terms. The symbolic algebraic calculations (using MACSYMA) reveal that all terms logarithmic in α cancel identically and lend to (3.1.4). This result justifies the proposed expansions (3.1.1) to (3.1.3) as simple power series in α.)

The asymptotic expression (3.1.4) appears in Figure 2a along with the exact results; the agreement for long waves is evident. Both the asymptotic and the exact results indicate that the growth rate becomes independent of J for long waves. This is because the dynamics at long waves becomes lubrication-like, and the influence of the fluids' inertia becomes negligible.

With the exact results we are in the position to assess how well lubrication theory describes the system dynamics (in the limit of $\varepsilon \to 0$). In lubrication theory the radial length-scale in the film is smaller than the axial scale and it easily follows (see Frenkel et al. (1987)) that, for m of order one (in ε), the growth rate is given by

$$\omega_r = \frac{\varepsilon^3}{3m}(\alpha^2 - \alpha^4). \tag{3.1.5}$$

Figure 3 is a comparison of the lubrication result and the exact solution. Clearly the agreement is exceptional even for ε as large as 0.2 for the parameters chosen. Finally in the limit of $\varepsilon \to 0$ the Yih result should coincide with the order α^2 term in the lubrication expression; in fact, a straightforward expansion of (3.1.4), in powers of ε for $a = 1/(1-\varepsilon)$, confirms that it does.

3.2 The Influence of a Double Layer of Charge for an Infinite Outer Region ($Q \neq 0, \varepsilon \to 1$)

In this section we include the effect of the electrostatic double layers ($Q \neq 0$) for the case of an infinite outer region ($\varepsilon \to 1$). In this limit the dispersion equation depends only on the parameters J, m, $k$and Q. Thus only the double layer around the interface contributes to the stability, and the sign of the interface potential does not effect the stability of the system.

The non-oscillatory neutral curves for this system derive solely from the normal stress balance and are given by

$$Q\,\mathcal{E}+1-\alpha^2=0, \tag{3.2.1}$$

where $\mathcal{E}$ is the electrostatic contribution given generally by (2.3.26) and specifically in the limit $\varepsilon \to 1$ by

$$\mathcal{E}_\infty=\frac{k^2 K_1(k)}{(K_0(k))^2}\left[\frac{\gamma K_1(k) K_1(\gamma)}{K_0(\gamma)}-kK_0(k)-K_1(k)\right]. \tag{3.2.2}$$

As noted they are independent of the hydrodynamics and are only a function of the electrical parameters Q and k. For $Q=0$ the capillary instability of Tomotika (1935) obtains and the system is stable only to disturbances having $\alpha \geq 1$.

As the dimensional interfacial radius $R_1 \to \infty$, the system becomes planar. Equation (3.2.1) with dimensional variables and with leading order, large argument expansions of the Bessel functions (e.g. Abramowitz & Stegun (1972)) gives

$$-\alpha^2\sigma+\frac{\varepsilon_e}{4\pi}\Phi_I^2 k^2(\gamma-k)+\frac{\varepsilon_e}{4\pi}\Phi_I^2 k(\gamma-k)\frac{1}{R_1}$$
$$+\left[\sigma+\frac{\varepsilon_e}{4\pi}\Phi_I^2\left(\frac{k^2-9\gamma k+6\gamma^2}{-16\gamma}\right)\right]\frac{1}{R_1^2}+O\left(\frac{1}{R_1^3}\right)=0. \tag{3.2.3}$$

As $R_1 \to \infty$ (with $\zeta=\gamma/k$), it becomes

$$\alpha^2\sigma-\frac{\varepsilon_e}{4\pi}\Phi_I^2 k^3(\zeta-1)=0. \tag{3.2.4}$$

This recovers Miller & Scriven's (1970) planar, constant surface potential, marginal interfacial stability result for two fluids with equal densities.

Figure 4 shows neutral curves for different values of the inverse debye length parameter k. For comparison Figure 5 shows growth rate curves for the same values of k at a particular value of Q ($Q=0.3$) and for $J=10^3$ and $m=1$. The

crossing points of the $Q = 0.3$ line with the neutral curves of Figure 4 agree perfectly with the changes of sign of the growth rate curves of Figure 5. Figure 5 also includes the growth rate curve for pure hydrodynamics $Q = 0$ in which case the system is stable for $\alpha \geq 1$. The intersections of the pure hydrodynamic growth rate curve with the other growth rate curves (points a, b, c, d, e, and f in Figure 5) are the points where the electrostatic contribution is zero ($\mathcal{E}_\infty = 0$) since even for the dynamic case, the influence of the double layer enters only through the parameter $\mathcal{E}_\infty$. Since $\mathcal{E}_\infty$ is zero at these points, from (3.2.1), they coincide with the neutral curves' singular points manifest in Figure 4.

To interpret the marginal curves, consider first long and moderately long waves. A short calculation shows that as $\alpha \to 0$ the electrostatic contribution $\mathcal{E}_\infty$ up to order α^2 is

$$\mathcal{E}_\infty = -b_0 + b_2 \alpha^2, \tag{3.2.5}$$

where b_0 and b_2 are given by

$$b_0 = -\frac{k^2 K_1(k)}{(K_0(k))^2}\left[\frac{k(K_1(k))^2}{K_0(k)} - kK_0(k) - K_1(k)\right], \tag{3.2.6}$$

and

$$b_2 = \frac{k^2 (K_1(k))^2}{(K_0(k))^2}\left[\frac{k^2 K_0(k)K_3(k) - 2k^2 K_1(k)K_2(k) + (k^2 - 8)K_0(k)K_1(k)}{8k(K_0(k))^2}\right]. \tag{3.2.7}$$

Numerical calculation shows that, for every k, b_0 and b_2 are both positive and b_2 is always greater than b_0 ($b_2 > b_0 > 0$).

By inserting the above expansion into the neutral stability equation (3.2.1) the following criterion for stability emerges for long and moderate waves

$$(1 - Q\, b_0) - (1 - Q\, b_2)\, \alpha^2 < 0 \qquad (\textit{stable})$$

$$> 0 \qquad (\textit{unstable}). \qquad (3.2.8)$$

Thus for this range of wavelengths one can interpret the electrostatic influence as a pure reduction of the surface tension for both the circumferential and the longitudinal curvature. However, the reduction in the surface tension corresponding to each of these curvatures is different, it being $Q\, b_0$ for the circumferential and $Q\, b_2$ for the longitudinal. From Figure 4 and the above expansion we can see that, for very long waves, only the order α^0 terms in (3.2.8) are important. If Q is larger than a critical value $Q^* = 1/b_0$ the destabilizing effect of the circumferential curvature can be eliminated and the system becomes stable to such disturbances. However, at some wave number α^*

$$\alpha^* = \sqrt{\frac{1 - Q\, b_0}{1 - Q\, b_2}}, \qquad (3.2.9)$$

the fact that the corresponding longitudinal tension is negative $(1 - Q\, b_2 < 0)$ and $(b_2 > b_0)$ causes the system to become unstable for shorter wavelength disturbances (see Figure 4 points (A, B and C)). Figure 5 also includes this effect; for the chosen value of Q ($Q = 0.3$) the last three growth rate curves (k= 8, 10 and 12) start as negative (stable) and then at some wave number they become positive (unstable) (see Figure 5 points (A, B and C)). For even shorter waves the system becomes stable again because the lower right branches of the neutral curves asymptote to infinity. This behavior is given analytically by

$$\underset{\alpha\to\infty}{\mathcal{E}_\infty} = \left[\frac{kK_1(k)}{K_0(k)}\right]^2 \alpha + O(\alpha^0); \quad \underset{\alpha\to\infty}{Q} = \left[\frac{K_0(k)}{kK_1(k)}\right]^2 \alpha + O(\alpha^0). \qquad (3.2.10)$$

A physical interpretation is in order. For very short waves $\mathcal{E}$ is positive (destabilizing) and linear in α. The asymptote of the lower branch, described by (3.2.10) becomes a balance of the order α^2 stabilization of the longitudinal curvature and this order α destabilization of $\mathcal{E}$. Thus at high α the electrostatic destabilization has been reduced from order α^2 (cf. (3.2.8)) to order α. As in Miller & Scriven's case, wave-wave interactions of double layers at very short wavelengths account for this suppression of electrical destabilization allowing surface tension's stabilization to dominate in this regime.

If, on the other hand, Q is less than $1/b_0$, the stabilizing electrostatic effect does not overcome the unstable nature of the circumferential curvature and the system is unstable for the longest waves (i.e. for $(1-Qb_0)>0$). For this case there are two possibilities: (*i*) $Qb_2<1$ or (*ii*) $Qb_2>1$. If $Qb_2<1$, then the longitudinal surface tension ($1-Qb_2$) is positive and stabilizes the system at a value of α given by (3.2.9) (see Figure 4 and 5 points (D and E) or, in fact, the purely hydrodynamic point $(\alpha,Q)=(1,0)$.). Since $b_2>b_0$, $\alpha^*>1$, which accounts for the receding of the critical wave number to shorter waves relative to the pure hydrodynamics. Moreover, the electrical effect is stabilizing to the left of $\bar{\alpha}$:$\mathcal{E}_\infty(\bar{\alpha})=0$ and destabilizing to its right. Thus since $\bar{\alpha}<1$, the points $(\alpha,Q)=(0,1/b_0)$ and $(1,0)$ have qualitatively different behavior with increasing Q and therefore can not lie on the same branch of the neutral curve.

If $Q\ b_2>1$, then the longitudinal surface tension is negative and also destabilizes the system. In this range of Q $(1/b_0>Q>1/b_2)$ the system never becomes stable in the quadratic range (cf. (3.2.9) has no real roots), but it does become stable at higher α because of unfavorable wave-wave interactions described by (3.2.10)

and discused above. This accounts for the sudden flattening of the right branches of the neutral curves in Figure 4 and explains why the ($Q = 0.3$) line does not intersects the ($k = 6$) neutral curve in the quadratic range.

From Figure 4 it appears that the larger the debye length (the smaller the k) the larger the Q has to be in order for the electrostatic contribution to stabilize for long waves or to destabilize for short waves. This can be explained as follows: At constant potential the debye length is a measure of the length over which the electrostatic potential changes from its interfacial value due to absorbed ions to its reference value far from the interface. Thus a larger debye length defines a weaker gradient of the base state potential Φ^0, i.e., a weaker electric field. Clearly, then, a larger Q is needed to achieve the critical electrostatic effect.

It is worth noting that these results apply equally well to the problem of a jet of uniform velocity in a vacuum or a gas. By a simple coordinate transformation, one can see that the growth rate in the case of a jet differs from our results solely by the addition of an imaginary part equal to the jet's velocity. Jet problems in the presence of axial electric fields were the subject of previous investigators (Saville (1970), Saville (1971), Melcher & Taylor (1969)).

3.3 The Influence of a Double Layer of Charge for a Finite Outer Region ($Q \neq 0, R_2 < \infty$)

In this section we present the results for the most general case where the outer region is finite and the electrostatic effects are present. These results reduce to those of section 3.1 when $Q = 0$ and to the results of section 3.2 when $\varepsilon \to 1$. The dispersion equation of this section depends on all the parameters ε, J, m, k, Q and $\Delta\Phi/\Phi_I$.

The non-oscillatory neutral curves again obtain from (3.2.1) with $\mathcal{E}$ given by the general expression (2.3.26). As before, the neutral curves are independent of the hydrodynamics but are now functions of the film parameter ε and the electrical parameter $\Delta\Phi/\Phi_I$ as well as of Q and k. Two cases have qualitatively different neutral curves and thus merit independent discussions. The first case is when the base state volume charge density is everywhere of the same sign. Interfacial perturbations cause unfavorable like-charge interactions between the interfacial and wall double layers in the regions where the perturbation has thinned the film. These interactions stabilize the system and motivate the name double layer repulsion. In the second case, the diffuse layer adjoining the fluid interface is opposite in sign to that next to the wall. Here film thinning leads to favorable interactions between these opposite charges and this tends to destabilize the system. This case is referred to as double layer attraction.

(i) Double Layer Repulsion

The nondimensional base state volume charge density ρ_e^0, nondimensionalized with $e\, n_0$, is given by

$$\rho_e^0(\mathbf{r}) = -2\,\Phi^0(\mathbf{r}). \tag{3.3.1}$$

It is clear from (3.3.1) that ρ_e^0 is everywhere of the same sign as long as $\Phi^0(\mathbf{r})$ has that property. This can be realized when $\Delta\Phi / \Phi_I \le 1$. For discussion purposes in this subsection we shall chose the simplest case of $\Delta\Phi / \Phi_I = 0$. Two types of neutral curves (A and B) exist. Type B neutral curves are similar to those from the previous section where a singularity appears at some $\alpha < 1$. Type A neutral curves

are new; a singularity appears at some $\alpha > 1$. These curves appear in Figures 6a and 6b which vary ε at fixed k. Figure 6c is corresponding potential profiles for the values of ε, k and $\Delta\Phi/\Phi_I$ chosen.

As in the previous section, expanding the parameter $\mathcal{E}$ in powers of α up to order α^2 greatly aids in the explanation of the resulting curves; thus $\mathcal{E} = -b_0 + b_2\,\alpha^2$, where

$$b_0 = -\frac{\Phi_r^0}{\Phi_I^2}\left(\frac{K_0(ka)\,I_1(k) + I_0(ka)\,K_1(k)}{I_0(ka)\,K_0(k) - I_0(k)\,K_0(ka)}\,k\Phi_r^0 + \Phi_{rr}^0\right), \tag{3.3.2}$$

and b_2 is detailed in the appendix. Again from (3.2.1), the system is stable to long and moderate wavelength disturbances when

$$(1 - Q\,b_0) - (1 - Q\,b_2)\,\alpha^2 < 0\,,$$

and unstable to such disturbances when greater than zero. Consider first neutral curves 6a and 6b which describe the influence of changing the film thickness with the debye length (k) held fixed. When ε is large ($\varepsilon \geq 0.5$) the film is thick enough for the debye length chosen ($k = 10$) so that the diffuse double layers adjoining the interface and wall effectively do not interact and a region of nearly zero volume charge density exists (cf. Figure 6c). Only the double layer next to the interface affects the stability and marginal curves like those of the infinite outer region case obtain. As in that case b_0 and b_2 are both positive and b_2 is greater than b_0 ($b_2 > b_0 > 0$). For $Q > 1 / b_0$ the system is stable for small α, then becomes unstable (at α^* as given by (3.2.9)) and finally becomes stable due to the asymptotic behavior of $\mathcal{E}$ as $\alpha \to \infty$ given by

$$\underset{\alpha\to\infty}{\mathcal{E}} = \left[\frac{\Phi_r^0}{\Phi_I}\right]^2 \alpha + O(\alpha^0). \tag{3.3.3}$$

For $Q < 1 / b_0$ long waves are unstable and then eventually stabilize at α^* as given by (3.2.9) if $Q\, b_2 < 1$ and outside the quadratic range if $Q\, b_2 > 1$. As can be seen in Figure 6b the neutral curves for $\varepsilon = 0.6$ and above quickly merge in to the infinite case curve ($\varepsilon \rightarrow 1$).

When ε is less than 0.5 the region of zero volume charge density in the film disappears, and the double layers interact (cf. Figure 6c). This interaction stabilizes the system increasing b_0 (for $\varepsilon > 0.1$) and decreasing b_2 as ε decreases (cf. Figure 6d)[1]. As b_2 becomes less than b_0, the two branch neutral stability structure transforms from that of Figure 6b to that of Figure 6a. For the longest waves, the stability is qualitatively unchanged in Figure 6a from Figure 6b since only b_0 is relevant there. For $Q > 1 / b_0$, the system is stable while for $Q < 1 / b_0$ it is unstable. However since $b_2 < b_0$, $\alpha^* < 1$ in (3.2.9) for $Q < 1 / b_0$ and the critical wave number shifts to longer waves. Since the singularity in the neutral curve, i.e., the $\bar{\alpha}$ for which $\mathcal{E}(\bar{\alpha})$ changes sign, is now to the right of one, the electrical effect is stabilizing for all $\alpha < 1$ with the magnitude of this stabilization increasing with Q. Thus one branch of the neutral curve can connect the points $(\alpha , Q) = (0 , 1 / b_0)$ and $(1 , 0)$; the axial curvature stabilizes the system at small α (< 1) and a small unstable lobe replaces the large unstable region between the branches of Figure 6b. For $Q > 1 / b_0$, long waves are stable. Importantly, a window of stability for all α exists from the value ($1 / b_0$) to the minimum of the upper branch, which can not be in the quadratic range. Note the window widens as ε decreases and double layer repulsion becomes more dominant.

---

1 As $\varepsilon \rightarrow 0$, b_0 and b_2 go to zero because the base state potential profiles become flat.

Lastly, for Q above the minimum the system is destabilized at smaller waves. This may be attributed to the change in sign of the coefficient of the axial curvature $1 - Q b_2 < 0$ as well when $b_2 > 0$ ($\varepsilon = 0.4$); this part of the upper branch is given by (3.2.9) which is in the quadratic range. For smaller ε however, b_2 is negative (cf. Figure 6d) and the axial curvature is stabilizing for all Q. Thus for these cases the transition to the unstable region for moderate α must be attributed solely to higher order terms in α in the expansion of $\mathcal{E}$. Here too unfavorable wave-wave interactions restabilize the system to the shortest wavelengths disturbances reducing the dependence of $\mathcal{E}$ on α to order α from order α^2 (cf. (3.3.3)). For this part of the upper branch the marginal point is determined as the competition between the order α destabilization caused by $\mathcal{E}$ and the order α^2 stabilization caused by the axial curvature.

The dependence of the neutral curves on k at fixed ε for the potential distributions (not shown) is similar to that of Figures 6a and 6b: As k decreases at fixed ε, the double layers interact more and a transition occurs from the marginal curve structure of the infinite case (type B as in Figure 6b) to that of type A (as in Figure 6a.) In the next subsection on Double Layer Attraction we discus further the relationship between small ε and large k.

The influence of double layer repulsion on the growth rate appears in Figure 8 as ω_r as a function of Q with $\Delta\Phi / \Phi_I = 0$ and with k, ε, J, and m fixed. Also plotted on the figure (for $Q = 0.05$) is the long wave Yih (1967) expansion for ω_r obtained from (3.1.1) to (3.1.3). Again $c^{(0)} = 0$, and $c^{(1)}$ is purely imaginary and given by

$$c^{(1)} = c_h^{(1)} (1 - Q\, b_0), \tag{3.3.4}$$

where $c_h^{(1)}$ is the same as in (3.1.4). The Yih approximation, which is J independent, and the numerically exact solution converge as $\alpha \to 0$. Figure 7 clearly shows three different behaviors. When $Q < 1/b_0$, the system is unstable for a band of long waves. These are located inside the unstable lobe of Figure 6a ($\varepsilon = 0.4$). For these values of Q, it is clear that double layer repulsion has retarded the growth rate relative to the growth rate exclusively due to capillarity (cf. the curve marked H). For $1/b_2 > Q > 1/b_0$ the window of stability exists and this is shown by the always-stable ($\omega_r < 0$, $Q = 0.15$) growth rate curve. Finally, for $Q > 1/b_2$, the upper branch of the type A neutral curves becomes important and positive growth rates occur at wave numbers greater than 1 ($\alpha > 1$), although they must again stabilize for sufficiently large α ($\omega_r \to -\infty$ as $\alpha \to \infty$). Importantly, the growth rates derived from the upper branch unstable band are much larger than the pure hydrodynamic rate ($Q = 0$). Again the intersections of the pure hydrodynamic curve with the ($Q \neq 0$) curves defines the value of α ($\bar{\alpha}$) at which the electrostatic contribution is zero ($\mathcal{E}(\bar{\alpha}) = 0$). Since $\mathcal{E}$ is only a function of ε, κ and $\Delta\Phi/\Phi_I$ and because these parameters are fixed in Figure 7, all the curves intersect at the same value of α. This value of α defines the singularity that separates the upper and lower branches of the marginal stability curve (cf. Figure 6a, $\varepsilon = 0.4$).

(ii) Double Layer Attraction

In this subsection we examine the case in which the diffuse layers next to the fluid interface and the wall have volume charge densities ρ_e^0 of opposite sign. It is clear from (3.3.1) that in order to obtain diffuse layers of opposite charge the sign of Φ_I must be opposite to Φ_W, or $\Delta\Phi/\Phi_I > 1$. Plots of potential distributions $(\Phi - \Phi_I)/\Phi_I$ for various negative and positive values of $\Delta\Phi/\Phi_I$ appear in Figure 8c, and Figures 8a and 8b give the corresponding neutral curves. As expected, when

$\Delta\Phi/\Phi_I \leq 1$ and the volume charge density is everywhere of the same sign, the double layers repel, and for the values of ε and κ chosen (0.3 and 10, respectively) in Figure 8a, type A neutral curves characterizing strong double layer repulsion obtain. As $\Delta\Phi/\Phi_I$ increases from one, the charge of the diffuse layers next to the wall and next to the fluid interface take on opposite signs. This change in diffuse layer sign destabilizes the system because in regions where the film thickness has decreased charges of unlike sign (favorably) approach one another.

As $\Delta\Phi / \Phi_I$ increases from an initially strong double layer repulsion configuration, b_0 decreases and b_2 increases, and the unstable lobe of the type A neutral curves grows. At a critical value of $\Delta\Phi / \Phi_I$ (≈ 1 for the values of ε and κ chosen) b_2 becomes greater than b_0, and a transition back to type B neutral curves occurs (Figure 8b). Finally, as $\Delta\Phi / \Phi_I$ increases further, b_0 decreases through zero to negative values and the upper branch of the type B curves disappears leaving only the lower branch. This branch, (described by (3.2.9) when $Q\, b_2 < 1$), recedes with increasing $\Delta\Phi / \Phi_I$ as b_2 increases, i.e., the stabilization of the axial curvature decreases. Finally, as in the previous cases the lower branch of Figure 8b goes as $O(\alpha)$ for $\alpha \rightarrow \infty$; thus in the case of double layer attraction for which there is only one branch ($b_0 \leq 0$), the system becomes unstable to an increasingly wider band of wavelengths as Q increases.

Figure 9 shows the influence of double layer attraction on the growth rate for $m = 1$, $J = 10^3$ and $Q = 0.4$ and for the same values of ε and κ as in Figure 8. Points A, B, C and D in Figures 8a, 8b and 9 are the wavelengths of zero growth. Figure 9 shows that as double layer repulsion fades (increasing $\Delta\Phi / \Phi_I$) the win-

dow of stability disappears and as double layer attraction takes over, the maximum growth rate and the wave number of maximum instability increase until they exceed those for pure capillarity (the curve marked H).

Double layer attraction can also occur even when the volume charge density is everywhere of the same sign if the *surface* charge densities of the two interfaces (film-core and film-tube) are of opposite sign. This can be achieved either by reducing the film thickness ε keeping the debye length ($1 / k$) constant or by increasing the debye length (decreasing k) keeping the film thickness constant, in the case where the potential difference $\Delta\Phi$ is fixed and nonzero. This can be shown as follows: First the governing equation (2.2.2) for the base state potential is

$$\frac{d^2\Phi^0}{dr^2}+\frac{1}{r}\frac{d\Phi^0}{dr}=k^2\,\Phi^0; \tag{3.3.5}$$

then by defining a film variable y as $\varepsilon\, y=\frac{1}{1-\varepsilon}-r$, and letting ε go to zero $(\varepsilon\to 0)$ one gets

$$\frac{d^2\Phi^0}{dr^2}=0. \tag{3.3.6}$$

The solution of (3.3.6) is linear with respect to r so when $(\Delta\Phi\neq 0)$ the surface charge densities $(\sigma_e=-\mathbf{n}\cdot\nabla\Phi^0)$ of the two interfaces are of opposite sign. On the other hand if one lets the debye length go to infinity $(k\to 0)$, then (2.2.2) becomes

$$\frac{d^2\Phi^0}{dr^2}+\frac{1}{r}\frac{d\Phi^0}{dr}=0. \tag{3.3.7}$$

The solution of (3.3.7) is $\Phi^0=d_1\ln(r)+d_2$ which does not have a singular point; so, again the surface charge densities of the interfaces are of opposite sign.

Figure 10b shows plots of potential distributions $(\Phi-\Phi_I)/\Phi_I$ for some decreasing values of the film thickness ($\varepsilon=$ 0.6, 0.5, 0.4, 0.3, 0.2, 0.1). It is clear

from that Figure that as the film thickness decreases the potential distribution in the film becomes linear and the surface charge density at the film-core interface changes sign. Figure 10a shows the corresponding neutral curves. As expected, when the two interfaces are far apart ($\varepsilon = 0.6$ and 0.5) we get type B neutral curves, similar to the ones from the infinite outer region case. When the interfaces are brought closer together ($\varepsilon = 0.4, 0.3$ and 0.2) the double layers repel and type A neutral curves characterizing double layer repulsion obtain. At some critical film thickness, which is a function of the debye length and the potential difference, the potential distribution becomes linear, forcing the surface charge densities of the two interfaces to become of opposite signs; a strong double layer attraction results (see last graph in Figure 10a). Similar neutral curves arise for the second case ($k \to 0$).

4 SUMMARY AND CONCLUSIONS

The results presented in section 3, bear directly on the critical question of how to stabilize an annular film from the capillary instability. Figures 6a and 8a have windows of Q values that emerge only when the volume charge density is everywhere of the same sign. In such cases double layer repulsion is strong enough to stabilize the action of the circumferential curvature while not at the same time reducing the surface energy to the point where the axial curvature tension is no longer positive (i.e., $1/b_0 < Q < 1/b_2$). For moderate ε and k, decreasing $\Delta\Phi/\Phi_I$ may realize this. Physically, decreasing $\Delta\Phi/\Phi_I$ proceeds when one sets the wall potential higher than that of the reservoir for $\Phi_I > 0$. Then, at fixed ε and k, a decrease in $\Delta\Phi/\Phi_I$ brings on and then widens a band of complete stability (cf. Figures 8a and 8b). Alternatively, for fixed, negative Φ_W, adsorption of an anionic surfactant can force Φ_I negative by lowering the interface potential relative to the bulk.

Consider, as a numerical example of complete stabilization, an electrolyte film surrounding an oil core in a rock pore with a characteristic diameter of 100 μms and with the anionic surfactant sodium dodecal sulfate (SDS) introduced in the electrolyte film. SDS adsorbs onto the oil-water interface creating a surface potential. In this numerical example, we assume that the surfactant also adsorbs onto the rock wall the same way it adsorbs to the oil-water interface so the potential difference between the two interfaces is zero ($\Delta\Phi = 0$). Havenbergh & Joos (1983) and Bleys & Joos (1985) have shown that the adsorption of SDS at the air-water interface may be described by a Langmuir adsorption isotherm:

$$\sigma_e = -e\,\Gamma^- = -e\,\frac{\Gamma^-_\infty\,\rho_e^-(r=f)}{a+\rho_e^-(r=f)}, \tag{4.1}$$

where Γ^- is the surface surfactant concentration, Γ^-_∞ is the maximum surface surfactant concentration, a is the Langmuir constant and $\rho_e^-(r=f)$ is the volume charge density at the interface. The constants a and Γ^-_∞ have been calculated for the air-water interface. Assuming the same constants for adsorption onto an oil-water interface, one can calculate the surface charge density and surface potential. Then from (2.3.15) one can find the critical surface tension corresponding to the lower branch of the window of stability of type A neutral curves ($Q = 1/b_0$). Systems with surface tension below this critical value can lie in the window and be stable. Figure 11 shows curves of the critical surface tension versus the film thickness ε for various values of the surfactant concentration n_0. From this figure we see that as an example if the oil-water interfacial tension of the system is reduced to 10 dynes/cm (by, say, introducing a second, non-ionic surfactant), then for a trace surfactant concentration of SDS $n_0 = 8X10^{-10} mole/cm^3$ the system can become stable for film thicknesses in the range

($\varepsilon = 0.001$ to 0.01). When surface potentials exceeding the Debye-Hückel limit are necessary, for this regime, the above theory can only be used as a guideline for the calculation of stability windows.

This band window of stability which occurs with double layer repulsion represents the only case of stability to all wavelengths. In an infinite system ($R_2 \rightarrow \infty$ or $\varepsilon \rightarrow 1$) this stabilization is not possible: Although surface tension lowering can stabilize the circumferential tension at long waves (when $Q\ b_0 > 1$), $b_2 > b_0 > 0$ implies that the longitudinal tension is necessarily also negative ($Q\ b_2 > 1$), which leads to an unstable band for moderate wave numbers (cf. Figure 4). This behavior, however, both in the infinite case and in the finite case for weak or non-existent double layer repulsion can be advantageous for the emulsification of the fluids, i.e., to produce fluid droplets that have radii significantly smaller than R_1.

APPENDIX

The parameter b_2 from section 3.3 is given by

$$b_2 = \left[\frac{\Phi_r^0}{\Phi_I}\right]^2 \times$$

$$\left[\frac{\hat{\alpha}_1 K_1(k) + \hat{\alpha}_2 K_2(k) + \hat{\alpha}_3 K_3(k) + \hat{\alpha}_4 K_0(k) K_0(ka) + \hat{\beta}_0 K_0^2(ka) - \hat{\beta}_2 K_2(ka)}{8\, k (I_0(k) K_0(ka) - I_0(ka) K_0(k))^2}\right], \quad (A1)$$

where

$$\hat{\alpha}_1 = [\hat{\alpha}_{11} + (k^2 - 8) I_0(k) I_0(ka)] K_0(ka) + (k^2 - 8) I_0^2(ka) K_0(k), \quad (A2)$$

$$\hat{\alpha}_2 = 2\, k^2 I_0(ka) (I_0(ka) K_1(k) + K_0(ka) I_1(k)), \quad (A3)$$

$$\hat{\alpha}_3 = k^2 I_0(ka) (I_0(k) K_0(ka) - K_0(k) I_0(ka)), \quad (A4)$$

$$\hat{\alpha}_4 = ((8 - k^2) I_1(k) - I_3(k)) I_0(ka) + 2\, k^2 a^2 I_1(k) I_2(ka), \quad (A5)$$

$$\hat{\beta}_0 = (I_3(k) + I_1(k)) k^2 I_0(k) - (8 I_0(k) + 2\, k^2 I_2(k)) I_1(k), \quad (A6)$$

$$\hat{\beta}_2 = 2\, a^2 k^2 I_0(ka) (I_0(k) K_1(k) + K_0(k) I_1(k)), \quad (A7)$$

and

$$\hat{\alpha}_{11} = 2 (a^2 I_0(k) I_2(ka) - I_2(k) I_0(ka)). \quad (A8)$$

FIGURES

Figure 1: Schematic of the circular tube geometry detailing the electrolyte film and the dielectric core.

Figure 2: Dependence of the growth rate (ω_r) on the wave number (α) for capillary driven instability: (a) J dependence and the long wave expansion (b) m dependence and (c) ε dependence.

Figure 3: Comparison of the Lubrication result (3.1.5) and the exact numerical solution ($\varepsilon = 0.1, 0.2, 0.3, 0.4, 0.5$).

Figure 4: The k dependence of the neutral stability curves of Q against α for an infinite outer region containing a double layer.

Figure 5: The k dependence of infinite outer region growth rate curves (ω_r *vs.* α).

Figure 6: The ε dependence of the stability of an electrolyte film for $\Delta\Phi / \Phi_I = 0$:
(a)Neutral curves of type A for strong double layer repulsion ($\varepsilon = 0.1, 0.2, 0.3, 0.4$).
(b)Neutral curves of type B for weak double layer repulsion ($\varepsilon = 0.6, 0.7, 1.0$).
(c)Base state electrostatic potential profiles for different ε.
(d)Dependence of leading order terms in the expansion of $\mathcal{E}$ (3.2.5) as a function of ε.

Figure 7: Growth rate curves as a function of Q for double layer repulsion.

Figure 8: Stability of an electrolyte film in the presence of double layer attraction due to *volume* charge density:
(a)Type A neutral curves of double layer repulsion for $[\Delta\Phi / \Phi_I] < 1$.
(b)Type B neutral curves resulting from double layer attraction $[\Delta\Phi / \Phi_I] \geq 1$.
(c)Base state electrostatic potential profiles for incrementally larger values of $\Delta\Phi / \Phi_I$.

Figure 9: The acceleration of the growth rate in the presence of increasing double layer attraction at fixed Q.

Figure 10: Stability of an electrolyte film in the presence of double layer attraction due to *surface* charge density:
(a)The ε dependence of neutral curves for $\Delta\Phi / \Phi_I \neq 0$.
(b)Base state electrostatic potential profiles for different values of ε and $\Delta\Phi / \Phi_I \neq 0$.

Figure 11: Numerical example of complete stabilization (critical surface tension versus ε).

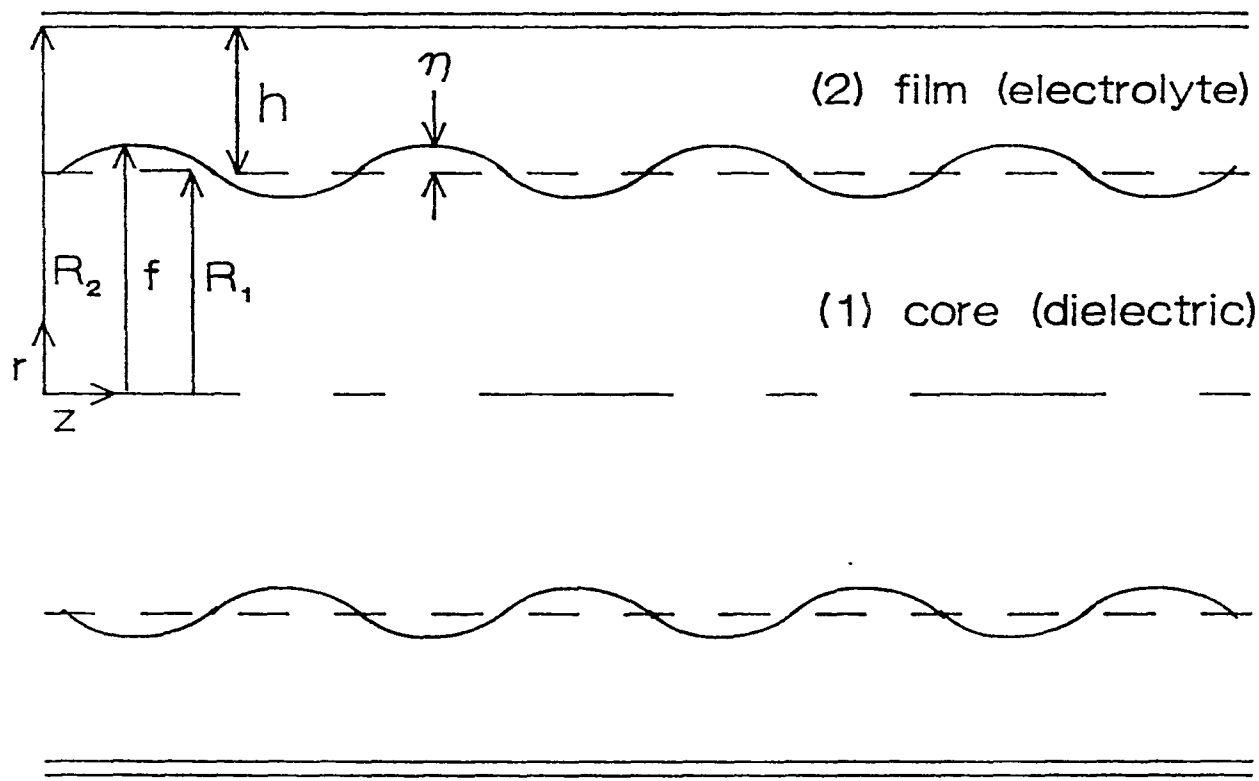

Figure 1

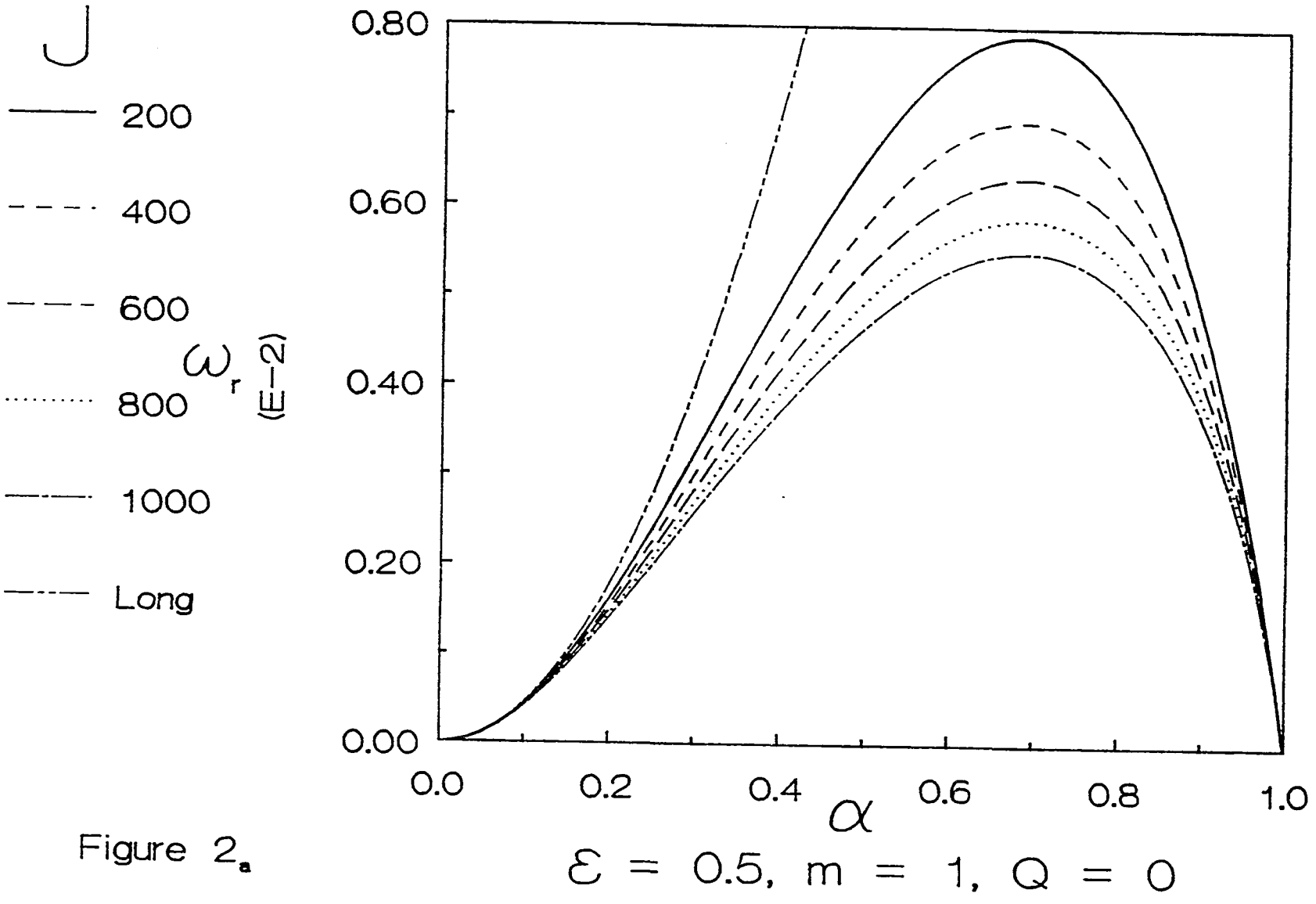
J
200
400
600
800
1000
Long
ω_r (E−2)
0.80
0.60
0.40
0.20
0.00
0.0
0.2
0.4
0.6
0.8
1.0
α
ε = 0.5, m = 1, Q = 0

Figure 2$_a$

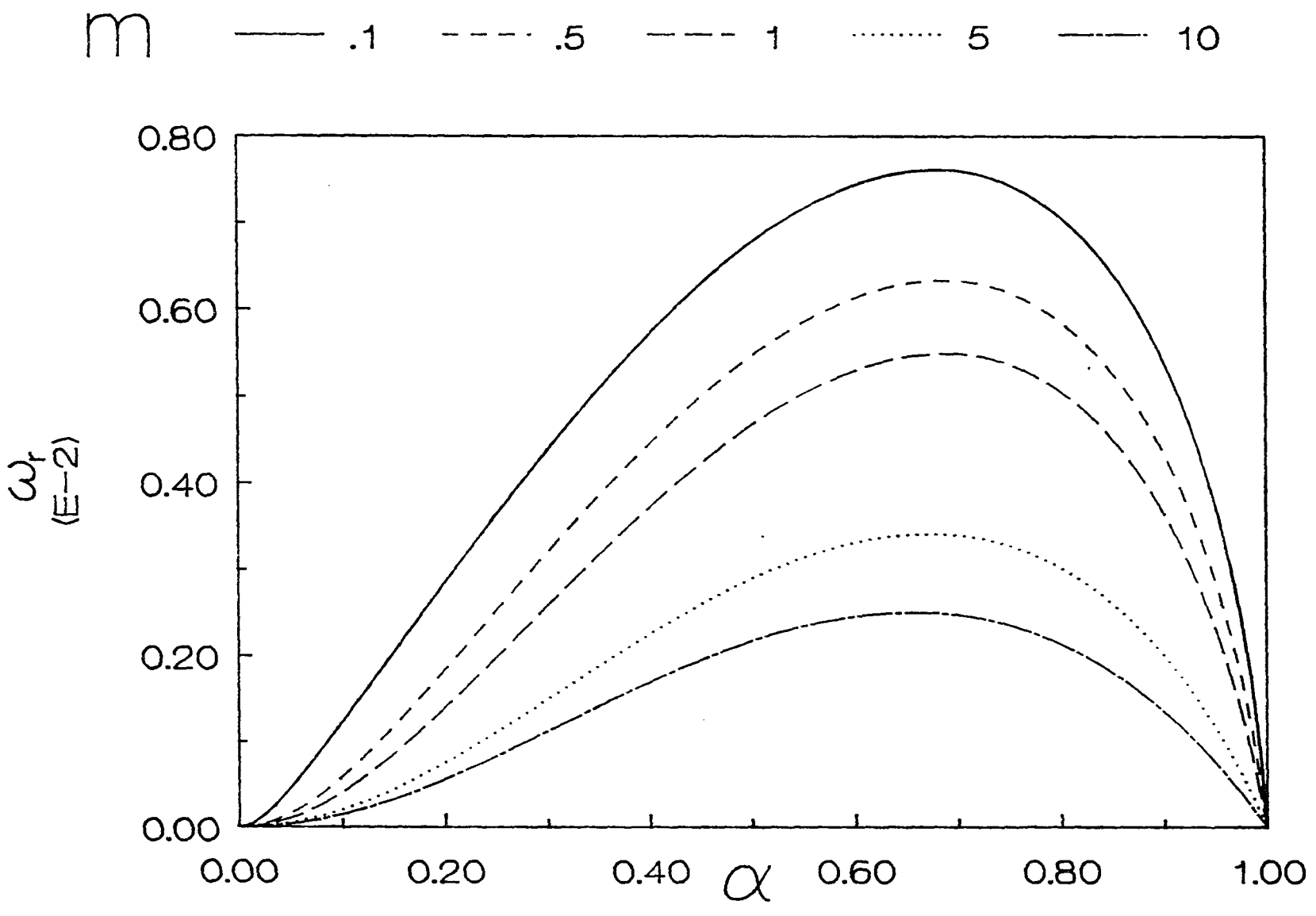

Figure 2_b $\varepsilon = 0.5,\ J = 1000,\ Q = 0$

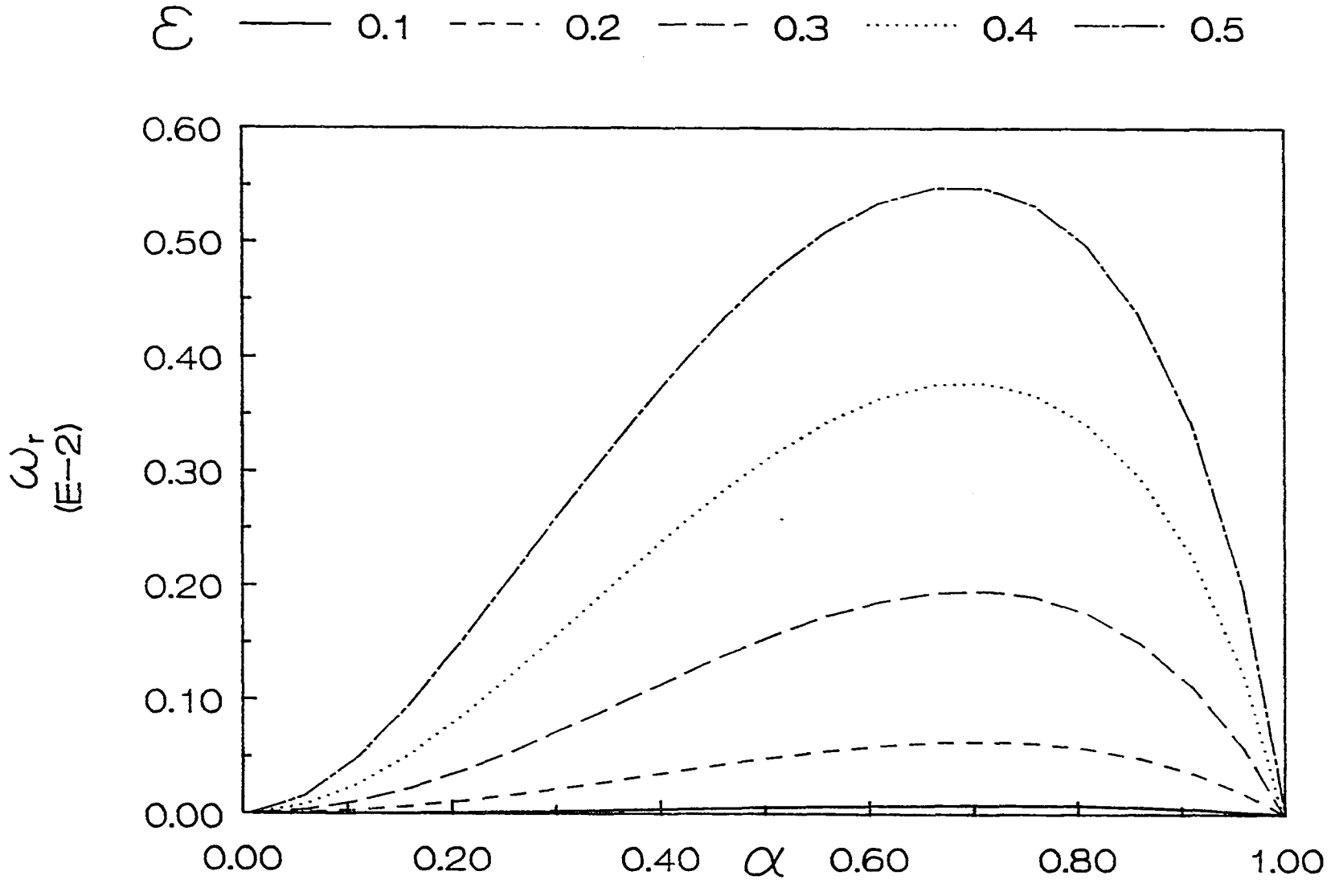

Figure 2_c J = 1000, m = 1, Q = 0

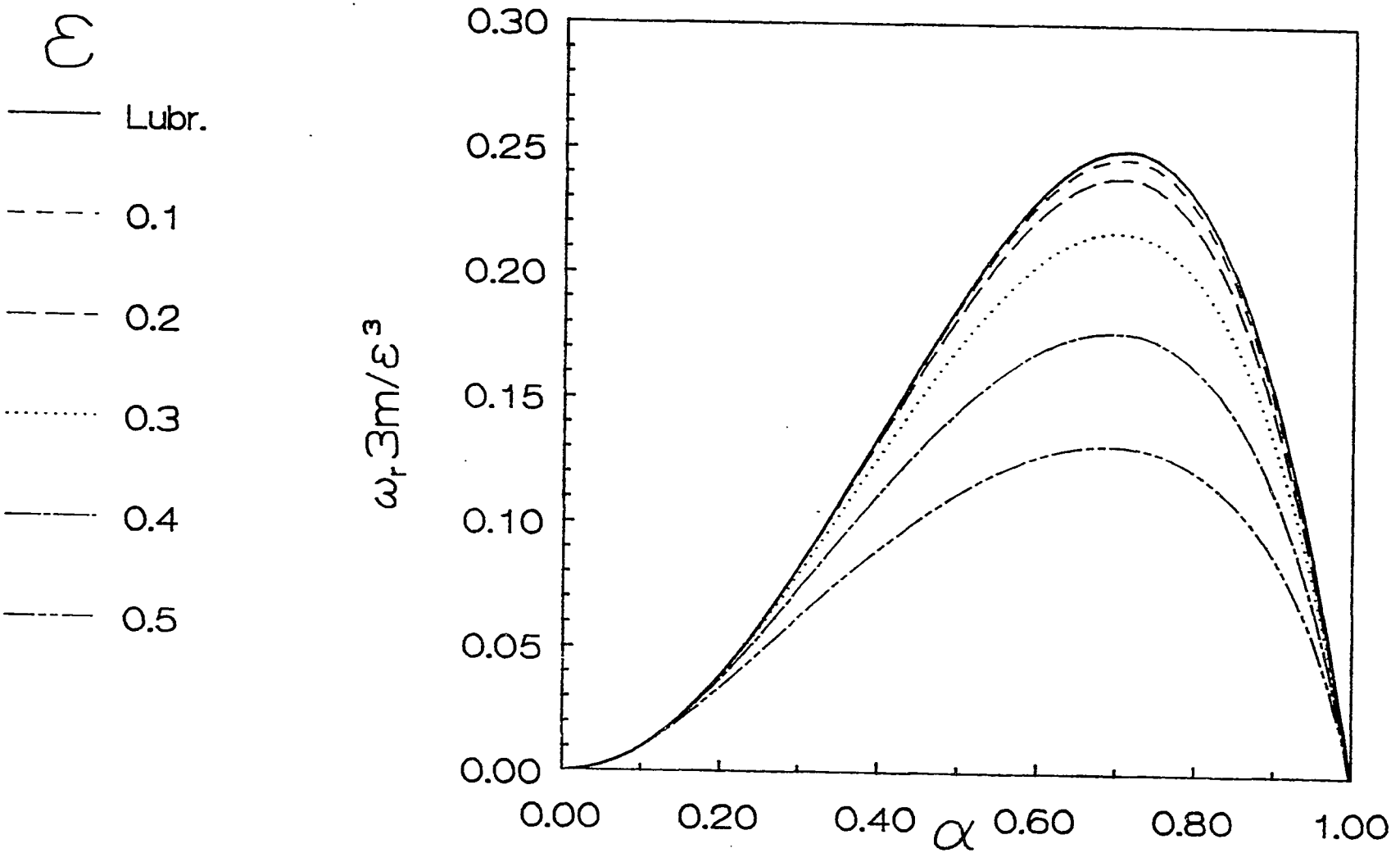
ε
Lubr.
0.1
0.2
0.3
0.4
0.5
$\omega_r 3m/\varepsilon^3$
0.30
0.25
0.20
0.15
0.10
0.05
0.00
0.00
0.20
0.40
α
0.60
0.80
1.00
J = 1000, m = 1, Q = 0

Figure 3

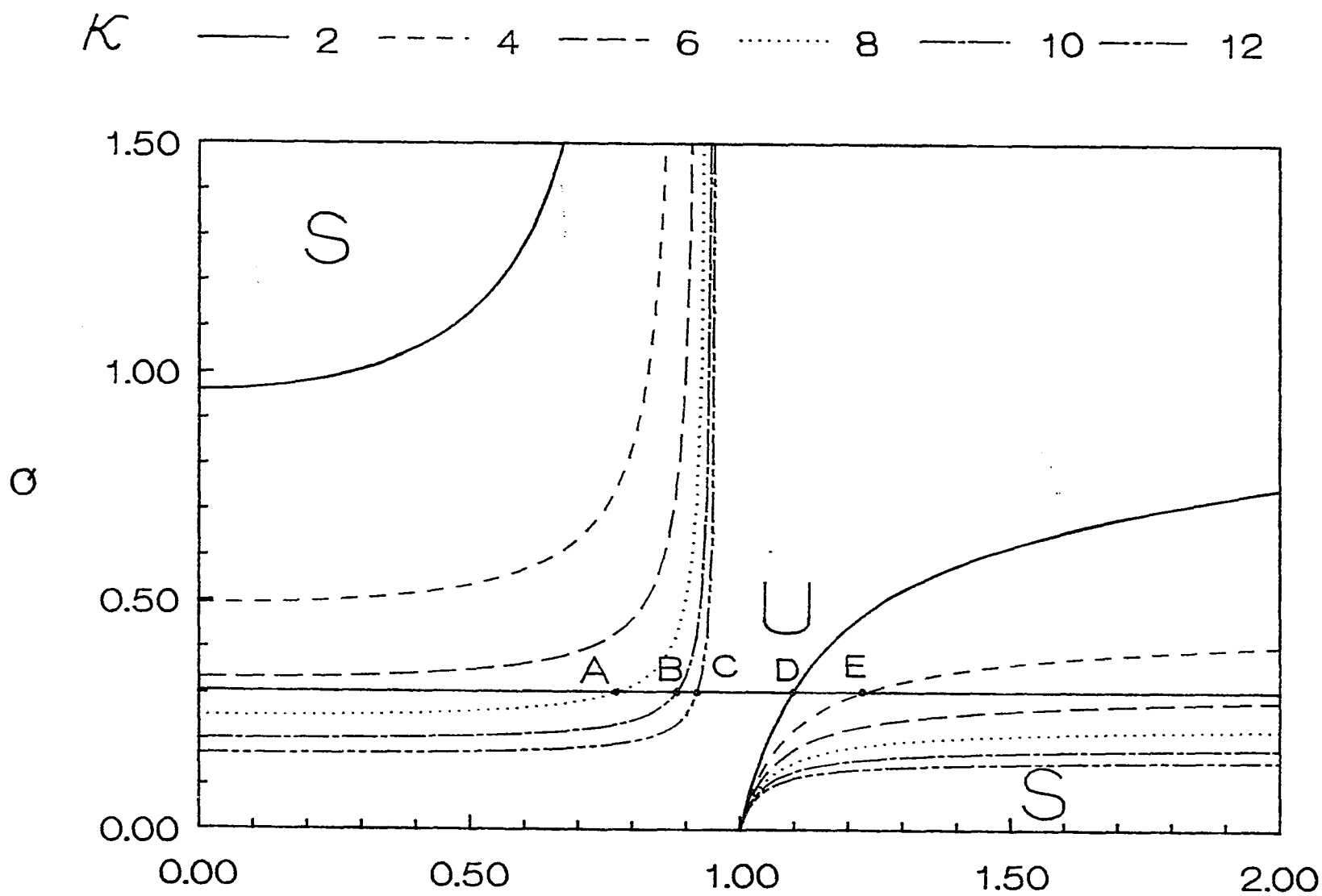

Figure 4

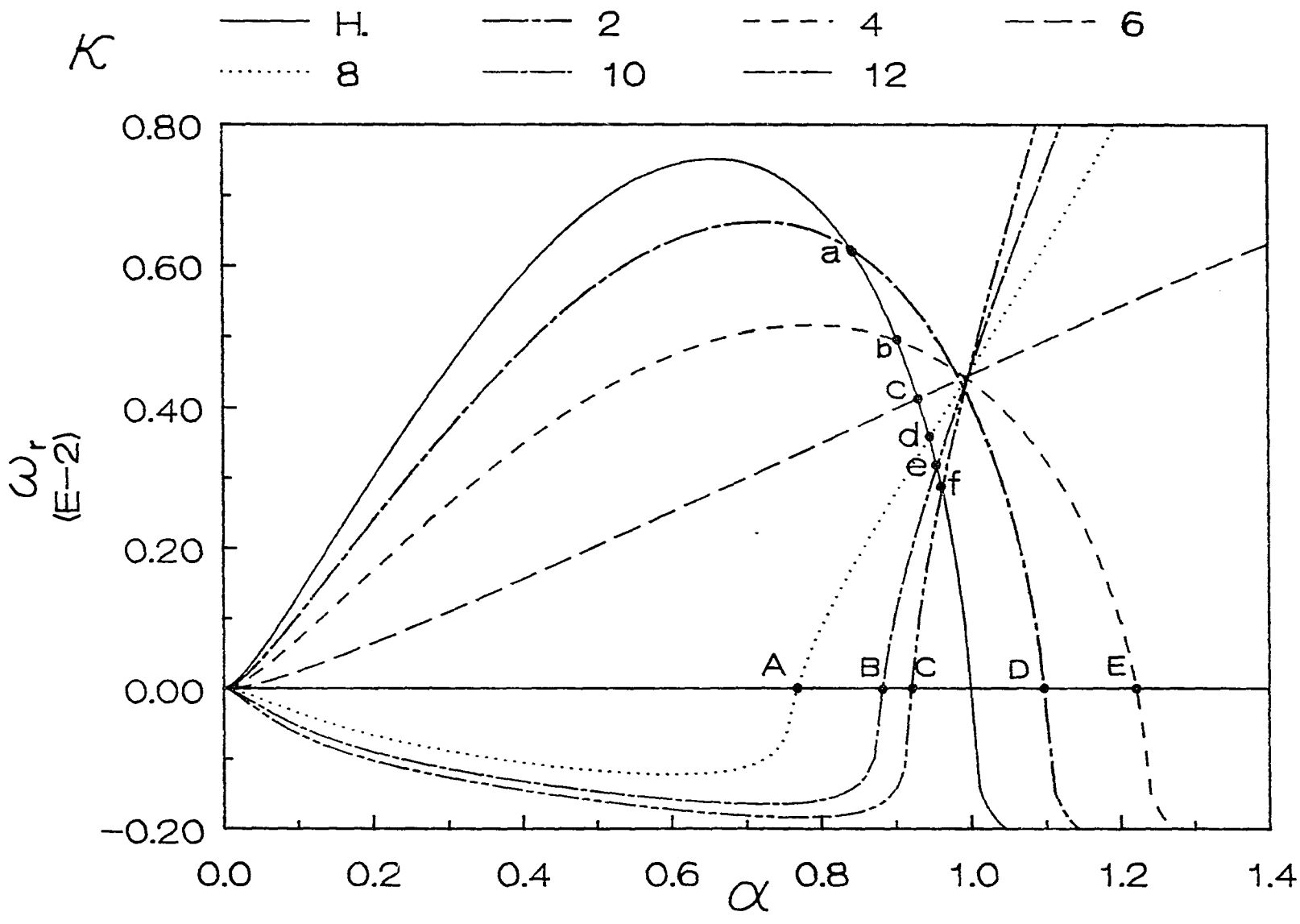

Figure 5 Q = 0.3, J = 1000, m = 1

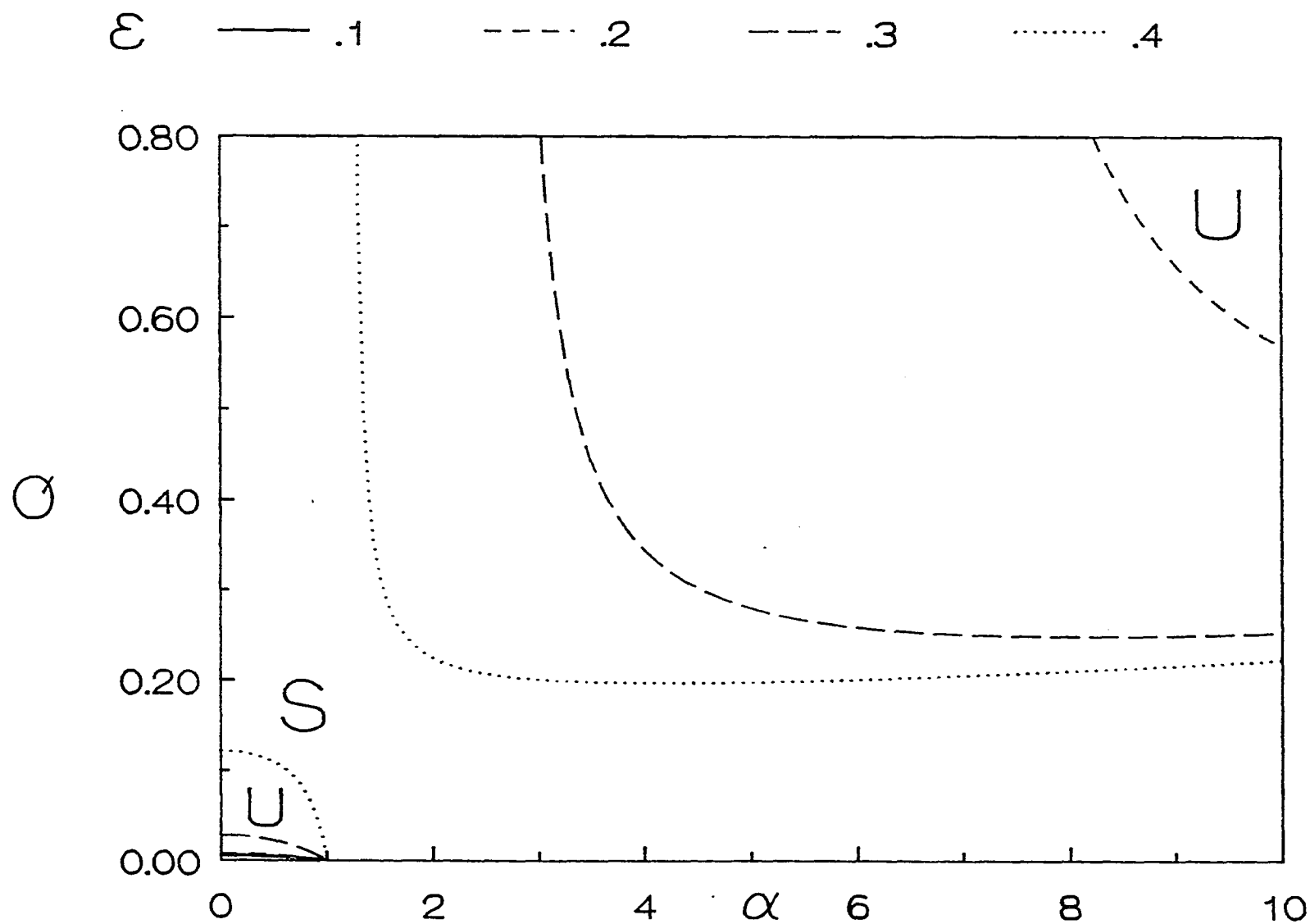

Figure 6_a $\kappa = 10,\ \Delta\Phi / \Phi_1 = 0$

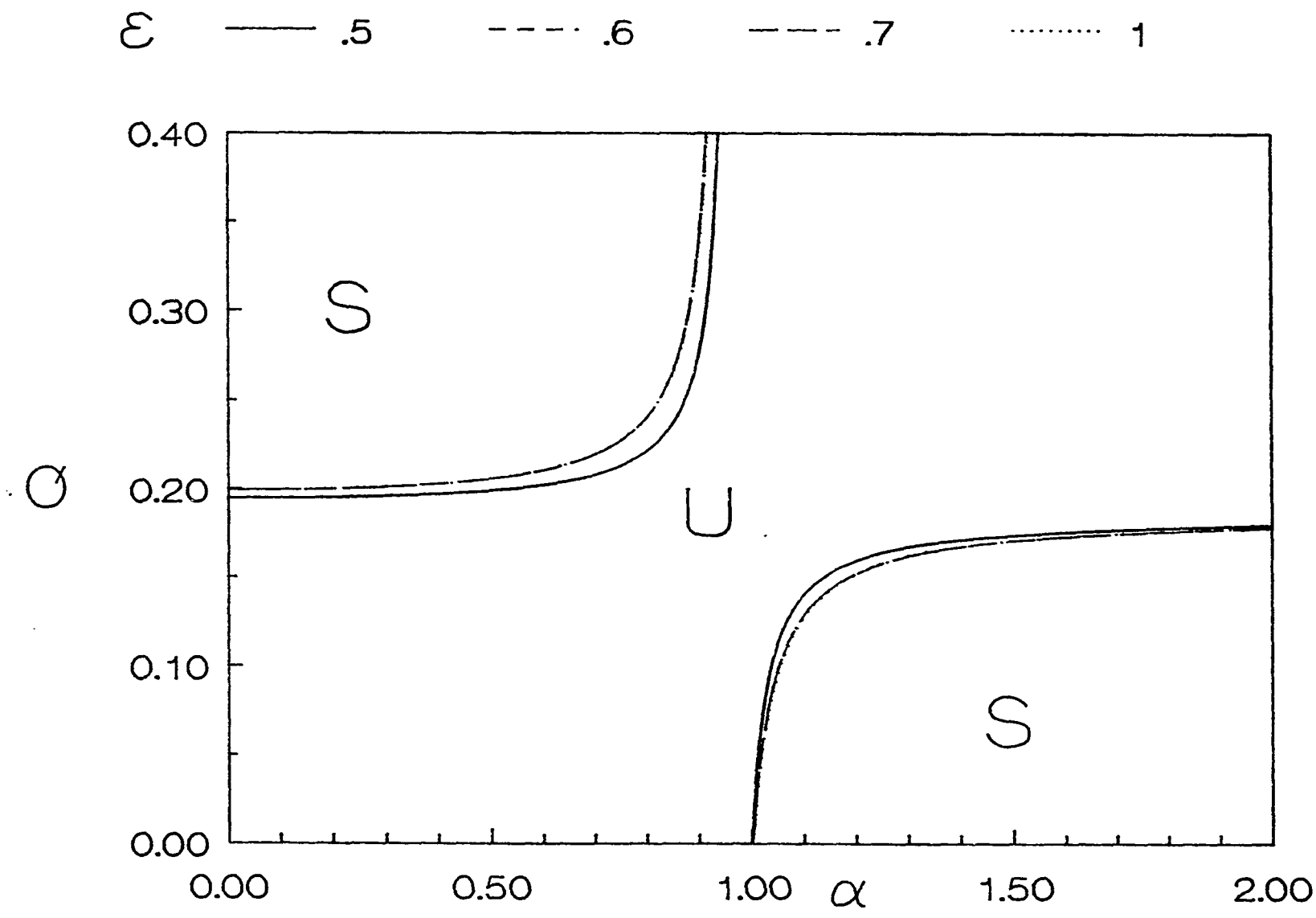

Figure 6_b $\kappa = 10,\ \Delta\Phi / \Phi_1 = 0$

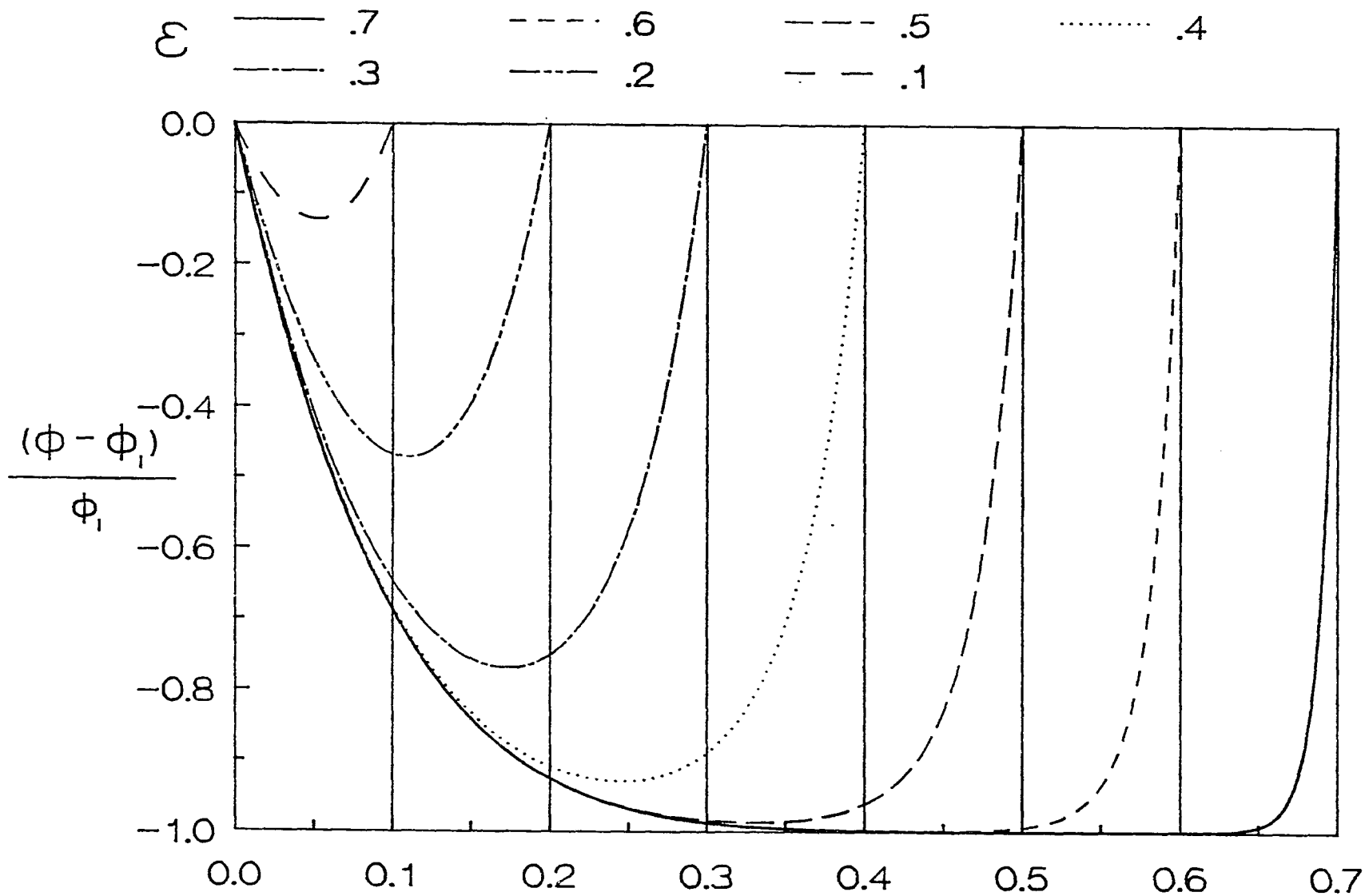

Figure 6_c $\kappa = 10,\ \Delta\Phi / \Phi_1 = 0$

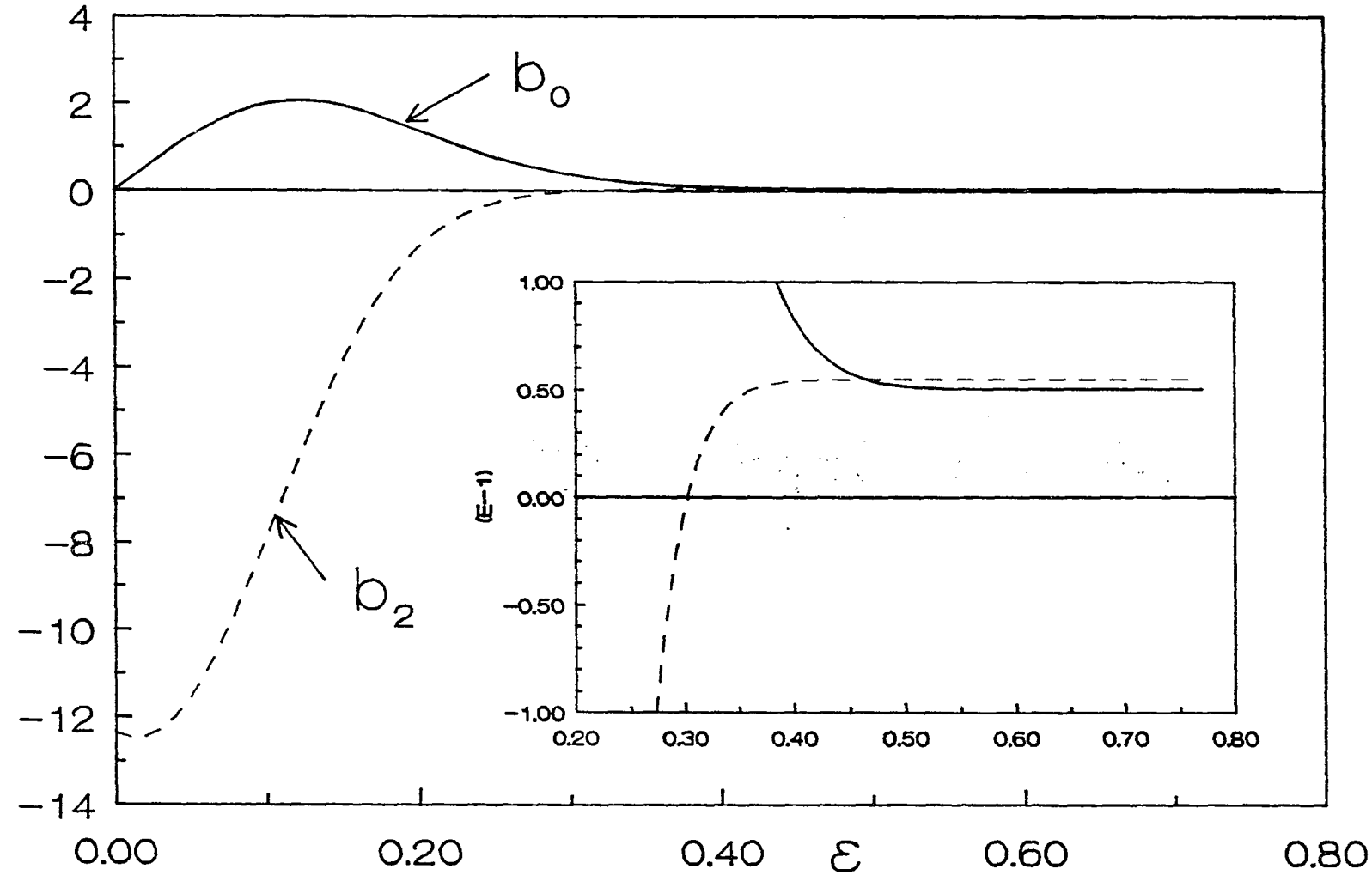

Figure 6_d $K=10,\ \Delta\Phi / \Phi_1 = 0$

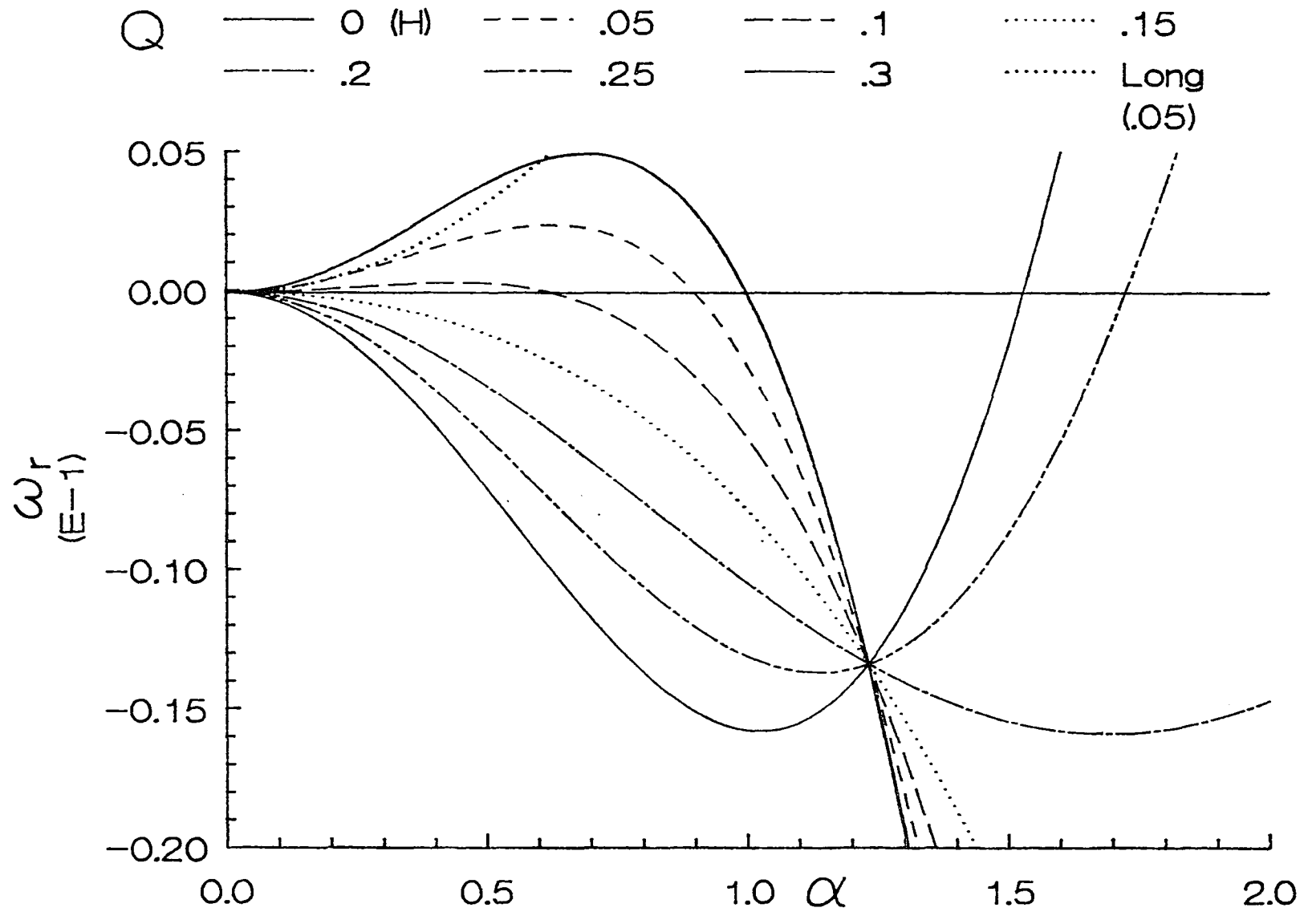

Figure 7 $\mathcal{E}=0.4$, $J=10$, $m=1$, $\mathcal{K}=10$, $\Delta\Phi/\Phi_1=0$

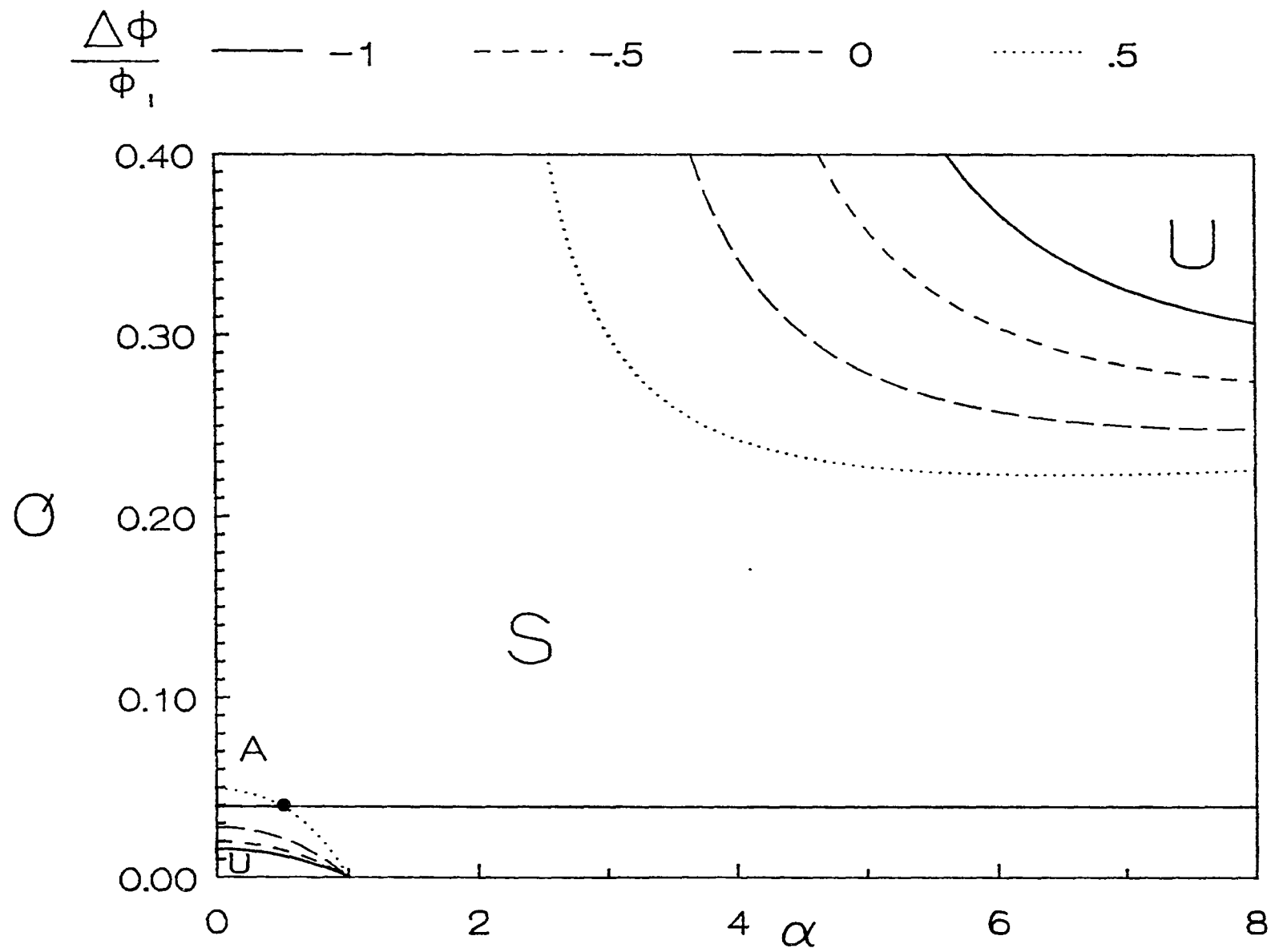

Figure 8_a $\kappa=10, \varepsilon=0.3$

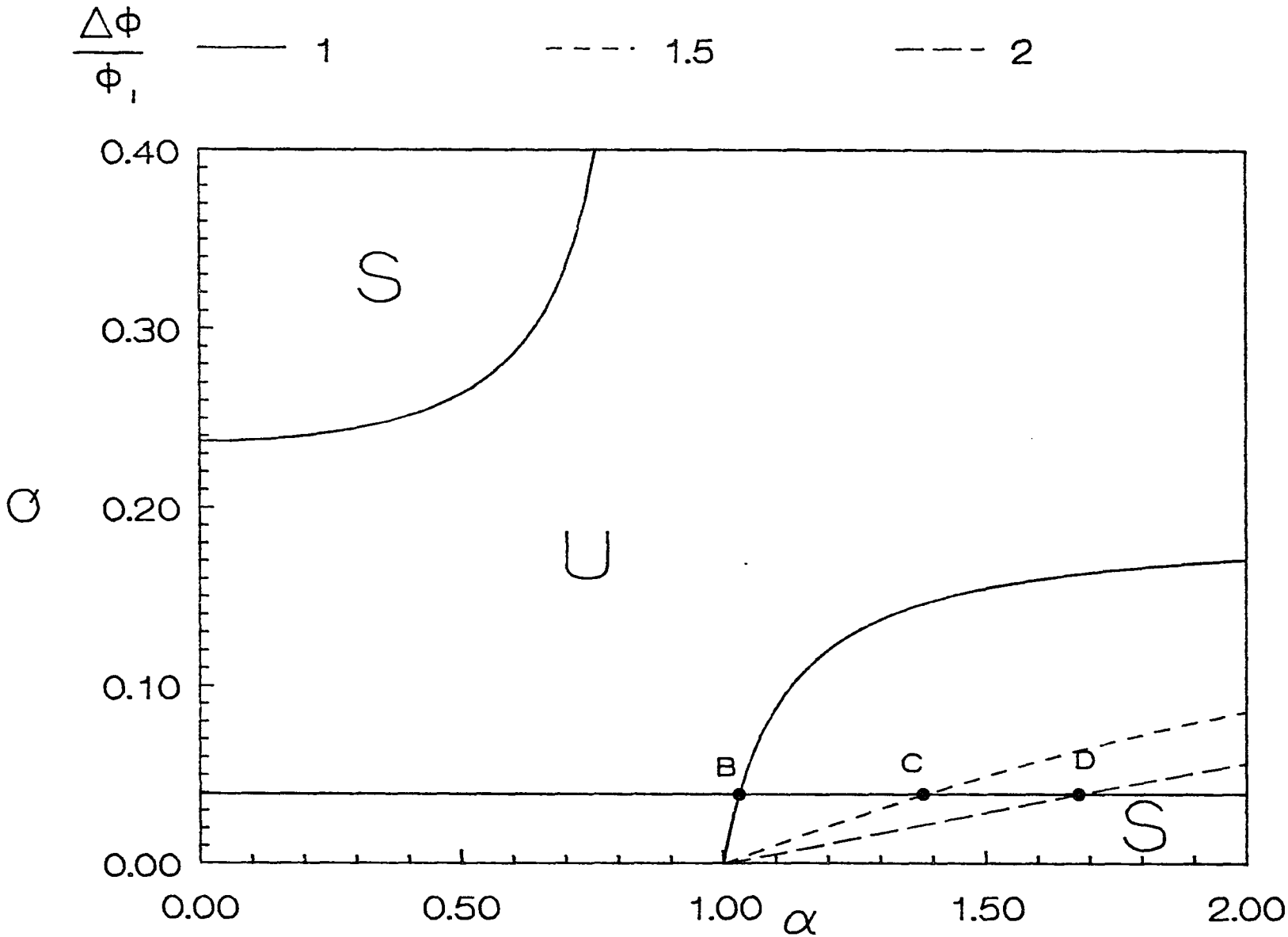

Figure 8_b $\kappa = 10, \quad \varepsilon = 0.3$

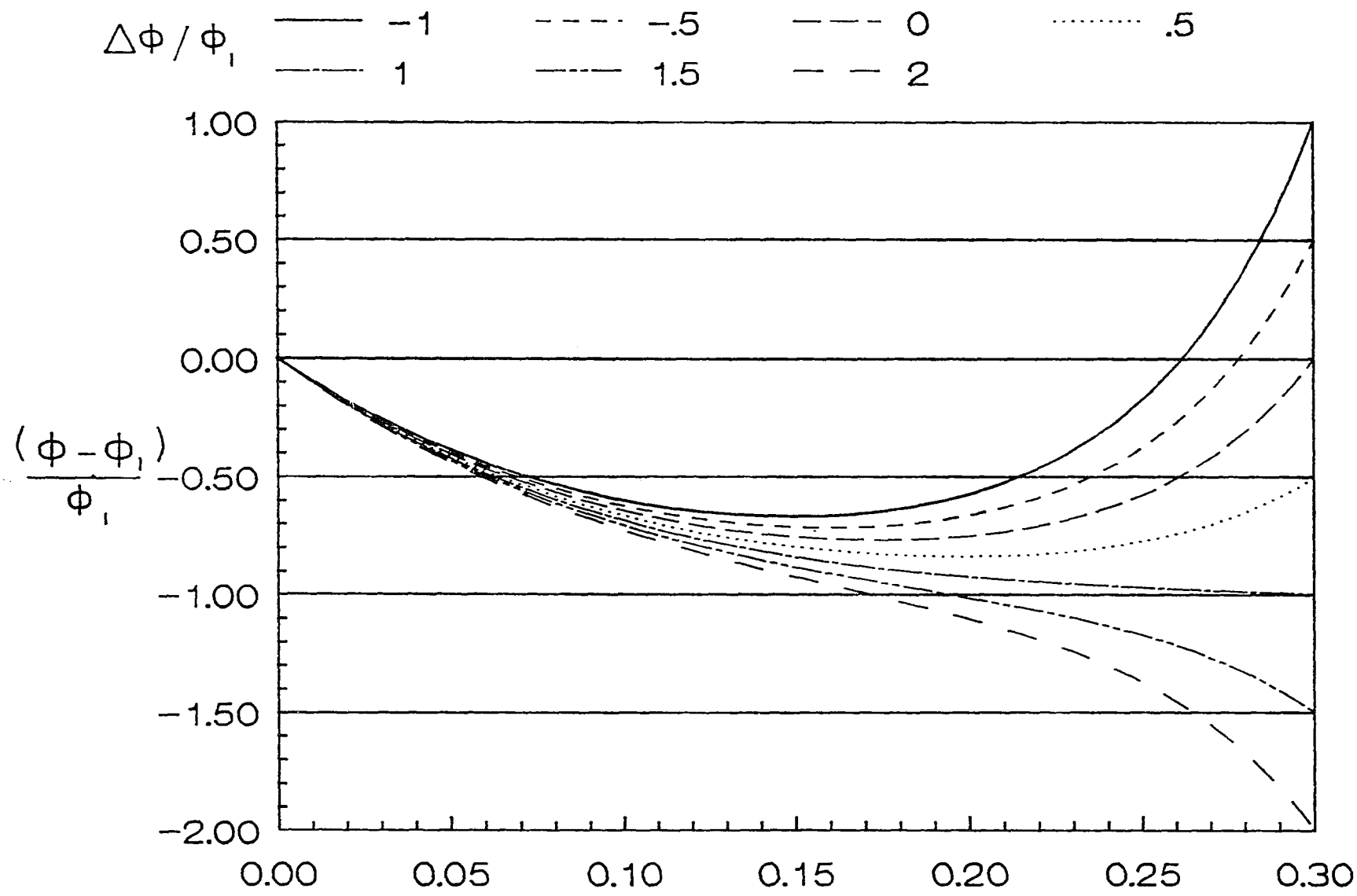

Figure 8c

$\kappa = 10, \quad \varepsilon = 0.3$

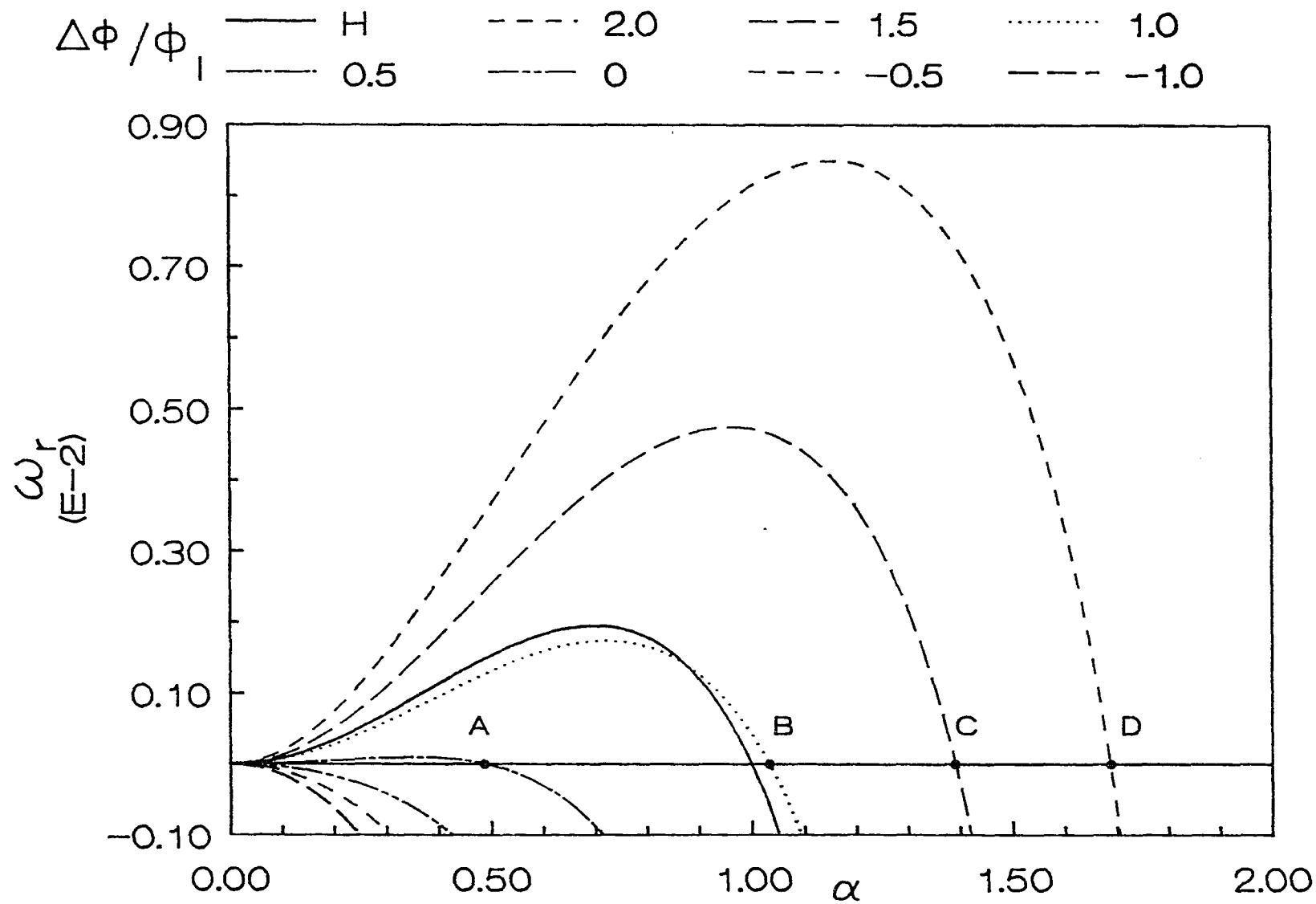

Figure 9 J=1000, m=1, Q=0.04, ε=0.3, κ=10

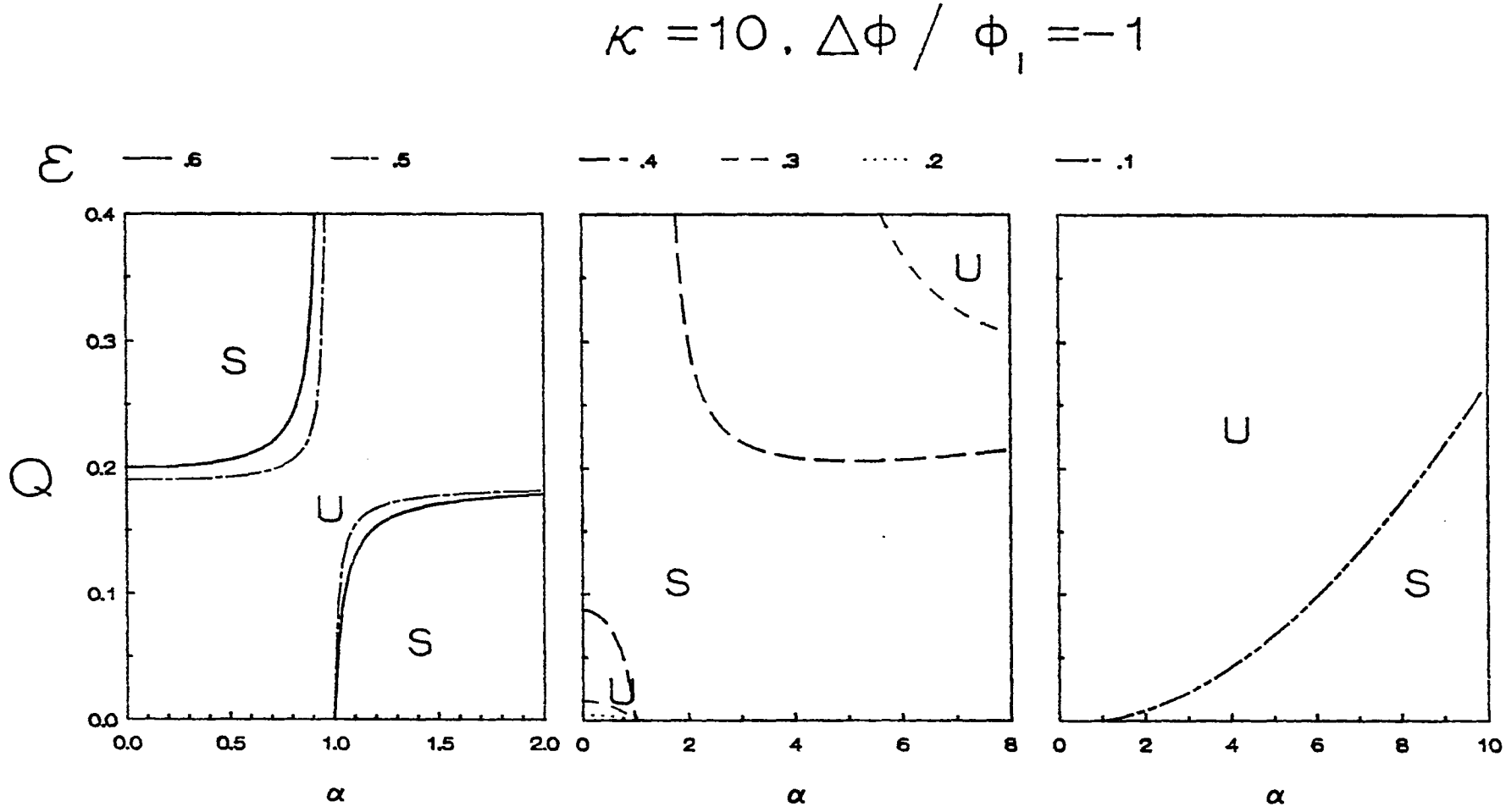
κ =10, Δφ / φ1 =−1
ε
.6
.5
.4
.3
.2
.1
Q
0.4
0.3
0.2
0.1
0.0
S
U
S
U
S
U
S
0.0
0.5
1.0
1.5
2.0
0
2
4
6
8
0
2
4
6
8
10
α
α
α

Figure 10_a

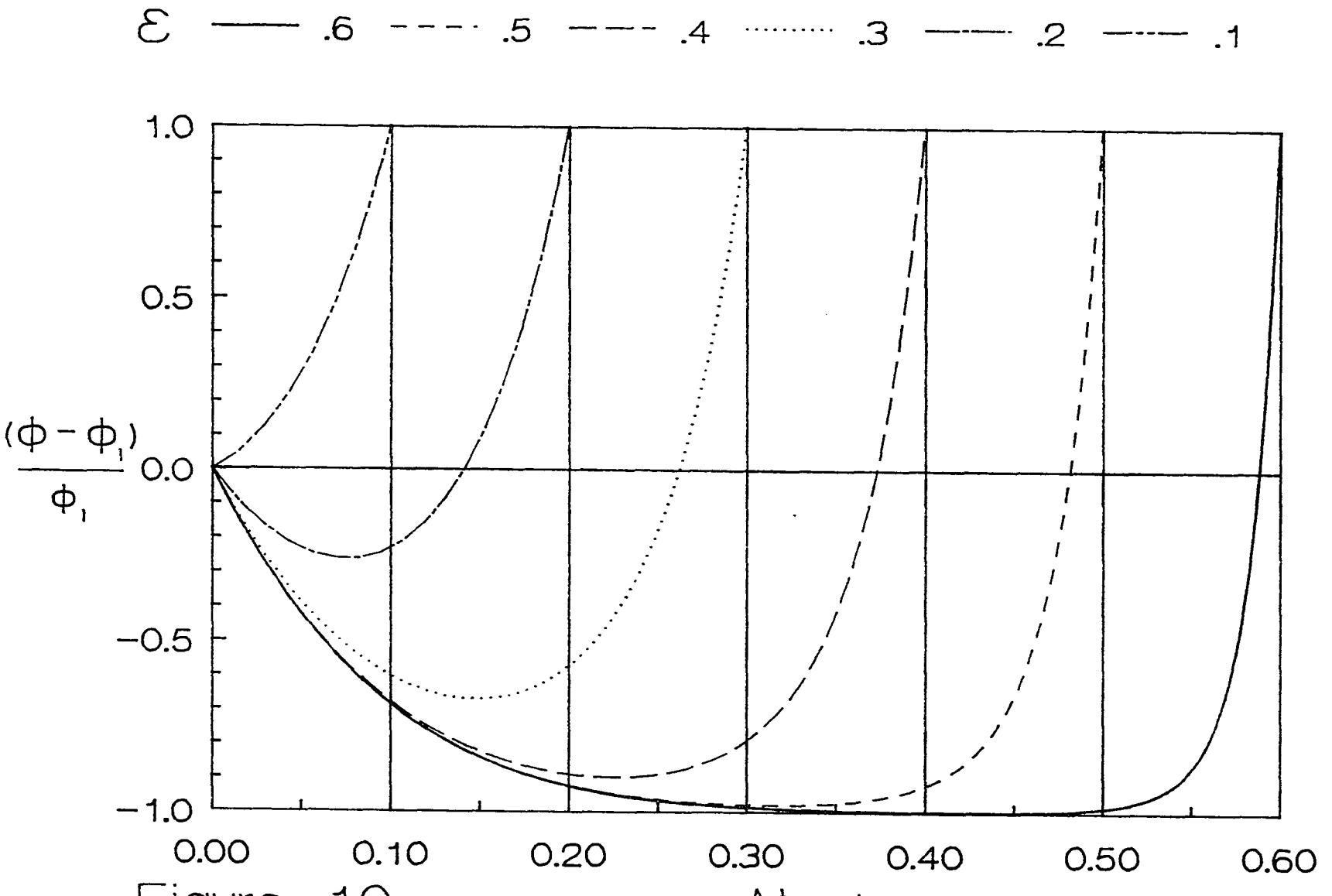

Figure 10_b $\kappa = 10$, $\Delta\Phi / \Phi_1 = -1$

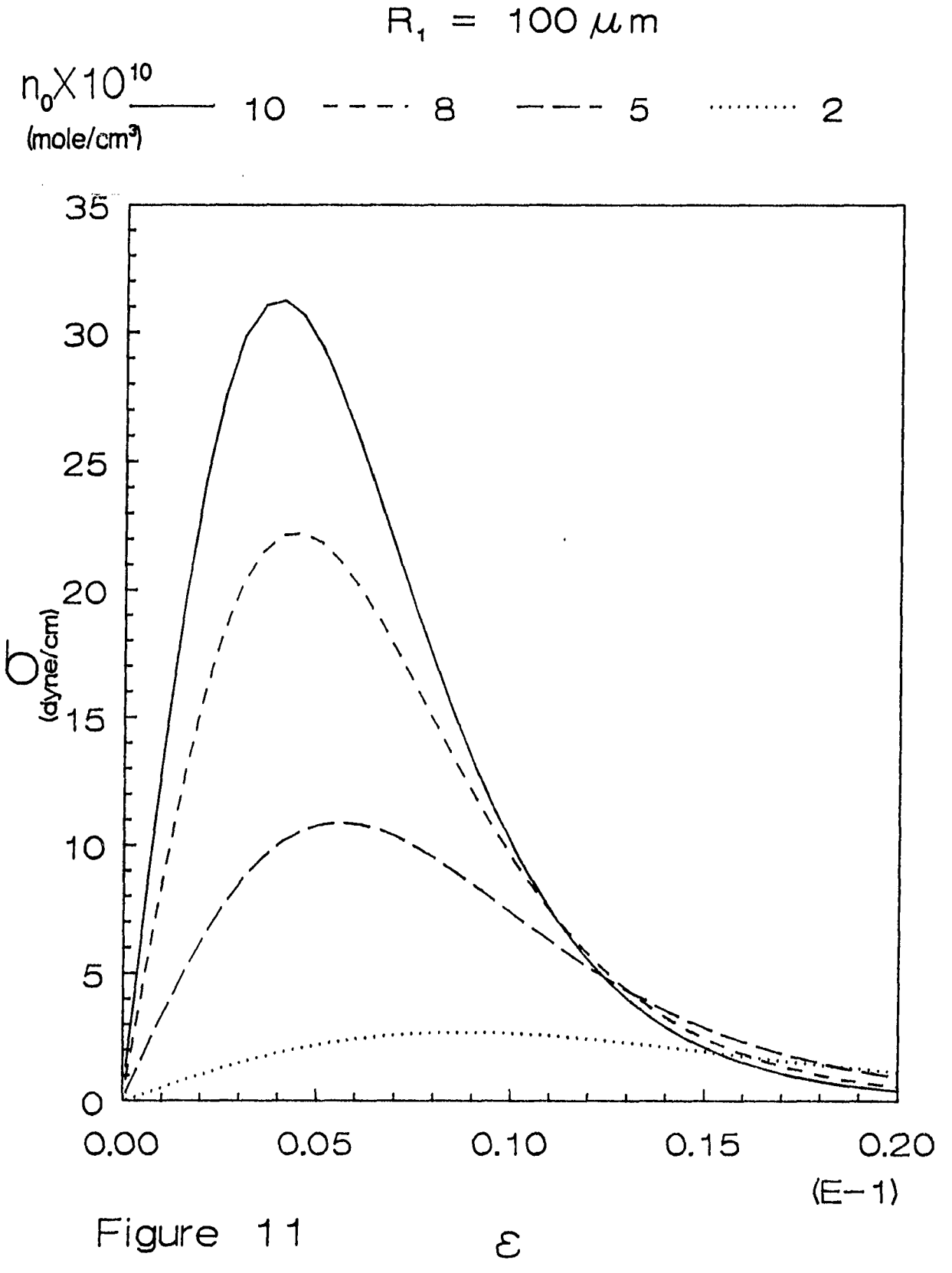
$R_1 = 100\,\mu m$
$n_0 X 10^{10}$ (mole/cm³)
10
8
5
2
35
30
25
20
15
10
5
0
σ (dyne/cm)
0.00
0.05
0.10
0.15
0.20
(E−1)
ε

Figure 11

IV An Asymptotic Theory for the Linear Stability of a Core Annular Flow in the Thin Annular Limit.

1 INTRODUCTION

To recover oil which is saturating capillary pores in a rock bed one can flush with a second, immiscible liquid, usually an aqueous solution of low interfacial tension with the oil. The type of flow pattern which develops as the aqueous phase displaces the saturating oil depends on the wetting properties of the oil and the aqueous solution. If the oil wets the pore wall more strongly than the aqueous phase, then the displacement takes the form of a winding train of long aqueous slugs separated by pools of oil and riding over a thin cushion of the oil. Alternatively, if the aqueous solution is more strongly wetting, then the fluids change places, and the displacement consists of slugs of oil moving over an aqueous film. In either case, the hydraulic resistance of rock pores is usually large enough that the train velocities are small, and the flow capillary numbers C_a (defined as the product of the slug centerline velocity U and the wetting layer viscosity divided by the interfacial tension) are usually much less than one. In addition, Reynolds numbers (defined as the product of the train velocity multiplied by the pore radius and divided by either the kinematic viscosity of the oil or the displacing phase) are commonly of order one or less. For these cases of small C_a and order one or less Reynolds numbers, the thickness of the wetting layer is set by the conditions at the leading edge of the slug, and is proportional, from the asymptotic theory of Bretherton (1961), to $C_a^{2/3}$.

In the central region of the slug, the flow locally resembles a core annular flow (CAF) with the nonwetting phase flowing centrally, and the wetting liquid moving in an annular ring. The interfacial stability of this CAF can significantly affect the

mobility of the train. Growing interfacial disturbances can cause the wetting layer to snap and bring the nonwetting fluid in contact with the capillary pore wall. If the respreading of the wetting layer is slow or inhibited, then contact line forces now attaching the slug to the wall can retard the movement of the slug and decrease the overall train mobility.

The aim of this paper is to study the linear stability of CAFs in an effort to better understand the mobility of the train flows which develop in displacing oil with aqueous solutions. A first step is to examine the linear stability of a perfect core annular flow (PCAF), which is a CAF in a precisely circular tube in which the core and annulus are exactly concentric with the tube wall. Joseph and collaborators in a series of articles (Joseph, Renardy and Renardy (1984), Preziosi, Chen and Joseph (1989), Hu and Joseph (1989), Hu, Lundgren and Joseph (1991), Chen, Bai and Joseph (1990) and Bai, Chen and Joseph (1991)) have used numerical and long wave techniques to establish a detailed picture of the linear stability of a PCAF mainly to axisymmetric disturbances. In this series, Chen, Bai and Joseph (CBJ) present the most general theoretical analysis. CBJ examine the stability of a PCAF to axisymmetric disturbances in a vertical tube driven by both gravity and a pressure gradient. Six dimensionless groups describe the neutral stability. These are (1) an aspect ratio a equal to the ratio of the inner radius R_2 of the tube to the undisturbed core radius R_1, (2) a viscosity stratification ratio m equal to the quotient of the annulus viscosity μ_2 to the core viscosity μ_1, (3) a density ratio l equal to the density of the annulus fluid ρ_2 divided by that of the core, ρ_1, (4) a Reynolds number based on a gravity driven flow ($R_g^2 = g\rho_1^2 R_1^3/\mu_1^2$), (5) a quotient F representing the ratio of a axial pressure gradient $\left(f = -\frac{dP}{dz}\right)$ to the force of gravity ($\rho_1 g$) ($F = f/\rho_1 g$), and (6) a parameter J describing the influence of the interfacial tension σ between the two phases ($J = \sigma R_1 \rho_1/\mu_1^2$).

The parameter F is a measure of the effect of pressure forcing on the flow direction in a vertical tube; for $l = 1$, when $F > -1$ the flow is downward, and when $F < -1$ pressure overcompensates for gravity and the flow is upward. When l is not equal to one, these demarcations are not strictly valid and mixed flow can occur. However, assuming that the density differences are not too great, when $F < -1$ the flow is predominantly up and when $F > -1$ the flow is predominantly down, and therefore in this paper we refer loosely to these ranges of F as "upflow" and "downflow". An extended discussion of the results of Joseph *et al.* follows in order to establish a background to which to compare our results.

We begin by discussing the case of density matched fluids ($l = 1$). For this case, the maximum base velocity V occurs at the centerline, and the stability analysis does not depend separately on R_g and F, but rather on these variables through the product

$$R_g^2 \frac{(1+F)(m+a^2-1)}{4m}$$

which defines a core Reynolds number R_e based on the centerline velocity ($R_e = \rho_1 R_1 V/\mu_1$). Preziosi, Chen & Joseph (1989) (PCJ) constructed neutral plots of R_e against the axial wavenumber α for fixed values of a, J and m. PCJ (and, for that matter, the entire series of Joseph articles) discuss only the case of $m < 1$ because of their interest in understanding the stability of CAFs structured when water is introduced to reduce the friction in the pipeline transport of heavy crude oil. In all of these plots, the $R_e = 0$ axis corresponds to the static capillarity interface of a cylindrical instability as studied by Plateau, Rayleigh (1879), Tomotika (1935) and Goren (1962). The circumferential component of the surface tension forces is destabilizing while the axial component is stabilizing. The competition is such that dimensional wavelengths

larger than $2\pi R_1$ ($\alpha < 1$) are unstable and those smaller are stable.

PCJ's neutral curves, computed for large J (~ 2000) are generically of two types, depending on the values of a and m . The first type occurs for intermediate values of m and thin annuli, and consists of two branches, one a lower curve extending from the capillary instability point (0,1) to an intersection point (R_{ec}, 0) on the ordinate, and a second upper branch parabola with a minimum in R_e denoted by R_u which is typically much larger than R_{ec} . The PCAF is unstable inside the lobe formed by the lower branch and above the parabola boundary of the upper branch. However, a window of global stability in R_e extends between the branches. The fact that an unstable lobe forms at finite but small R_e for $m < 1$ establishes the fact that the viscosity stratification in the base state shear flow stabilizes the capillary instability and shortens the band of unstable waves. At the critical value R_{ec} the stabilization for the longest waves is complete. Values of R_{ec} derive from the long wave limit $\alpha \rightarrow 0$ with J , R_e , m and a assumed to be of order one; for relatively large values of J (say 2000) and thin annuli ($1.0 < a < 1.2$), PCJ find that the values of R_{ec} vary between one and ten, while the minimum of the upper branch is equal to a few hundred.

When m approaches one from below or the film thickness is increased, R_{ec} increases, and the viscosity stratification becomes less effective in stabilizing the long wave capillary instability. At a critical value of m depending on a , the stability window in R_e is lost, and a new two- branch plot emerges. In this new plot, the capillary point (1,0) is the origin of a short wave branch in which R_e increases as α increases from one. A second branch begins at the ordinate (0, R_{ec}) and extends sharply to large values of R_e as α increases from zero. The PCAF is unstable in the space between the branches because of the destabilizing action of the circumferential component of the

surface tension. Viscosity stratification is only effective at high R_e in the narrow region between the ordinate and the upper branch, and the action of the axial component of the surface tension gives rise to the stable region beneath the lower branch.

Density differences between the core and annular fluids can also affect the stability, but only in a significant way when gravity is present and has a non-zero component acting along the flow direction. CBJ present the influence of a density difference superimposed upon capillarity and viscosity stratification in a vertical tube with $m = 0.5$. They present their data in the form of two types of neutral curves, R_g against α with $F = 0$ (free fall downflow), and F against α at fixed R_g (either downflow ($F > -1$) or upflow ($F < -1$)). As described above the free fall curve for the case $l = 1$ and a sufficiently thin annulus is the two branch window structure, with R_g^2 replacing R_e through the relation given above. As l increases from one, the R_g^2 axis intercept decreases and the unstable lobe becomes smaller. Thus in free fall downflow, density stratification stabilizes the PCAF when the heavier fluid is in the annulus. Placing the lighter fluid in the annulus is destabilizing, and CBJ demonstrate that as l decreases sufficiently (as determined by a) from one, the stability loci change into a plot resembling that of the second type in (R_e *vs* α) with no window of stability.

The effect of upflow uses the marginal plots of F against α for fixed R_g . Again, for $l = 1$ the curve derives from the (R_e *vs* α) plot rewriting R_e in terms of F and using the fixed values of m , a and R_g . Since the (R_e *vs* α) plot is reflectionally symmetric about the zero flow case of $R_e = 0$, the (F *vs* α) for equal densities is reflectionally symmetric about $F = -1$, which represents the point of zero flow for $l = 1$. The (F *vs* α) neutral curve for $l = 1$ is then a three branch structure with a hemispherical-like lobe and two parabolas referred to in CBJ as "positive- F" and "negative-F" upper branches. The regions within the lobe, above the "positive- F"

branch and below the "negative-F" branch are unstable while the connecting region is stable. Windows of global stability exist. As l becomes larger than one, the part of the hemispherical lobe corresponding to $F > -1$ (downflow) decreases indicating stabilization in downflow as before. However, the opposite part of the lobe which corresponds to upflow also decreases and so placing the heavier fluid in the annulus is destabilizing for upflow. Both (R_g *vs* α) and (F *vs* α) plots change into branch structures with no windows of global stability in R_g or F as the annulus thickness increases, and the impact of viscosity and density stratification decreases.

For reasons discussed above the series of Joseph's articles does not consider the case of a more viscous outer fluid ($m > 1$). However, one can anticipate some of its features for thin films. The analytical expressions given in PCJ and CBJ for the growth rate of long waves ($\alpha \to 0$) for J , F , R_g, m, l all of order one indicate that for $m > 1$ viscosity stratification, like capillarity, destabilize the longest waves. Hickox (1971) also obtained this long wave result for the more general case of nonaxisymmetric disturbances ($m > 1$). Because there is no long wave stabilization mechanism, we anticipate that the marginal plot of R_g will consist of a single branch beginning at (1,0) and extending for larger values of α and increasing values of R_g.

The objective of this study is to understand the stability of PCAFs with thin layers in order to draw conclusions on the ability of wetting layers around slugs to remain intact. The studies of Joseph and co-workers outlined above cannot directly apply to the thin layer problems considered here for three reasons. First, the layers are extremely thin; The nondimensional annular thickness $\varepsilon \equiv \frac{R_2 - R_1}{R_1} = a - 1$ can be of order 10^{-2} or smaller. Numerical calculations become extremely difficult in this limit because of the rapid variation of hydrodynamic variables in the wetting layer. Indeed Joseph *et al.* have undertaken studies only down to $\varepsilon = 0.1$. In addition, our thin film

theory, as indeed any analytic theory, facilitates assessment of the importance of competing effects as well as the influence of the pertinent parameters. Second, Joseph's work does not examine the case $m > 1$, which corresponds to the oil wetting case. Third, in the study of the stability of the wetting layer the computation of growth rates is essential in order to resolve how the time scale for the disturbance growth compares to the speed with which surface convection or dispersion moves the disturbance to the trailing edge of the slug.

To avoid numerical problems, we propose studying this thin annulus stability by constructing asymptotic solutions to the linear growth rate in the limit as $\varepsilon \to 0$ with the wavenumber α and the viscosity ratio m larger than ε. Since α is of order one, these asymptotic expressions describe dynamics for disturbances of the order of or larger than the core radius R_1, but not of the order of the annulus thickness. (Chen & Joseph (1990) point out that when ε is large or when $m = O(\varepsilon)$ and ε fairly small, the film's inertial becomes significant, and thus we require m to be asymptotically larger than ε.) In displacement problems, we have remarked that Reynolds numbers are of order one or smaller, and so we will take R_g and F to be of order one. Values of J for these problems are much larger than one since $J = \frac{R_e m}{C_a}$ and the capillary number is small, and we therefore take $J = O(1/\varepsilon)$. Other smaller scalings for J are also considered and we will show that they can be derived from the $J = O(1/\varepsilon)$ general expressions obtained by taking appropriate limits. Importantly, these other regimes are relevant to other CAF regimes such as lubricated pipelining where J is of order one or smaller in ε.

Once derived, we use the growth rate expansion in ε for the following purposes. First we show that the expansion, when used to construct neutral curves, can reproduce with exceptional accuracy the lower (order one) branches of the (R_g *vs* α)

and (F *vs* α) plots obtained numerically by Joseph *et al.* for ε as high as 0.2. Second, we construct neutral curves for the case of $m > 1$, not previously considered, and we detail growth rates for both $m > 1$ and $m < 1$. Third, using the Bretherton analysis in conjunction with our asymptotic expansion, we develop a theory for the stability of the wetting layer surrounding liquid slugs moving at low capillary numbers. Lastly, we briefly describe how the expansion can be incorporated into a weakly nonlinear theory of the interface's stability.

An outline of this study is as follows. In Sec. 2 we formulate the linear stability problem, and derive the exact governing equations in terms of nondimensional variables. In Sec. 3 we derive the long wave expansions for the exact problem and then for the asymptotic analysis. The long wave expansions anticipate the orderings that we use to construct the asymptotic expansions in Sec. 4. With these orderings in mind we use scaling arguments to set up asymptotic solutions in the film and in the core which, when matched, produce the linear stability dispersion equations for the first two orders in ε. In Sec. 5, 6 and 7 we discuss results and applications as described in the previous paragraph.

2 FORMULATION OF THE EXACT LINEAR STABILITY THEORY

Two immiscible, Newtonian, incompressible fluids are flowing in a perfect core-annular arrangement in a vertical pipe of inner radius R_2. The interface is given by $r = R_1$. A fluid of viscosity μ_1 and density ρ_1 occupies the core region $0 \le r \le R_1$. A second fluid with viscosity μ_2 and density ρ_2 occupies the film region $R_1 \le r \le R_2$. We use cylindrical polar coordinates (r, θ, z) with the z axis oriented in the direction of the gravitational acceleration $\mathbf{g}$ (see Fig. 1). Gravity and a uniform, constant pressure gra-

dient $-\frac{dP}{dz}=f$ drive the flow. The velocity field is unidirectional and depends only on r. Nondimensionalizing the velocity by the gravity scale $[\rho_1 g R_1^2/\mu_1]$ and the radial coordinate by the unperturbed core radius R_1, the base flow takes the following form

$$\mathbf{v}_i=[0,0,w_i^0(r)] \quad (i=1,2), \tag{2.1}$$

$$w_1^0(r)=\frac{F+1}{4}(1-r^2)+\frac{F+l}{4m}(a^2-1)+\frac{1-l}{2m}\ln a\,, 0\le r\le 1\,, \tag{2.2}$$

$$w_2^0(r)=\frac{F+l}{4m}(a^2-r^2)-\frac{1-l}{2m}\ln\left(\frac{r}{a}\right), \quad 1\le r\le a\,, \tag{2.3}$$

where subscripts 1 and 2 denotes the core and annular regions respectively. The non-dimensional parameters

$$F=\frac{f}{\rho_1 g}\quad,\quad m=\frac{\mu_2}{\mu_1},\quad l=\frac{\rho_2}{\rho_1},\quad \text{and}\quad a=\frac{R_2}{R_1}, \tag{2.4}$$

appear in (2.2) and (2.3) as a result of the nondimensionalization proposed above.

Consider axisymmetric disturbances of the interface $r(z,t)=S(z,t)$ which cause velocity disturbances to the core and annular base flows. All equations that follow are in nondimensional form with radial and axial variables nondimensionalized by R_1, velocities by $[\rho_1 g R_1^2/\mu_1]$ time by $[\mu_1/\rho_1 g R_1]$ and pressure by $[\rho_1^3 g^2 R_1^4/\mu_1^2]$. Since the fluids are incompressible, introduction of a disturbance stream function Ψ

$$u_i=\frac{1}{r}\frac{\partial\Psi_i}{\partial z}\quad\text{and}\quad w_i=-\frac{1}{r}\frac{\partial\Psi_i}{\partial r}, \tag{2.5}$$

automatically satisfies the continuity equation for the velocity disturbance.

The surface and the velocity disturbances can be ordered with a small parameter δ :

$$r(z,t) = 1 + \eta(z,t)\,\delta + O\,(\delta^2), \tag{2.6}$$

$$\Psi_i(\mathbf{r}) = \Psi_i^0(r) + \Psi_i^1(\mathbf{r})\,\delta + O(\delta^2). \tag{2.7}$$

We then insert these expansions into the Navier-Stokes equations and kinematic and stress boundary conditions at the fluid interface. Decomposition of the resulting equations into normal modes

$$\Psi_i^1(\mathbf{r}) = \psi_i(r) \quad \exp\,[\mathbf{i}\,\alpha\,(z - c\,t)], \tag{2.8}$$

and retention of only order δ terms define the following linear stability problem

$$D\,(D\,\psi_1) = \mathbf{i}\alpha R_g^2 (w_1^0 - c) D\,\psi_1\,, \tag{2.9}$$

and

$$D\,(D\,\psi_2) = \mathbf{i}\alpha R_g^2 \frac{l}{m}\left[\,(w_2^0 - c) D\,\psi_2 + \left(\frac{1}{r} w_{2_r}^0 - w_{2_{rr}}^0\right)\psi_2\right], \tag{2.10}$$

where

$$D \equiv \frac{d^2}{dr^2} - \frac{1}{r}\frac{d}{dr} - \alpha^2,$$

α is the wave number, c is the wave speed and w_i^0 is the nondimensional base velocity in region i , subject to

$$\frac{\psi_2}{r} = 0 \qquad \text{and} \qquad \frac{1}{r}\frac{d\psi_2}{dr} = 0 \qquad \text{at} \quad r = a, \tag{2.11}$$

$$\frac{\psi_1}{r} < \infty \qquad \text{and} \qquad \frac{1}{r}\frac{d\psi_1}{dr} < \infty \qquad \text{at} \quad r = 0, \tag{2.12}$$

$$\frac{1}{r}(\psi_1 - \psi_2) = 0, \qquad \text{at} \quad r = 1, \tag{2.13}$$

$$\frac{1}{r}\left(\frac{d\psi_1}{dr} - \frac{d\psi_2}{dr}\right) + \left(w_{1_r}^0 - w_{2_r}^0\right)\eta = 0, \qquad \text{at} \quad r = 1, \tag{2.14}$$

$$[D\,\psi_1 + 2\,\alpha^2\,\psi_1] - m\;\;[D\,\psi_2 + 2\,\alpha^2\,\psi_2] + r\left(w_{1_{rr}}^0 - m\;w_{2_{rr}}^0\right)\eta = 0, \quad \text{at} \quad r = 1, \tag{2.15}$$

$$\frac{m}{\mathbf{i}\alpha r}\frac{d}{dr}[D\psi_2]+2m\,\alpha\mathbf{i}\frac{d}{dr}\left[\frac{1}{r}\psi_2\right]-\frac{1}{\mathbf{i}\alpha r}\frac{d}{dr}[D\psi_1]-2\alpha\mathbf{i}\frac{d}{dr}\left[\frac{1}{r}\psi_1\right]-\frac{J}{R_g^2}[\alpha^2-1]\eta$$

$$+\frac{R_g^2}{r}\left[(w_1^0-c)\left(\frac{d\psi_1}{dr}-l\frac{d\psi_2}{dr}\right)+\left(l\,w_{2_r}^0-w_{1_r}^0\right)\psi_1\right]=0,\quad \text{at}\quad r=1, \tag{2.16}$$

and

$$\eta=\frac{1}{r}\frac{\psi_1}{(w_1^0-c)}\qquad \text{at}\quad r=1\,. \tag{2.17}$$

The dimensionless parameters

$$R_g=\left[\frac{g\rho_1^2R_1^3}{\mu_1^2}\right]^{1/2},\quad J=\frac{\sigma R_1\rho_1}{\mu_1^2},\quad \text{and}\quad J^*=J\,a, \tag{2.18}$$

appear in (2.9) through (2.17) as a result of the nondimensionalization proposed above. R_g^2 is the Reynolds number due to gravity and J is a surface tension parameter introduced by Chandrasekhar (1961) in his study of the capillary instability of jets of a viscous liquid in air. J^* is shown so all of the notation is consistent with CBJ.

3 LONG WAVE EXPANSIONS

We now turn to the stability problem for the longest waves and for thin films. Our aim is to see the ε-dependence of the various effects and to anticipate the scalings for our more general asymptotic theory. Consider the stability problem for waves which are long with respect to the undisturbed core radius R_1. Using Yih's (1967) method, one introduces a regular expansion in α for the stream function ψ_i and the wave speed c :

$$c=c^{[0]}+c^{[1]}\,\alpha+O(\alpha^2)\,, \tag{3.1}$$

and

$$\psi_i=\psi_i^{[0]}+\psi_i^{[1]}\,\alpha+O(\alpha^2)\,. \tag{3.2}$$

These expansions assume ε to be an order one quantity in α, and are thus *exact* long wave expansions. Hickox (1971), Joseph and co-workers and Smith (1989) (for the

case $m = 1$) have computed $c^{[0]}$ and $c^{[1]}$ for ε of order one. We consider here the behavior as $\varepsilon \to 0$.

Substituting the above expansions into the governing equations and boundary conditions we find that $c^{[0]}$ is real and therefore does not contribute to the stability, but only to dispersion that makes waves move with a velocity different from the base velocity at the interface:

$$c^{[0]} - w_1^0(1) = \frac{((1+\varepsilon)^2 - 1)^2}{4m\,((1+\varepsilon)^4 + m - 1)}(F+1)(m-1)$$

$$- \frac{2\,((1+\varepsilon)^4 + m - 1)\ln(1+\varepsilon) - ((1+\varepsilon)^2 - 1)(m + 2(1+\varepsilon)^2 - 2)}{4m\,((1+\varepsilon)^4 + m - 1)}(l-1), \quad (3.3)$$

To the next order in α, we find $c^{[1]}$ to be pure imaginary; so it does contribute to the stability:

$$c^{[1]} = \left[\frac{J}{R_g^2} f_1(\varepsilon, m) + R_g^2 f_2(\varepsilon, m, l, F)\right]\mathbf{i}, \quad (3.4)$$

where f_1 and f_2 are lengthy algebraic expressions detailed in the appendix to CBJ.

We study the linear stability for the long waves in the limit of small film thickness ($\varepsilon \to 0$) by Taylor expanding (3.4) in powers of ε:

$$c^{[1]} = \frac{J}{R_g^2}\left[\frac{\varepsilon^3}{3m} - \frac{\varepsilon^4}{m^2}\right]\mathbf{i}$$

$$+ R_g^2 \frac{F+1}{4}\left[(m-1)\left(\frac{(F+1)}{48m^2}\varepsilon^2 - \frac{(F+1)(m+8)}{48m^3}\varepsilon^3\right) - \frac{(l-1)}{24m^2}\varepsilon^3\right]\mathbf{i}. \quad (3.5)$$

The first square bracketed term on the right hand side of (3.5) represents the destabilizing effect of the circumferential curvature; the stabilizing effect of the longitudinal curvature enters at a higher order in α. The second square bracketed term represents the contribution of viscosity and density stratification. Eq. (3.5) indicates that viscosity stratification has a stabilizing effect when $m < 1$ for both down-flow ($F > -1$) and

up-flow ($F < -1$) and a destabilizing effect when $m > 1$. On the other hand density stratification has a stabilizing effect for down-flow and a destabilizing effect for up-flow when $l > 1$ and the opposite when $l < 1$. From (3.5) we draw four important conclusions concerning the effects of capillarity, and viscosity and density stratifications for long waves on thin films. First, for R_g^2 of order one in ε, the destabilizing effect of capillarity can only compete with the stabilizing effect of viscosity stratification ($m < 1$) when J is of order $1/\varepsilon$. Second, the influence of density differences is one order in ε higher than viscosity stratification. Third, when the fluids are viscosity matched, competition between stabilizing density stratification occurs for $J = O(1)$. Lastly, we note that the expansion (3.5) is nonuniform in m as $m \to 0$. The region of nonuniformity appears to be of order ε because it is at this order of m that the ε^2 and ε^3 terms become comparable. Below we extend these observations for small α to a theory valid up to order one in α.

As mentioned in the introduction neutral curves of R_g against α intersect the ordinate at a single point. This point derives implicitly from (3.4) by setting $c^{[1]} = 0$ and is given by

$$R_{gc}^4 = \frac{J f_1(\varepsilon, m)}{f_2(\varepsilon, m, l, F)}. \tag{3.6}$$

This value is a critical Reynolds number since on the $\alpha = 0$ axis, the longest waves are stable for $R_g > R_{gc}$ and are unstable for $R_g < R_{gc}$. This region of global stability typically starts either at R_{gc} or at a value of R_g close to R_{gc}.

Expanding R_{gc}^4 in (3.6) in powers of ε gives us our first opportunity to evaluate how well an asymptotic expansion in ε reflects the exact stability picture as $\varepsilon \to 0$. As such, Figure 2a compares the exact solution to (3.6) with the order ε^2 and ε^3

approximations to it as a function of m for $\varepsilon = 0.1$, $l = 1$ and $J^* = 2000$. It is clear from Figure 2a that the order ε^3 expression is a significant improvement over the order ε^2 expression. Figure 2b compares the agreement for different values of ε. It demonstrates that for fixed ε the agreement begins to break down for m of order ε; this is consistent with the fact that the region of nonuniformity in m of (3.5) is of order ε. As ε increases not only does the applicable range of m decrease, but also the accuracy of the ε^3 approximation decreases.

4 ASYMPTOTIC EXPANSIONS

In this section we derive the asymptotic expansions for the case of an asymptotically thin film, for a Reynolds number that is asymptotically of order one in ε. The axial length scales in the film and in the core, and the radial length scale in the core remain order one quantities while the radial length scale in the film is small [of $O(\varepsilon)$]. Thus lubrication equations will be valid in the film. In order to separate the radial length scales in the film and in the core, we introduce a new, order one, stretched film variable y given by

$$r = 1 + \varepsilon - \varepsilon y. \tag{4.1}$$

This stretched film radial scale forces the radial derivatives in the film to be large ($O(1/\varepsilon)$), whereas they are order one in the core. This will motivate a set of scalings which, as we shall see, agree with those suggested from the long wave analysis (cf. (3.5)) given earlier.

From the problem formulation in Sec. 2, one can see that the perturbation flows derive from the interfacial displacement η appearing in the normal and tangential stress balances and in the continuity of axial velocity boundary conditions. As such, the circumferential curvature forces ($J \neq 0$) in the normal stress balance can generate a

perturbation pressure, the viscosity stratification ($m \neq 1$) can generate a large perturbative axial velocity or the density difference ($l \neq 1$) can cause a perturbative tangential stress; in principle, any combination of these effects can drive the flows.

In typical thin, lubricating film problems, it is the large perturbation pressure that sets the variables' scales. As we shall see below, this is a salient case in our context, and leads to a set of consistent scalings that are relevant to liquid-liquid displacement in rock pores. Interestingly, however, essentially the same scales and the resulting analysis can apply even when the surface tension is no longer as predominating. Thus, we will construct an analytic structure sufficiently general to encompass both cases which will allow one to formally reduce the former to the latter by simply pushing the surface tension parameter J to a higher order in ε in the final equation for the (imaginary part of the) wave speed. It is worth recalling that the long wave length analysis (3.5) can be understood to have foreseen the confluence of regimes.

Let us begin with the first case where the circumferential curvature induces a pressure perturbation across the interface that drives the lubrication film flow. The perturbation pressure, however, does not appear explicitly in the stream function formulation, and we must therefore examine (2.9) through (2.17) a bit more closely. By virtue of the film's large radial derivatives the leading order hydrodynamic term (whose origin is from P) in the normal stress balance (2.16) which must balance the curvature terms is

$$\frac{m}{\mathrm{i}\alpha r}\frac{1}{\varepsilon^3}\frac{d^3\psi_2}{dy^3}=\frac{J}{R_g^2}(\alpha^2-1)\,\eta.$$

Since α , η , m and r are all order one quantities, one has

$$\psi_2 \sim J\,\varepsilon^3 / R_g^2 .$$

The continuity of axial velocity at the interface (2.14) is the source of Yih's viscous stratification instability. For $m \neq 1$, the order one term $(w_{1r}^0 - w_{2r}^0)\,\eta$ represents in linearized form the discontinuity of the base flow at the disturbed interfacial position. This introduces a perturbation at least to the core velocity $\frac{1}{r}\frac{d\psi_1}{dr}$ to preserve the continuity of velocity at the interface. (If the film quantity dominated in (2.14) it would also dominate in (2.15) and overditermine the film.) Noting that core radial derivatives are order one quantities gives $\psi_1 \sim 1$. As a result both the leading order continuity of radial (2.13) and axial (2.14) velocity equations involve only core quantities, while the leading order normal stress balance is purely a film equation.

In order not to overdetermine the core, the tangential stress balance, to leading order, must contain the dominant film term

$$\frac{m}{\varepsilon^2}\frac{d^2\psi_2}{dy^2}.$$

Thus,

$$\frac{J\varepsilon}{R_g^2} \geq \psi_1 \sim 1.$$

Equality in this expression couples the film and core through this boundary condition whereas strict inequality would allow one to close the film problem independently of the core and thereby lead to linear growth totally governed by capillarity

$$\frac{J}{R_g^2} \sim \frac{1}{\varepsilon^{1+\delta}}. \quad (0 \leq \delta \leq 1)$$

In the case of interest here, a strong yet less overwhelming surface tension (i.e., equality above)

$$\frac{J\varepsilon}{R_g^2} \sim \psi_1 \sim 1,$$

turns out to result in the perturbation core velocity accounting for the total axial velocity discontinuity to leading order. Finally, the kinematic condition written in terms of film variables yields $c \sim \psi_2$. Thus the complete set of scales is

$$\frac{J}{R_g^2} \sim \frac{1}{\varepsilon}, \quad \psi_1 \sim 1, \quad \psi_2 \sim \frac{J\varepsilon^3}{R_g^2} \sim \varepsilon^2, \quad c \sim \varepsilon^2. \tag{4.2}$$

Let us turn now to the second case where the surface tension parameter J is less controlling, say $J \leq O(1)$ in ε, as in the case for lubricated pipelining. J, now of reduced importance, no longer determines the scales. In fact, the leading order term in the normal stress (2.16) dominates and is thus zero at the interface:

$$-\frac{2mi\alpha}{r\varepsilon^3} \frac{d^3\psi_2}{dy^3} = 0 \qquad \text{at} \quad r = 1.$$

This has at least four pertinent consequences: (1) The perturbation pressure across the interface is now zero to leading order. Thus, (2) the film's leading order velocity profile is linear rather than parabolic; and (3) the scale on ψ_2 must be either

$$\psi_2 > O\left(\frac{J\varepsilon^3}{R_g^2}\right) \quad \text{or} \quad \frac{J}{R_g^2} < O\left(\frac{\psi_2}{\varepsilon^3}\right).$$

(4) The leading order normal stress boundary condition again involves only film quantities.

From the long wave analysis, one sees that when $m \neq 1$, viscosity stratification is more important than density stratification, and must therefore drive the flow. Thus, we turn to the order one viscous-stratification-derived perturbation in the continuity of axial velocity. In order for the film problem to be neither overdetermined nor have a trivial solution, the core again takes up this perturbation and requires $\psi_1 \sim 1$. To not overdetermine the core the tangential stress balance must again contain both film and core contributions, which finally requires $\psi_2 \sim \varepsilon^2$ and $c \sim \varepsilon^2$.

We may now return to the normal stress balance and see what orderings for J this latter analysis allows. Certainly, $(J/R_g^2) < O(1/\varepsilon)$, which for $R_g^2 = O(1)$ allows J to be of order one or less, as in the case in lubricated pipelining. Again, as suggested from the long wavelength analysis, only viscosity stratification will be present for these J orderings to leading (ε^2) order in c. In fact, viscosity stratification alone determines the thin film's leading order linear stability according to the sign of $m - 1$; the density difference provides an order ε correction.

Finally, we construct a third set of scales in order to bring out the effect of the density difference and to have it interact with capillarity at leading order. To accomplish this one must first suppress viscosity stratification by, say, taking $m = 1$, and then make the effect of surface tension an order below that given in the first analysis above, i.e., $J = O(1)$, $R_g^2 = O(1)$, $m = 1$. This is again in complete agreement with the long wavelength analysis.

Before proceeding, it is worth noting the following point. The bottom line for all three of the sets of scaling arguments just presented is the derived scales for c, ψ_2, ψ_1, η which are the only explicitly asymptotic-expanded dependent variables entering the stream-function formulated linear stability problem. In all three of these treatments, η is of order one and the asymptotic expansions for the remaining variables are:

$$c = c^{(2)}\varepsilon^2 + c^{(3)}\varepsilon^3 + \cdots, \tag{4.3}$$

$$\psi_2 = \psi_2^{(2)}\varepsilon^2 + \psi_2^{(3)}\varepsilon^3 + \cdots, \tag{4.4}$$

and

$$\psi_1 = \psi_1^{(0)} + \psi_1^{(1)}\varepsilon + \cdots. \tag{4.5}$$

Thus we employ a single, unified treatment, leading to expressions for the wave speed and the growth rates. The scheme to arrive at the wave speed and growth rates

requires substituting the asymptotic expansions into the problem formulation and assembling the leading order problem. We then solve the resulting core and lubricating film equations and match them with the boundary conditions at the interface. As seen in the above scaling arguments, the core dynamics couple nontrivially to the film's through the mechanisms of viscosity stratification and density difference and this necessitates solution of the core problem.

Substituting these expansion to the governing equations and boundary conditions of a system with new coordinates traveling with the base state velocity at the interface $[w_1^{(0)}(1)]$, we get, to leading order in ε:

$$D\,(D\,\psi_1^{(0)}) = \mathbf{i}\,\alpha R_g^2 \frac{F+1}{4}(1-r^2)\,D\,\psi_1^{(0)}, \tag{4.6}$$

$$\frac{d^4\psi_2^{(2)}}{d\,y^4} = 0, \tag{4.7}$$

$$\psi_1^{(0)} = 0, \tag{4.8}$$

$$\frac{d\psi_1^{(0)}}{dr} - \left(1-\frac{1}{m}\right)\frac{F+1}{2}\frac{\psi_2^{(2)}}{c^{(2)}} = 0, \tag{4.9}$$

$$D\psi_1^{(0)} - m\frac{d^2\psi_2^{(2)}}{dy^2} + 2\,\alpha^2(1-m)\,\psi_1^{(0)} + (l-1)\frac{\psi_2^{(2)}}{c^{(2)}} = 0, \tag{4.10}$$

and

$$-\mathbf{i}\,\alpha m\frac{d^3\psi_2^{(2)}}{dy^3} - \frac{J_0}{R_g^2}(\alpha^4-\alpha^2)\frac{\psi_2^{(2)}}{c^{(2)}} = 0, \tag{4.11}$$

where $J_0 = J\varepsilon$.

The next order in ε gives

$$D\,(D\,\psi_1^{(1)}) = \mathbf{i}\,\alpha R_g^2 \frac{F+1}{4}(1-r^2)\,D\,\psi_1^{(1)}, \tag{4.12}$$

$$\frac{d^4\psi_2^{(3)}}{d\,y^4}=-\frac{2}{r^3}\frac{d^3\psi_2^{(2)}}{d\,y^3}, \tag{4.13}$$

$$\psi_1^{(1)}=0, \tag{4.14}$$

$$\frac{d\psi_1^{(1)}}{dr}-\left(1-\frac{1}{m}\right)\frac{F+1}{2}\frac{\psi_2^{(3)}}{c^{(2)}}=-\frac{d\,\psi_2^{(2)}}{d\,y}-\left(1-\frac{1}{m}\right)\frac{F+1}{2}\frac{\psi_2^{(2)}c^{(3)}}{(c^{(2)})^2}, \tag{4.15}$$

$$D\psi_1^{(1)}-m\frac{d^2\psi_2^{(3)}}{dy^2}+2\alpha^2(1-m)\psi_1^{(1)}+(l-1)\frac{\psi_2^{(3)}}{c^{(2)}}=m\frac{d\,\psi_2^{(2)}}{d\,y}+(l-1)\frac{\psi_2^{(2)}c^{(3)}}{(c^{(2)})^2}, \tag{4.16}$$

and

$$-\mathbf{i}\,\alpha m\frac{d^3\psi_2^{(3)}}{dy^3}-\frac{J_0}{R_g^2}(\alpha^4-\alpha^2)\frac{\psi_2^{(3)}}{c^2} =$$

$$\mathbf{i}\,\alpha m\frac{d^2\psi_2^{(2)}}{dy^2}-\frac{J_0}{R_g^2}(\alpha^4-\alpha^2)\frac{\psi_2^{(2)}c^{(3)}}{(c^{(2)})^2}+\mathbf{i}\,\alpha\frac{d}{dr}(D\,\psi_1^{(0)}-2\alpha^2\psi_1^{(0)}). \tag{4.17}$$

Following Papageorgiou *et al.* (1990) one can solve the leading order core problem in terms of Kummer or confluent hypogeometric functions $M(\Lambda,2,\lambda r^2)$ (see Abramowitz and Stegun (1972)),

where

$$\Lambda=1+\alpha^2/8\,\lambda-\lambda/2, \tag{4.18}$$

and

$$\lambda=\frac{1}{4}[\alpha R_g^2(F+1)]^{1/2}e^{-\mathbf{i}\pi/4}. \tag{4.19}$$

The solution for the stream-function in the core becomes

$$\frac{1}{r}\psi_1^{(0)}=A_1(\alpha)I_1(\alpha r)+B_1(\alpha)N_1(\alpha r), \tag{4.20}$$

where

$$N_1(\alpha r)=\int_0^r[I_1(\alpha r)K_1(\alpha t)-I_1(\alpha t)K_1(\alpha r)]\,t^2e^{-\lambda t^2}M(\Lambda,2,2\lambda t^2)\,dt. \tag{4.21}$$

The solution in the annulus that satisfies no slip at the wall ($y=0$) is

$$\psi_2^{(2)}=A_2y^3+B_2y^2. \tag{4.22}$$

Applying the leading order interfacial boundary conditions (4.8) through (4.11) we get a (4X4) system of equations of the form

$$\mathbf{A}\,\mathbf{x} = \mathbf{0}\,. \tag{4.23}$$

The matrix

$$\mathbf{A} = \begin{bmatrix} I_1(\alpha) & N_1(\alpha) & 0 & 0 \\ \alpha I_0(\alpha) & \alpha N_2(\alpha) & -\left(1-\frac{1}{m}\right)\frac{F+1}{2c^{(2)}} & -\left(1-\frac{1}{m}\right)\frac{F+1}{2c^{(2)}} \\ 2\alpha^2(1-m)I_1(\alpha) & \begin{matrix} e^{-\lambda}M(\Lambda,2,2\lambda) \\ +2\alpha^2(1-m)N_1(\alpha) \end{matrix} & -6m+\frac{(l-1)}{c^{(2)}} & -2m+\frac{(l-1)}{c^{(2)}} \\ 0 & 0 & 6m\,\mathbf{i}\,\alpha+\frac{J_0}{R_g^2}\frac{\alpha^2(\alpha^2-1)}{c^{(2)}} & \frac{J_0}{R_g^2}\frac{\alpha^2(\alpha^2-1)}{c^{(2)}} \end{bmatrix}$$

in (4.23) contains the coefficients of the constants of integration in these linearized boundary conditions. The constants appearing in **A** are

$$N_1(\alpha) = \int_0^1 [I_1(\alpha)\,K_1(\alpha t) - I_1(\alpha t)\,K_1(\alpha)]\,t^2\,e^{-\lambda t^2}\,M(\Lambda,2,2\lambda t^2)\,dt\,, \tag{4.24}$$

$$N_2(\alpha) = \int_0^1 [I_0(\alpha)\,K_1(\alpha t) + I_1(\alpha t)\,K_0(\alpha)]\,t^2\,e^{-\lambda t^2}\,M(\Lambda,2,2\lambda t^2)\,dt\,, \tag{4.25}$$

Finally **x** is the vector of the constants of integration

$$x = [A_1 \quad B_1 \quad A_2 \quad B_2]^t\,. \tag{4.26}$$

The amplitude equation follows by solving the equation $det(\mathbf{A}) = 0$ in terms of the wave speed $c^{(2)}$ (to order ε^2); the result is

$$c^{(2)} = \frac{J_0}{3\,m\,R_g^2}\alpha\,(\alpha^2-1)\,\mathbf{i} + \frac{1}{m}\frac{F+1}{4}\left[-\frac{N(\alpha)}{\alpha}\left(1-\frac{1}{m}\right)\right] + \frac{(l-1)}{2m}\,, \tag{4.27}$$

where

$$N(\alpha) = \frac{I_1(\alpha)\,e^{-\lambda}M(\Lambda,2,2\lambda)}{N_1(\alpha)\,I_0(\alpha) - N_2(\alpha)\,I_1(\alpha)}\,, \tag{4.28}$$

which is, in general, complex. From (4.27) one can immediately conclude that in the strong surface tension case [$J = O(1/\varepsilon)$] , density difference only contributes to dispersion to leading order in ε .

The general solution to the governing equation in the core remains the same to the next order in ε but the solution to the governing equation in the film that satisfies no slip on the wall becomes:

$$\psi_2^{(3)} = a_2 y^3 + b_2 y^2 - \frac{A_2}{2} y^4 . \tag{4.29}$$

Applying the second order boundary conditions (4.14) to (4.17) we get a system of equations of the form

$$\mathbf{A}\,\mathbf{x} = \mathbf{b}, \tag{4.30}$$

where **A** is the same as in (4.23) and **x** is the new vector of the constants of integration to this order in ε . Finally, **b** is a vector containing the inhomogeneities to this order in ε given by:

$$\mathbf{b} = \begin{bmatrix} 0 \\ -\left(\frac{(1-1/m)\,(F+1)}{2c^{(2)}}\left(\frac{1}{2}+\frac{c^{(3)}}{c^{(2)}}\right)+3\right)A_2 - \left(\frac{(1-1/m)\,(F+1)}{2\,(c^{(2)})^2}+2\right)B_2 \\ \left(\frac{(l-1)}{c^{(2)}}\left(\frac{1}{2}+\frac{c^{(3)}}{c^{(2)}}\right)-3m\right)A_2 + \left(\frac{(l-1)c^{(3)}}{(c^{(2)})^2}+2m\right)B_2 \\ \left(\frac{J_0\alpha^2(\alpha^2-1)}{R_g^2 c^{(2)}}\left(\frac{1}{2}-\frac{c^{(3)}}{c^{(2)}}\right)+6mi\alpha\right)A_2 - \left(\frac{J_0\alpha^2(\alpha^2-1)c^{(3)}}{R_g^2(c^{(2)})^2}-2mi\alpha\right)B_2 \\ -2i\alpha^4 I_0(\alpha)A_1 + \left(-2i\alpha^4 N_2(\alpha) + i\alpha\frac{d}{dr}\left(r^2 e^{-\lambda r^2} M(\Lambda,2,2\lambda r^2)\right)\right)B_1 \end{bmatrix}$$

Using the solvability (adjoint) method we solve (4.30) for the wave speed $c^{(3)}$ (to order ε^3); the result is

$$c^{(3)} = -\frac{J_0}{R_g^2}\frac{N(\alpha)}{4m^2}(\alpha^2-1)\,\mathbf{i} + \left[-\frac{1}{6m}+\frac{N(\alpha)}{2\alpha m^2}\right](l-1)$$
$$-\left[\frac{2\alpha^2}{3m}+\frac{2T(\alpha)-N(\alpha)}{6\alpha m}+\frac{N^2(\alpha)}{2\alpha^2 m^2}\right]\left(1-\frac{1}{m}\right)\frac{F+1}{2}, \qquad (4.31)$$

where
$$T(\alpha) = \frac{I_1(\alpha)\, e^{-\lambda} M(\Lambda+1,3,2\lambda)}{N_1(\alpha)\, I_0(\alpha) - N_2(\alpha)\, I_1(\alpha)}, \qquad (4.32)$$

which is also, in general, complex. Comparison with the long wave expansion in the previous section suggests that the combination of these two orders of ε results will give excellent agreement with the exact results. It is interesting to note that if the flow becomes asymptotically slow, i.e., $R_g^2 = O(\varepsilon)$ the complex Kummer functions reduced to real valued modified Bessel functions. Thus, to this order viscosity and density stratifications contribute only dispersion in this limit. In fact, this is also true for the exact problem (i.e., even for thick films) for asymptotically small values of R_g^2. It is also important to note that in the long wave limit ($\alpha \to 0$) (4.27) and (4.31) reduced to (3.5) by asymptotically taking the limit of $N(\alpha)$ and $T(\alpha)$ as ($\alpha \to 0$) :

$$\underset{\alpha\to 0}{N(\alpha)} = -4\alpha - \frac{R_g^2(F+1)\alpha^2}{48}\,\mathbf{i},$$

and
$$\underset{\alpha\to 0}{T(\alpha)} = -4\alpha + \frac{R_g^2(F+1)\alpha^2}{48}\,\mathbf{i}.$$

The main task in the numerical calculation based on (4.27) and (4.31) that appears below is the accurate evaluation of the kernels $N(\alpha)$ and $T(\alpha)$ for each value of α. For moderate values of α we use an NCAR Bessel function package to calculate the Bessel functions. The calculation of the Kummer function $M(\Lambda, 2, 2\lambda r^2)$ was more

involved, however. Following PMR we obtained the Kummer function for each α by numerical integration of the ordinary differential equation (4.6) (in terms of $g(r)$ where $D\psi_1^{(0)} = g(r)$) in the complex plane along a contour joining 0 to 2λ. For convenience we used a straight line contour and stored the values of M at the mesh points in order to compute $N_1(\alpha)$ and $N_2(\alpha)$ by quadrature from (4.24) and (4.25). A fourth order Runge-Kutta method performed the integration of the differential equation and Simpson's rule the quadrature. Refinement tests were made to insure numerical convergence. The extension to negative values of α follows from the identity

$$N(-\alpha) = -N^*(\alpha), \tag{4.33}$$

where * denotes complex conjugate. When a contour from 0 to $2\lambda^*$ is used in the computation of Kummer function in the complex plane (as in the case of up-flow ($F < -1$)), the result is $N^*(\alpha)$. With the kernels known numerically, the numerical implementation is now complete.

5 RESULTS AND DISCUSSION

5.1 Neutral Curves

We begin with a discussion of neutral curves. Neutral conditions follow by equating the imaginary part of c to zero. This leads to an implicit dependence of R_g^2 or F in the critical wavenumber α which may be expanded in ε :

$$R_g^2 = R_g^{2(0)} + R_g^{2(1)}\varepsilon + \cdots, \tag{5.1}$$

$$F = F^{(0)} + F^{(1)}\varepsilon + \cdots. \tag{5.2}$$

Inserting either of these expressions into the defining relation for the neutral state,

$$Im[c(R_{eg}, F, \varepsilon, J, m, \alpha)] = 0,$$

and noting the expansion for c, leads to equations for the expansion coefficients in (5.1) and (5.2). For example, in terms of the Reynolds number:

$$c^{(2)}\left[R_g^{2(0)}\right]=0, \tag{5.3}$$

$$R_g^{2(1)}\frac{dc^{(2)}}{dR_g^2}\Big|_{R_g^{2(0)}}+c^{(3)}\left(R_g^{2(0)}\right)=0\,. \tag{5.4}$$

Newton-Raphson based schemes provide numerical solutions for $R_g^{2(0)}$ from (5.3); $R_g^{2(1)}$ obtains by evaluating the derivative in (5.4) numerically. The determination of further terms in (5.1) and (5.2) requires expanding c to higher order. However, we show below that the two term expansion is usually sufficient for $\varepsilon < 0.2$ when $m > O(\varepsilon)$.

(i) The Case of the Less Viscous Annulus ($m < 1$)

Figure 3 shows neutral curves for pure gravity driven flow for different values of the film thickness ε. From this figure one can see that the agreement between our asymptotic calculations (lines) and CBJ's results (points) is excellent even for relatively large values of ε ($\varepsilon \le 0.2$). These curves demonstrate CBJ's result that viscosity stratification stabilizes the capillary instability and that this stabilization becomes more effective the thinner the film, i.e., it becomes stable at smaller values of R_g. Figures 4 (a and b) also show (R_g *vs* α) neutral curves but for different values of l with m, J, and F as in Figure 3. As noted in the last section and evident in figures 4, the influence of $l \neq 1$ is an order ε effect on the $l = 1$ neutral curve. It is apparent from the very good agreement with CBJ that this provides a sufficient description of this effect for thin films. For $\varepsilon = 0.2$, $l \neq 1$, the agreement is less satisfactory. In particular, for $l = 2$, a smaller value of ε is needed for order ε accuracy in R_g. For $l = 0.5$, CBJ's curve is actually no longer of the

canonical form displaying global stability. In fact the branch beginning from the R_g axis increases rapidly to high values of R_g beyond $\alpha \sim 0.3$ and thus lies outside the domain of our order one R_g theory. Again, as CBJ note, one should use a heavier lubricant to achieve stability at lower values of R_g for pure gravity driven flows.

Figure 5 shows a neutral curve for a forced flow (F *vs* α) for various values of the density ratio l with the other parameters as in CBJ. Again the agreement is excellent and confirms CBJ's results that for forced flow heavy lubricants are stabilizing for down-flow ($F > -1$) and light ones for up-flow ($F < -1$). It is also interesting to note that when $l = 1$, the neutral curves is symmetric about $F = -1$. This is also clear from the equations. Since the term $F + 1$ only enters the stability problem through the base flow and since for $l = 1$, a change in sign of $F + 1$ just changes the direction of the base flow, such a change can not affect the stability.

The final forced flow neutral curve (Figure 6) for $m < 1$, not given by CBJ, examines the effect of the viscosity ratio m : For down-flow there exist a critical pressure gradient above which the system is stable and the pressure gradient needed for stability becomes smaller as the viscosity ratio gets smaller (see Figure 6). The up-flow region of this graph is not shown on this figure because for ($l = 1$) the up-flow curves are a mirror image of the down-flow curves. As m increases the unstable lobe increases into a range of F in which the theory is no longer valid.

(ii) The Case of the More Viscous Annulus ($m > 1$)

Since CBJ's interests lie in lubricated pipelining, they did not consider Hickox's $m > 1$ arrangement. However, since our concern is CAF stability in the content of liquid-liquid displacements of oil by water, the $m > 1$ situation is pertinent. Since F unlike R_g is proportional to the experimentally manipulated pressure

gradient, we present only the (F *vs* α) type neutral curve. For $m > 1$ (Figure 7) viscosity stratification is destabilizing and thus the band of unstable waves contains at least the band $0 < \alpha < 1$. In fact, this band grows as F or, in fact, as R_g (not shown) increases. Note again that for the $l = 1$ case, the up-flow curve is just the reflection of the given (down-flow) curve about $F = -1$. Hu & Joseph (1989) reported similar nuetral curves [($R_e$vsα)] for fixed $m > 1$.

(iii) The Case of Equal Viscosities and Unequal Densities ($m = 1$, $l \neq 1$)

As mentioned in the Sec 4, in the absence of viscosity stratification ($m = 1$) density difference itself can compete with capillarity for moderate surface tension ($J = O(1)$). This is shown in Figure 8 where we show neutral curves for different values of the density ratio l for $m = 1$ $J^* = 10$, $R_g^2 = 10$, and $\varepsilon = 0.1$. Obviously, the neutral curve at $\alpha = 1$ represents pure capillarity, the only surviving effect when $l = 1$. From this figure one sees that density stratification plays the same qualitative role as in the case $m < 1$, where it had only an order ε-effect on the stability. That is, heavy lubricants are stabilizing for down-flow and destabilizing for up-flow, while for light lubricants the opposite is true. The only difference is that in the absence of viscosity stratification, the density difference becomes a leading order effect which can stabilize the capillary instability for sufficiently large pressure gradients that are downwards for heavy lubricants and upwards for light ones. Note that the figure displays a certain symmetry: When l is replaced by $2 - l$ (for $2 \geq l \geq 0$) and F by $(-2 - F)$, the curve remains unchanged. This, again, follows because the base flow simply changes direction upon these replacements.

5.2 Growth Rates

This brings us to a discussion of growth rates. We begin with the large surface tension, less viscous annulus situation, where we choose F to lie within the unstable lobe at the lower left of the canonical neutral curve. In Figure 9 we show the wave length of maximum instability from the linear analysis. For $m = 1$, there is no viscous stratification, and the wavelength of maximum instability is just the value determined by pure capillarity, which is independent of F. On the other hand, as m decreases from one, the film becomes less viscous and the effect of viscous stratification grows. The neutral curves exhibit this in that the intersection point of the neutral branch defining the surface-tension-derived unstable lobe with the F axis decreases to -1. Similarly, since the maximally unstable wave is closely related to the critical wave, the curves in Figure 9 (also symmetric about $F - 1 = 0$) diverge at values of F that also recede towards $F = -1$ as m decreases from one.

The corresponding maximum growth rates (cf. Figure 10) display competing effects. First, as the film becomes less viscous (i.e., m decreases from one), the system stabilizes, i.e., the maximum growth rate goes to zero, at lower values of F. Second, however, for values of F sufficiently far in the unstable region, the less viscous the film is, the less viscous resistance can inhibit the growth of unstable waves; thus small m systems will grow faster than those with larger m values. This accounts for the cross shape in Figure 10.

Finally, we turn to the $m > 1$ and large J case where, as already discussed, viscous stratification acts to destabilize the system (for small ε). The first trend that is clear in Figure 11 is that as F increases and the unstable band of waves

broadens, the corresponding maximum growth rates also increase. The second trend is that as the film becomes more viscous, the maximum growth rates decrease; this is just the same effect that explained the left side of Figure 10.

6 STABILITY OF WETTING LAYERS IN LOW CAPILLARY NUMBER SLUG FLOWS

When an aqueous phase displaces oil in a rock pore, slug flow regimes can arise in which the nonwetting phase takes the form of a train of long slugs moving over, and separated by, the wetting liquid. These flows are usually at very low capillary and slug phase Reynolds numbers, where, in the notation of this paper, $C_a = \mu_2 U/\sigma$ and $R_e = \rho_1 V R_1/\mu_1$ and U is the slug velocity which for thin annuli, is just $\frac{1}{2}V$.

Bretherton (1961) studied the motion of a long gas slug moving through a Newtonian liquid filling a straight cylindrical tube at low capillary and Reynolds numbers. Bretherton divided the slug interface and surrounding fluid into five regions: (i) a center region where the wetting layer achieves a constant thickness, (ii) two tip regions where capillary forces are important and the interfacial shapes are, to leading order, sections of spheres and (iii) two transition regions which bridge the tip and the constant wetting layer regions and in which capillary and viscous forces are both important and the wetting layer fluid mechanics is described by the lubrication equations. By matching solutions in each of these regions in powers of the capillary number to the one third power, Bretherton established the following leading order equation for ε as $C_a \to 0$:

$$\varepsilon = 1.337\, C_a^{2/3} + O(C_a^{4/3}). \tag{6.1}$$

Park and Homsy (1984) reexamined Bretherton's problem for the case of interest here of a liquid slug, and demonstrated that the above expression for ε remains valid as long as the viscosity ratio m is larger than $C_a^{1/3}$.

We use Bretherton's result to develop a theory for the stability of the wetting layer around a long liquid slug at low capillary numbers. We neglect density differences and express the stability equations in terms of R_e rather than F and R_g by the identification

$$R_e = \frac{(F+1)}{4}\frac{(a^2-1+m)}{m}R_g^2 .$$

The growth rate may be expressed as an asymptotic expansion in $C_a^{1/3}$ by introducing Bretherton's expression for ε into (4.27) and by equating J/mR_e to $\frac{1}{2C_a}$. The results to order $C_a^{4/3}$ is:

$$c = (1.337)^2 C_a\left(\frac{1.337}{2}\mathbf{i}\,\alpha\frac{\alpha^2-1}{3}+\frac{1}{\alpha m}\left(1-\frac{1}{m}\right)N(\alpha)\,C_a^{1/3}+O(C_a^{2/3})\right), \qquad (6.2)$$

where c is now nondimensionalized by the centerline velocity as in Preziosi, Chen and Joseph (1989). In the expression (4.19) for λ used in defining $N(\alpha)$, (6.2) replaces $(F+1)R_g^2/4$ by R_e. Recall that (4.27) is valid for $m > \varepsilon$ or $m > C_a^{2/3}$ and the Bretherton expression is valid for $m > C_a^{1/3}$. Since the latter is the more restrictive on m for $C_a \ll 1$, the above expansion in C_a is valid for $m > C_a^{1/3}$. Even with this restriction, one can draw some very interesting asymptotic conclusions regarding the growth dynamics:

(i) When $m < 1$ (oil slugs in water) and $C_a^{1/3}$ is in the range $m > C_a^{1/3} > m^2$, the stability is dominated by the stabilization due to viscosity stratification.

(ii) When $m < 1$ (again oil slugs in water), and $C_a^{1/3}$ is smaller than or of the order as m^2, capillarity competes with and then dominates the stabilizing

effect of viscosity stratification.

(iii) When $m > 1$ (water drops in oil), for all $C_a < 1$, viscosity stratification is destabilizing, but capillarity dominates.

Aul & Olbricht (1990) performed experiments with $m > 1$ using oil as the wetting phase and water in the core. The critical wavelength of the most unstable wave they observed is very closed to the one predicted by pure capillarity. They used an equation similar to (6.2) including only the capillarity term and showed very good agreement with the experimental values of the critical wavelength. A simple calculation of the capillarity and viscosity stratification terms of (6.2) using their material parameters ($R_2 = 27\mu m$, $R_e = 0.0277$, $[m_1 = 173, m_2 = 80, m_3 = 19]$ and $[C_{a1} = 0.022$, $C_{a2} = 0.01$, $C_{a3} = 0.0024]$) showed that indeed capillarity dominates (viscosity stratification is several orders of magnitude smaller than capillarity) for all three cases.

Equation (6.2) can be the basis for constructing stability plots in R_e, C_a space for fixed $m < 1$. By setting the imaginary part of c equal to zero, one obtains:

$$0 = 1.337\frac{\alpha(\alpha^2-1)}{3} + \frac{1}{\alpha m}\left(1-\frac{1}{m}\right) Im(N(\alpha))\, C_a^{1/3}, \tag{6.3}$$

One can calculate neutral stability plots of R_e against α for fixed $C_a^{1/3}$ and m that would be of the same form as the (R_g vs α) plots of Sec. 5. We suspect that for a fixed, small value of ε (and hence of C_a) and $m < 1$, there is a range of m larger than $C_a^{1/3}$ yet small enough so that the lower branch of the neutral curves (e.g. Figures 4, 5 and 6) is monotonic. In such cases, R_{ec}, just the limit of (6.3) as $\alpha \to 0$ given by:

$$R_{ec} = 1.337\,\frac{2\,m^2\,C_a^{-1/3}}{(1-m)}, \tag{6.4}$$

is the beginning of the window of global stability. The above equation defines a lobe in the $C_a^{1/3}$, R_e plane with unstable values lying inside the lobe. In view of the approximations involved in deriving (6.4), m must be less than one and $C_a^{1/3}$ must be smaller than m. Also note that these approximations require that R_e be of order 1 in ε or $C_a^{2/3}$. From (6.4) it is clear that this will be the case as long as $C_a^{1/3}$ is larger than m^2, so (6.4) is valid for $m < 1$ and for capillary numbers in the interval $m < C_a^{1/3} < m^2$.

One can use (6.4) to determine critical velocities above which oil slugs travel over linearly stable, thin water wetting layers. For such stable cases $R_e > R_{ec}$ and therefore, (6.4) leads to

$$U > \left[\left(\frac{1.337}{\rho_1 R_1 \mu_1}\right)^3 \mu_2^5 \sigma\right]^{1/4}. \tag{6.5}$$

As a typical example, consider oil slugs of unit specific gravity and $\mu_1 = 10cp$, traveling over a water film ($\mu_2 = 1cp$) with an interfacial tension of 10 dynes/cm in a 250 μm diameter pore. The slug-film interface is linearly stable for $U > 0.6cm/s$. However, in as much as the Bretherton theory breaks down for $C_a^{1/3} > m$, this prediction formally holds only to $U \cong 1cm/s$ for the numbers given. Naturally, one would hope that the situation would not change qualitatively by exceeding the Bretherton restriction.

7 WEAKLY NONLINEAR INTERFACIAL EVOLUTION

An important aspect of developing a linear theory in the thin film thickness asymptotic regime, is its capability of readily producing the dominant weakly nonlinear system out of a gradual linear instability. (A much larger initial disturbance would make both linear and weakly nonlinear theories redundant.) Such analyses have been

performed by PMR for the present geometry and for $m < 1$ but without density differences between the phases; the same formal procedure can be applied here also and the interested reader is referred to PMR for details.

The main outcome of the asymptotic analyses of PMR, is the derivation of nonlinear evolution equations by incorporation of weak nonlinearities (as in the Burgers equation for example) along with the linear operator that derives from the linear stability theory. Thus, it is easy to see that the evolution equation corresponding to our dispersion relation (4.27) is given by

$$\eta_\tau - \frac{2}{m}\eta\eta_z + \frac{J_0}{3mR_g^2}(\eta_{zz} + \eta_{zzzz}) - \frac{(l-1)}{2m}\eta_z$$

$$- \frac{\mathbf{i}}{2\pi m}\left(1 - \frac{1}{m}\right)\int_{-\infty}^{\infty} N(\alpha) \int_{-\infty}^{\infty} \eta(z',\tau) \quad e^{\mathbf{i}\alpha(z-z')}\, dz'd\alpha = 0 \,. \quad (7.1)$$

Equation (7.1) above covers a wide range of physical situations and is the result of "large" surface tension as explained earlier. In the regime where J/R_g^2 is order one and $m = 1$, disturbances grow on a relatively longer time scale (of order $1/\varepsilon^3$ in fact) by virtue of the relative magnitude of density difference instabilities (note that to leading order, a dispersive effect appears which is removed by a suitable Galilean transformation). The spectrum for this case is given by equations (4.27) and (4.31) and the evolution equation is

$$\eta_\tau - \frac{2}{m}\eta\eta_z + \frac{J}{3mR_g^2}(\eta_{zz} + \eta_{zzzz}) + \frac{(l-1)}{6m}\eta_z$$

$$+ \frac{\mathbf{i}}{4\pi m^2}(l-1)\int_{-\infty}^{\infty} N(\alpha) \int_{-\infty}^{\infty} \eta(z',\tau) \quad e^{\mathbf{i}\alpha(z-z')}\, dz'd\alpha = 0 \,. \quad (7.2)$$

Most of the qualitative features of both evolution equations (7.1) and (7.2) have been explained by the numerical experiments of PMR. For instance, these experi-

ments indicate that in the presence of capillarity the large time nonlinear evolution of the system remains bounded and can, in many cases depending on relative magnitudes of flow parameters, produce intricate and varied behavior ranging from trivial solutions to steady-state traveling waves to highly oscillatory chaotic behavior. There is one regime, however, which is different and merits further discussion. This weakly nonlinear evolution arises from the problem of "small" surface tension characterized by $J \sim 1$ and $R_g^2 \sim 1$. The evolution equation is obtained by setting $J_0 = 0$ in (7.1) above and so the equation contains the viscosity stratification mechanism alone (similar comments and conclusions also apply for (7.2) again with $J = 0$). The flow becomes linearly unstable depending on whether m is greater than or less than unity respectively. The unstable case $m > 1$ has some novel nonlinear consequences and we describe a possible senario next.

The large wavenumber (short wave) behavior of the kernel $N(\alpha)$ is of particular importance. The asymptotic behavior is $N(\alpha) \rightarrow \alpha \mid \alpha \mid$ as $\alpha \rightarrow \pm \infty$. So short waves, in the case of $m > 1$ at least, grow the fastest and there does not exist a regularizing cut-off. The problem is then expected to break down within a finite time (note that special initial conditions need to be used - see comments and analysis in Papageorgiou & Smith (1988)), the dominant structure being a shock formation in the interfacial shape. This shortening of axial length scales will invalidate our original assumptions of O(1) wavelengths and bringing a new shorter length scale, governed by the structure of the finite-time singularity. New physics enters through the upgraded role of the surface tension terms which are now in balance with viscous stratification due to the shorter scales involved. Overall then, the shock is expected to be smoothed out by the new physics that comes into play, and the final wave-form should look like a saw-tooth wave. We note that this is a suggestion as to the final behavior of the system

when $J = O(1)$ and $R_g^2 = O(1)$.

8 CONCLUSIONS

Thus we have developed an *analytic* asymptotic theory that leads to three important conclusions: First the asymptotic theory depicts the linear stability for thin films (as $\varepsilon \to 0$) very well. Comparison with results of Joseph and co-workers who numerically solved the Orr-Sommerfeld equations, shows excellent agreement (cf. Fig. 3,4 and 5). Second, the theory allows the ordering of the destabilizing forces in terms of the film thickness ε for thin films. In particular one sees that as $\varepsilon \to 0$: (i) The film inertial is not important and is a second order effect. (ii) For moderate sufrace tension, viscosity stratification dominates and the system is stable when the less viscous fluid is in the film and unstable when the less viscous fluid is in the core. (iii) For strong surface tension, capillarity competes with viscosity stratification and (iv) density stratification is a second order effect and to leading order is purely dispersive. Finally, for films of sufficiently low viscosity, viscosity stratification and capillarity determine the growth rates of wetting layers in slug flows.

FIGURES

Figure 1: Schematic of the circular tube geometry arranged vertically.

Figure 2: Comparison of the Lubrication results with the exact solution for long waves ($\alpha \to 0$) :
(a)Comparison of the order- ε^2 with the order- ε^3 .
(b)ε dependence for the order- ε^3 .

Figure 3: The ε dependence on the free-fall flow neutral curves [R_g vs α] and comparison with CBJ ($\varepsilon = 0.2, 0.1, 0.05, 0.01$).

Figure 4: (a)The l dependence on the free-fall flow neutral curves [R_g vs α] and comparison with CBJ for $\varepsilon = 0.1$ ($l = 0.5, 1.0, 2.0$).

Figure 4: (b)The l dependence on the free-fall flow neutral curves [R_g vs α] and comparison with CBJ for $\varepsilon = 0.2$ ($l = 0.5, 1.0, 2.0$).

Figure 5: The l dependence on the forced flow neutral curves [F vs α] and comparison with CBJ for $\varepsilon = 0.1$ ($l = 0.5, 1.0, 2.0$).

Figure 6: The m dependence on the forced flow neutral curves [F vs α] for $\varepsilon = 0.1$, $l = 1$ and $m < 1$ ($m = 0.3, 0.5, 0.7$).

Figure 7: The m dependence on the forced flow neutral curves [F vs α] for $\varepsilon = 0.1$, $l = 1$ and $m > 1$ ($m = 2, 10, 100$).

Figure 8: The l dependence on the forced flow neutral curves [F vs α] in the absence of viscosity stratification ($m = 1$) for $\varepsilon = 0.1$
($l = 0.1, 0.5, 0.8, 1.0, 1.2, 2.0, 10.0$).

Figure 9: The m dependence of the critical wavelength curves [λ_c vs F] for $m < 1$ ($m = 0.3, 0.5, 0.7$).

Figure 10: The m dependence of the maximum growth rate curves [ω_{rm} vs F] for $m < 1$ ($m = 0.3, 0.5, 0.7$).

Figure 11: The m dependence of the maximum growth rate curves [ω_{rm} vs F] for $m > 1$ ($m = 2, 10, 100$).

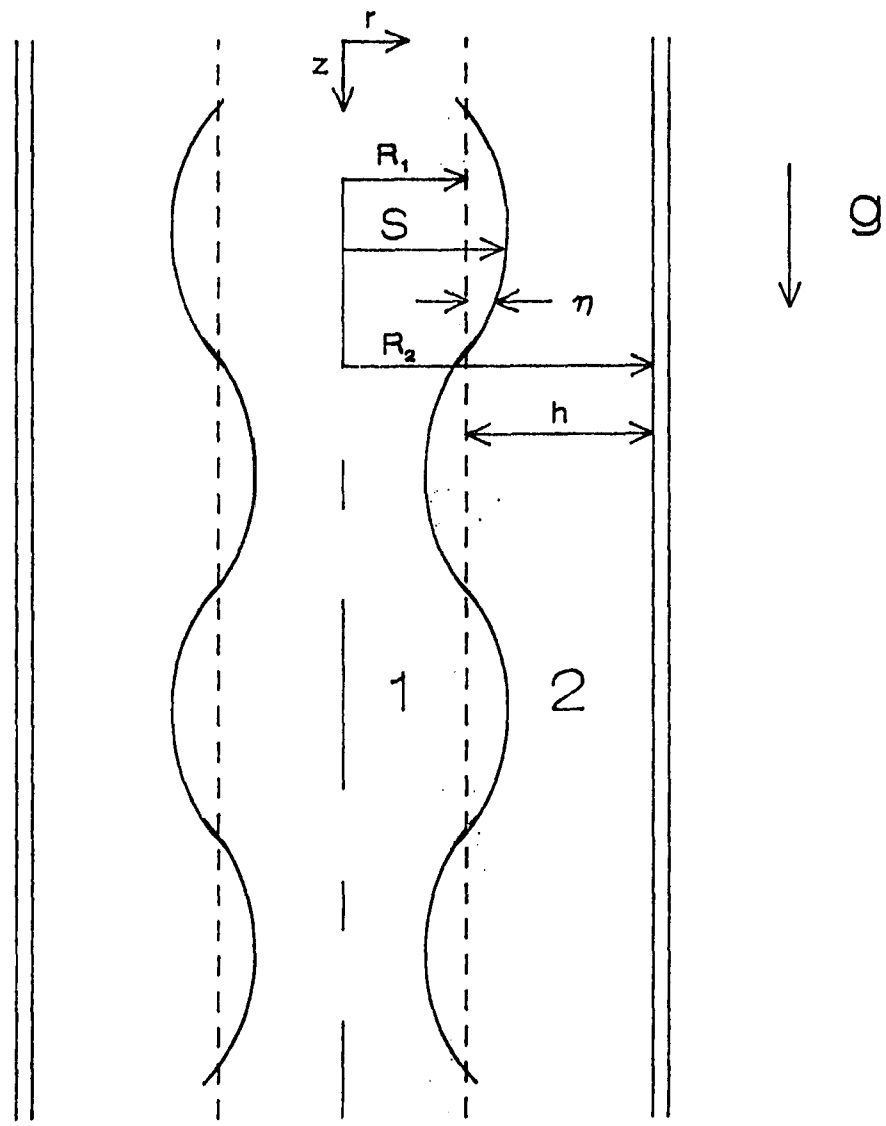

Figure 1

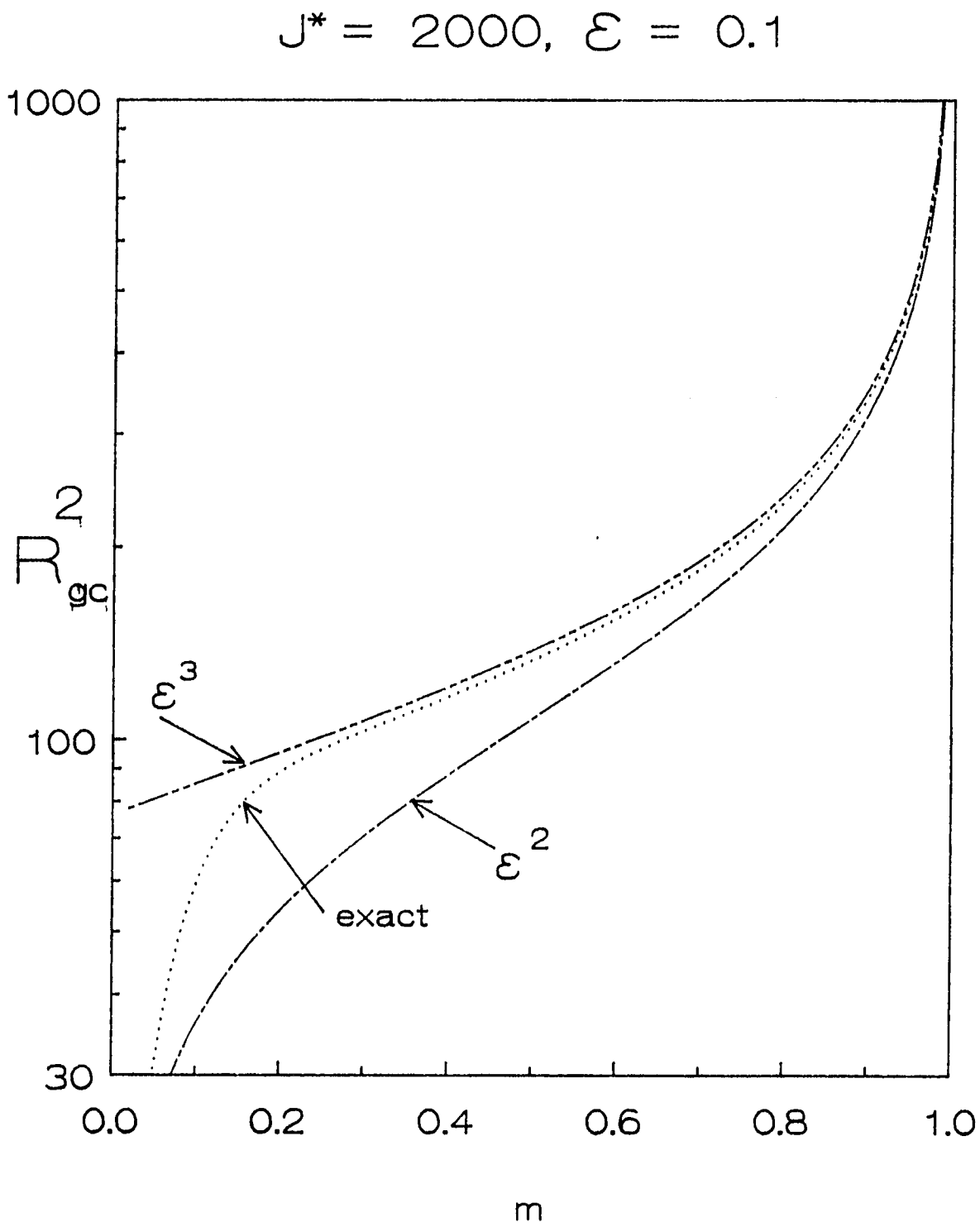
J* = 2000, ε = 0.1
1000
100
30
R^2_{gc}
ε^3
ε^2
exact
0.0
0.2
0.4
0.6
0.8
1.0
m

Figure 2_a

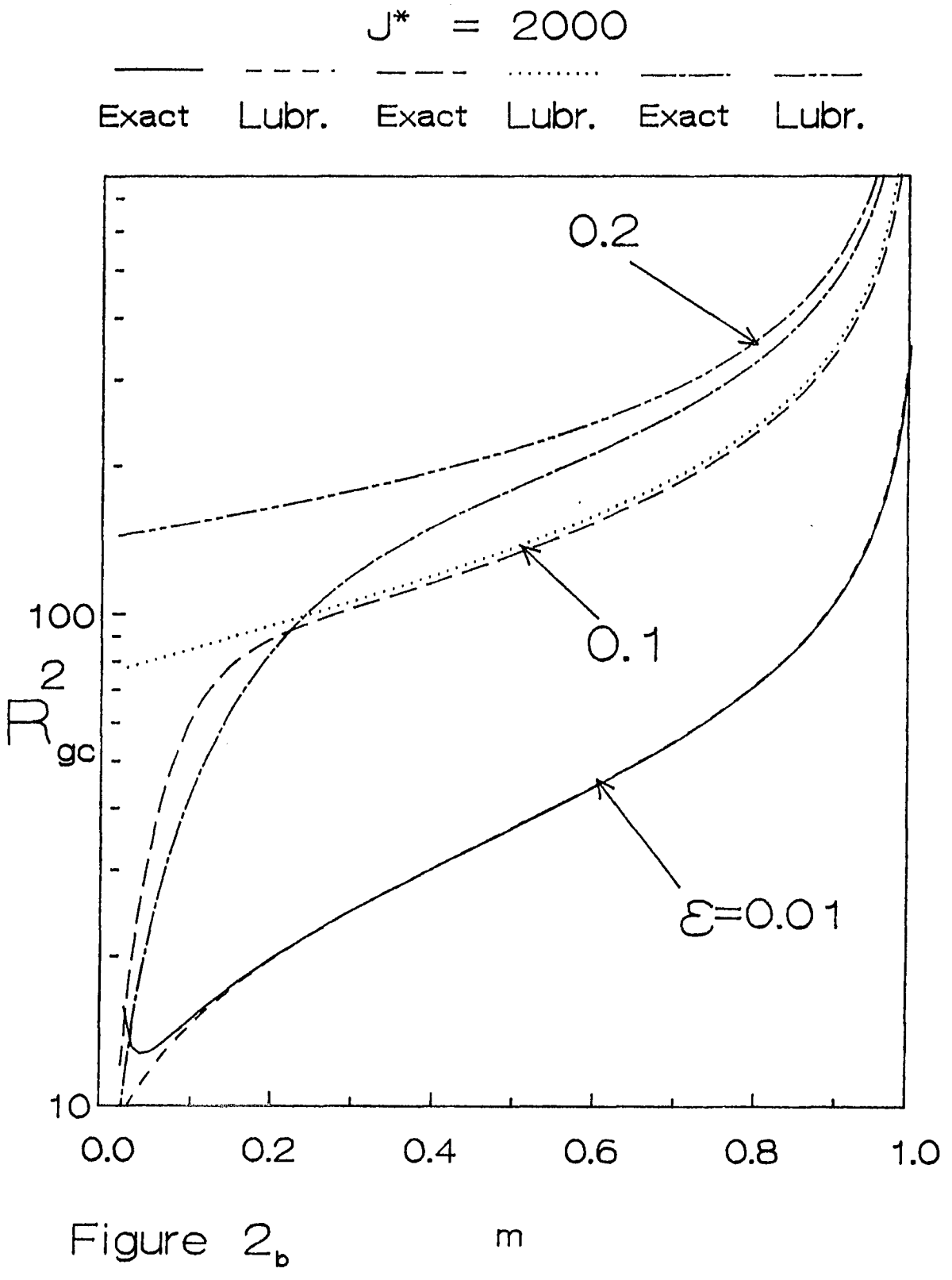
J* = 2000
Exact
Lubr.
Exact
Lubr.
Exact
Lubr.
0.2
0.1
ε=0.01
100
10
R^2_{gc}
0.0
0.2
0.4
0.6
0.8
1.0
m

Figure 2_b

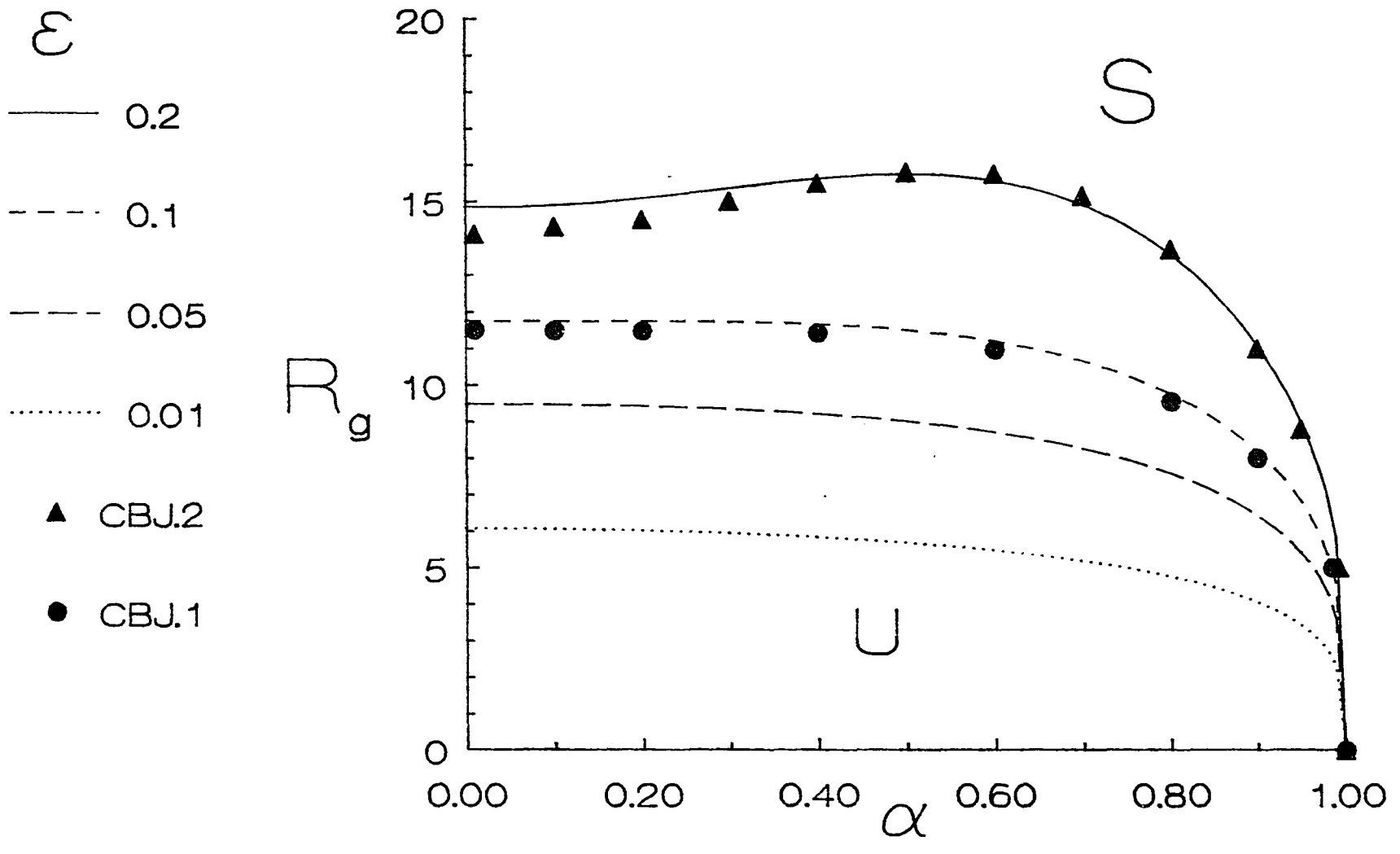

Figure 3 l=1, m=0.5, J*=2000

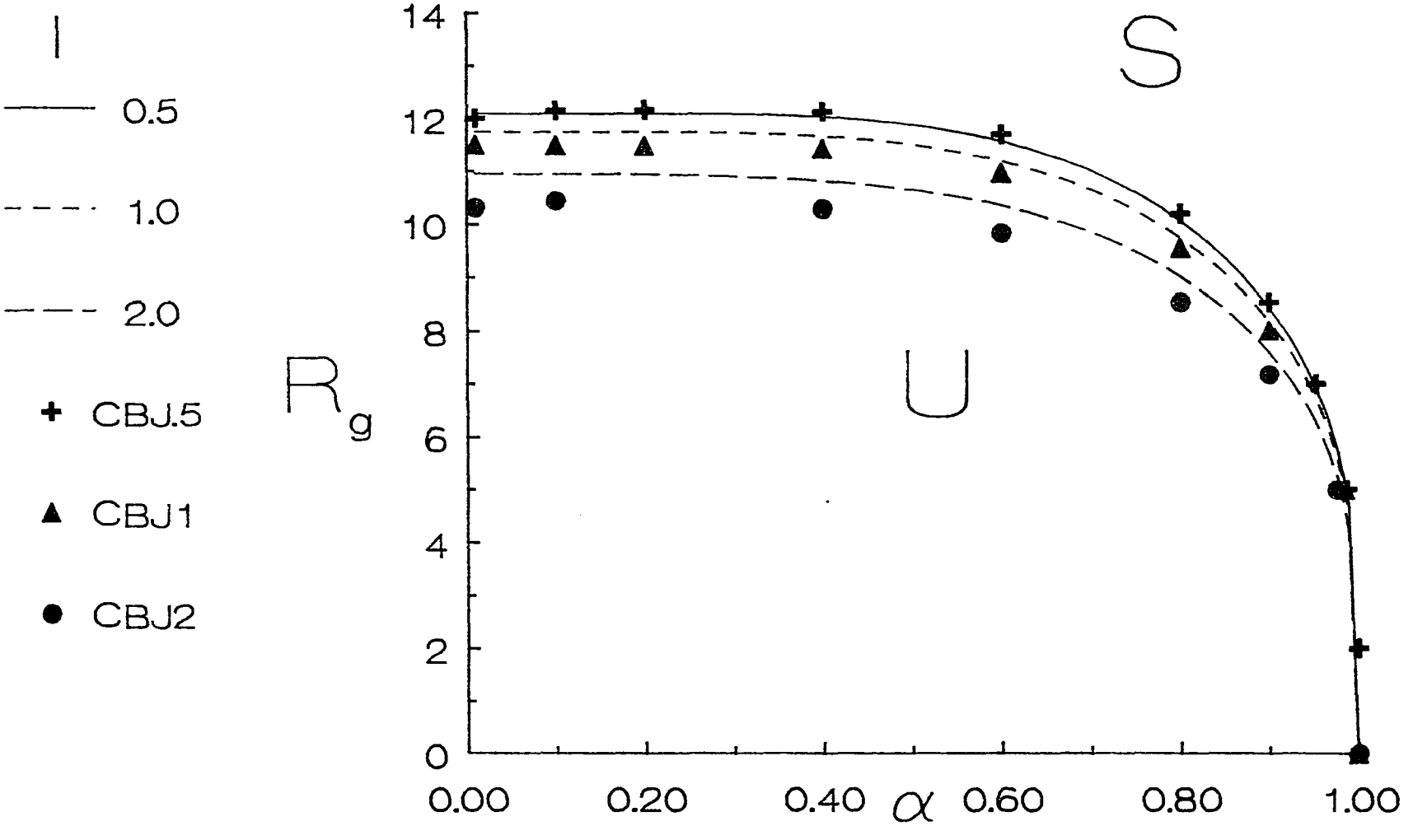

Figure 4_a ε =0.1, m=0.5, J^*=2000

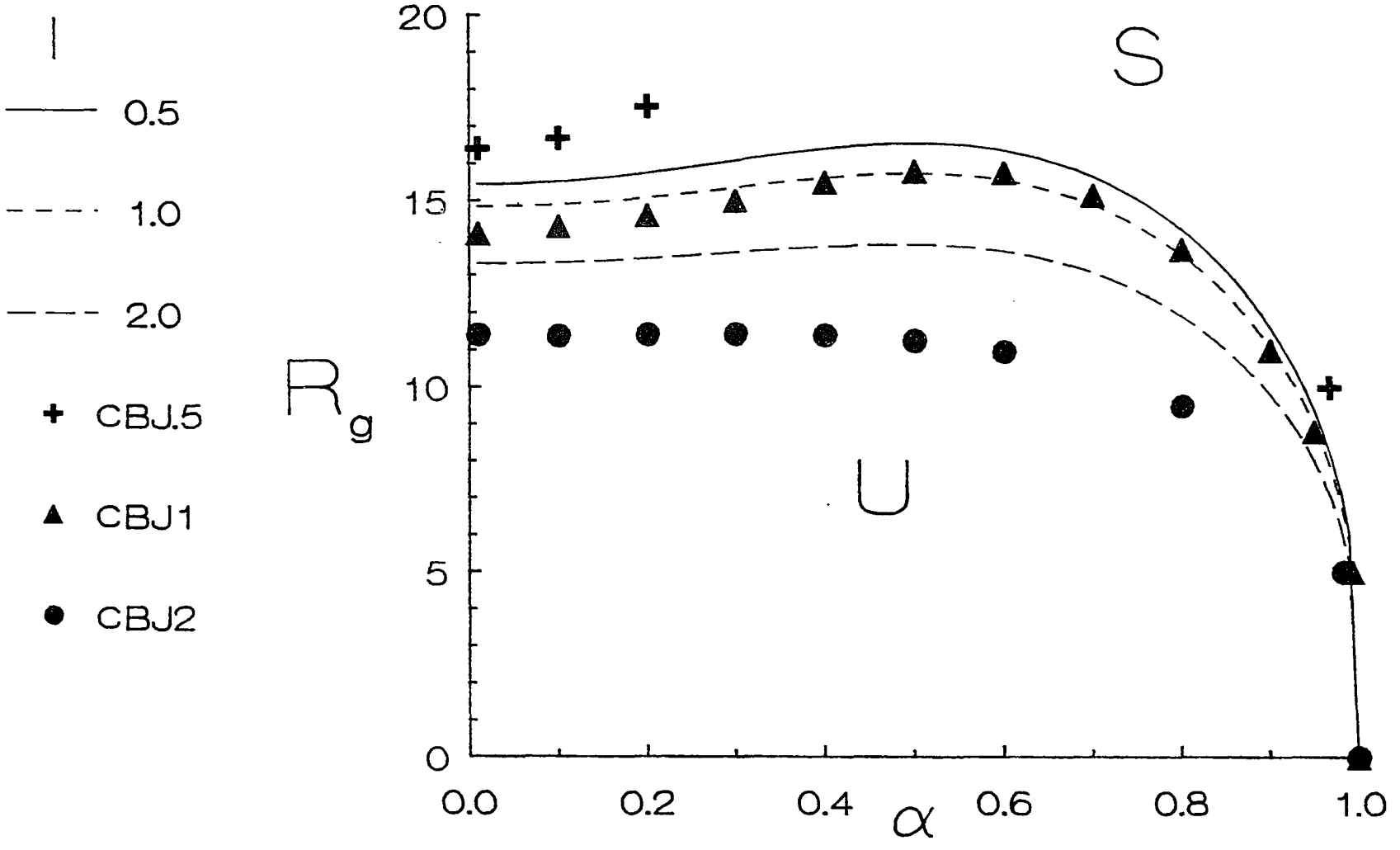
I
0.5
1.0
2.0
CBJ.5
CBJ1
CBJ2
R_g
20
15
10
5
0
S
U
0.0
0.2
0.4
0.6
0.8
1.0
α
ε=0.2, m=0.5, J*=2000

Figure 4_b

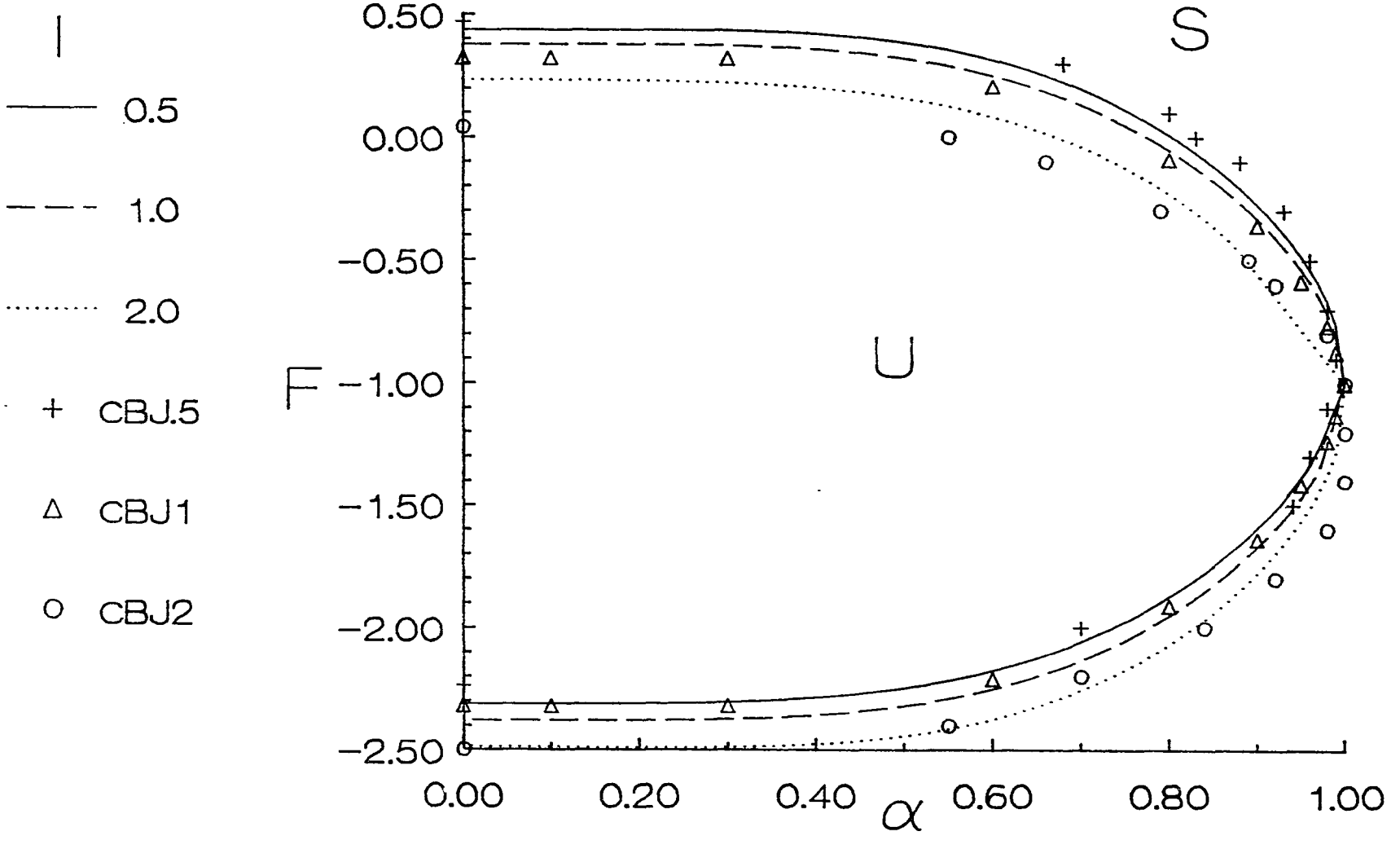

Figure 5

ε=0.1, m=0.5, J*=2000, Rg=10

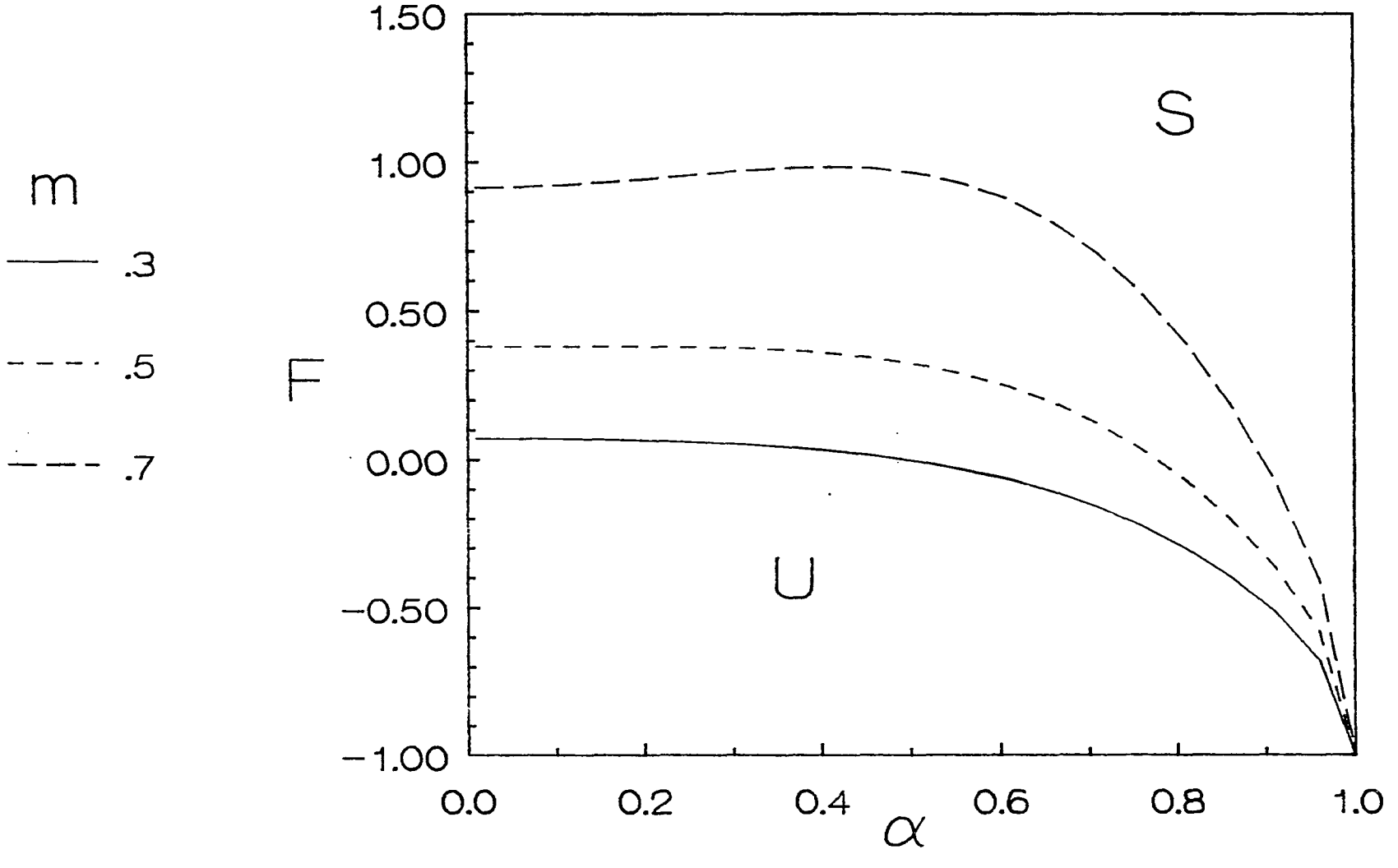

Figure 6

ε=0.1, I=1, J *=2000, Rg=10

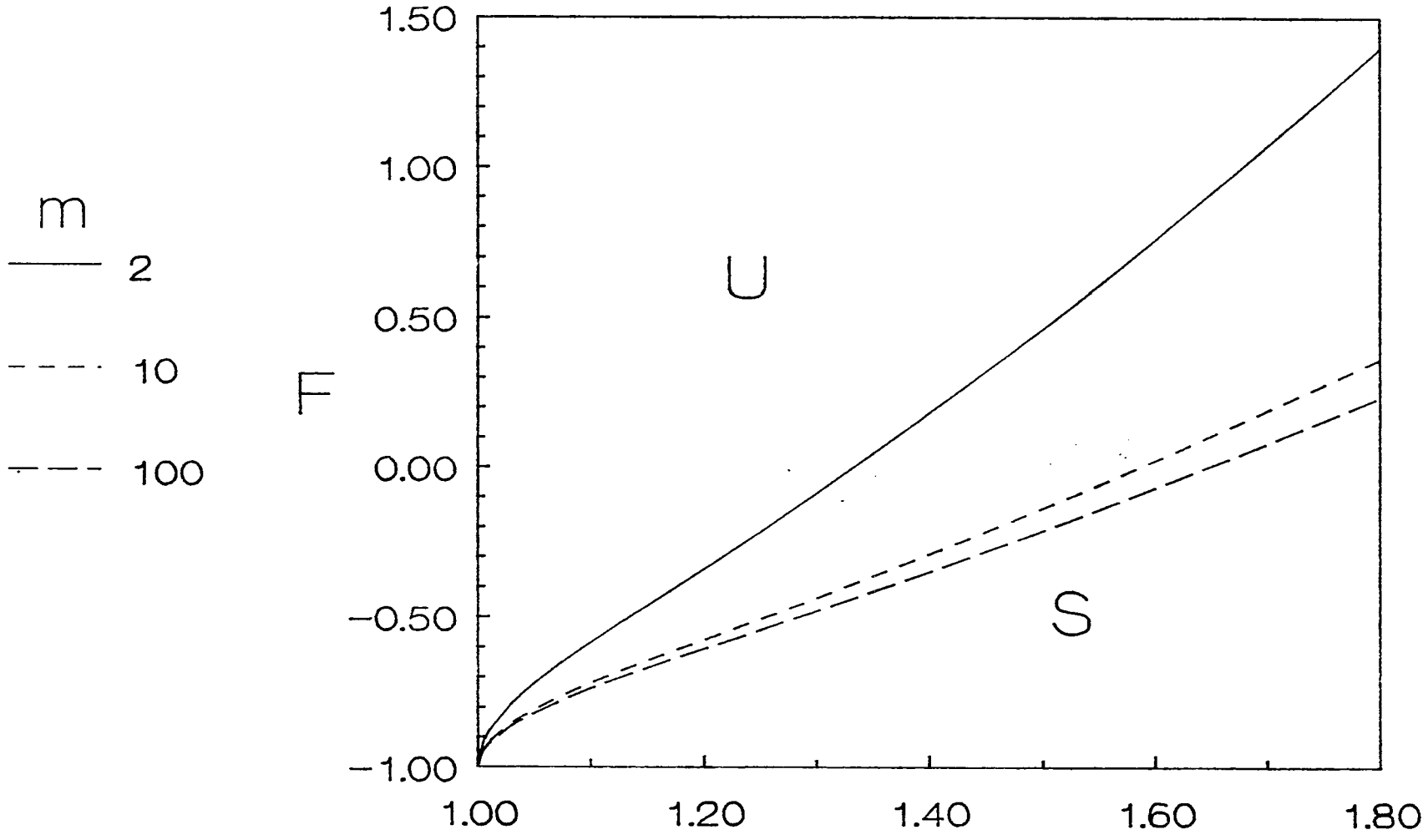

Figure 7

$\mathcal{E}$ =0.05, l=1, J=2500, R^2g=150

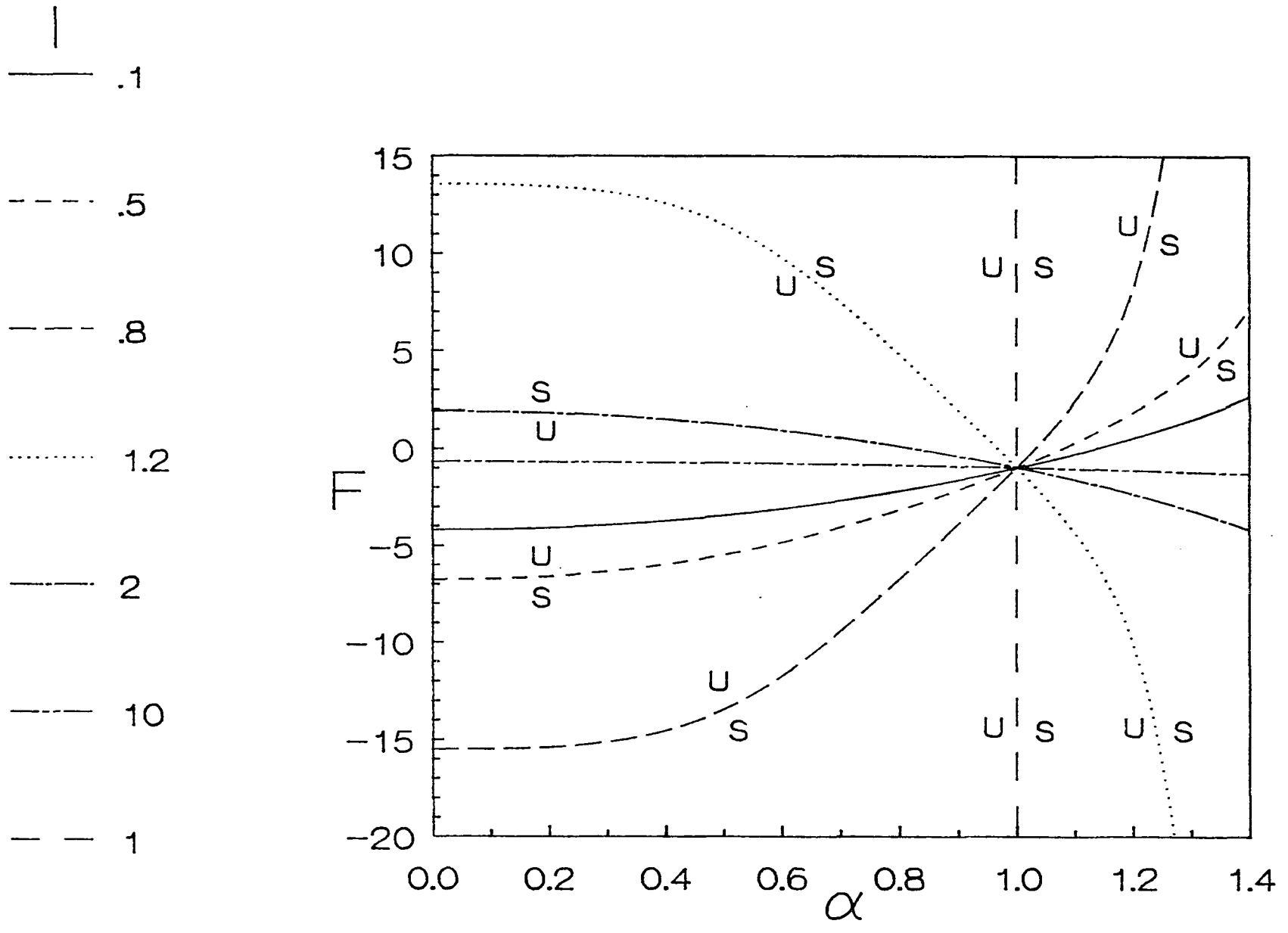

Figure 8 $\varepsilon = 0.1,\ m = 1,\ J^* = 10,\ R^2g = 10$

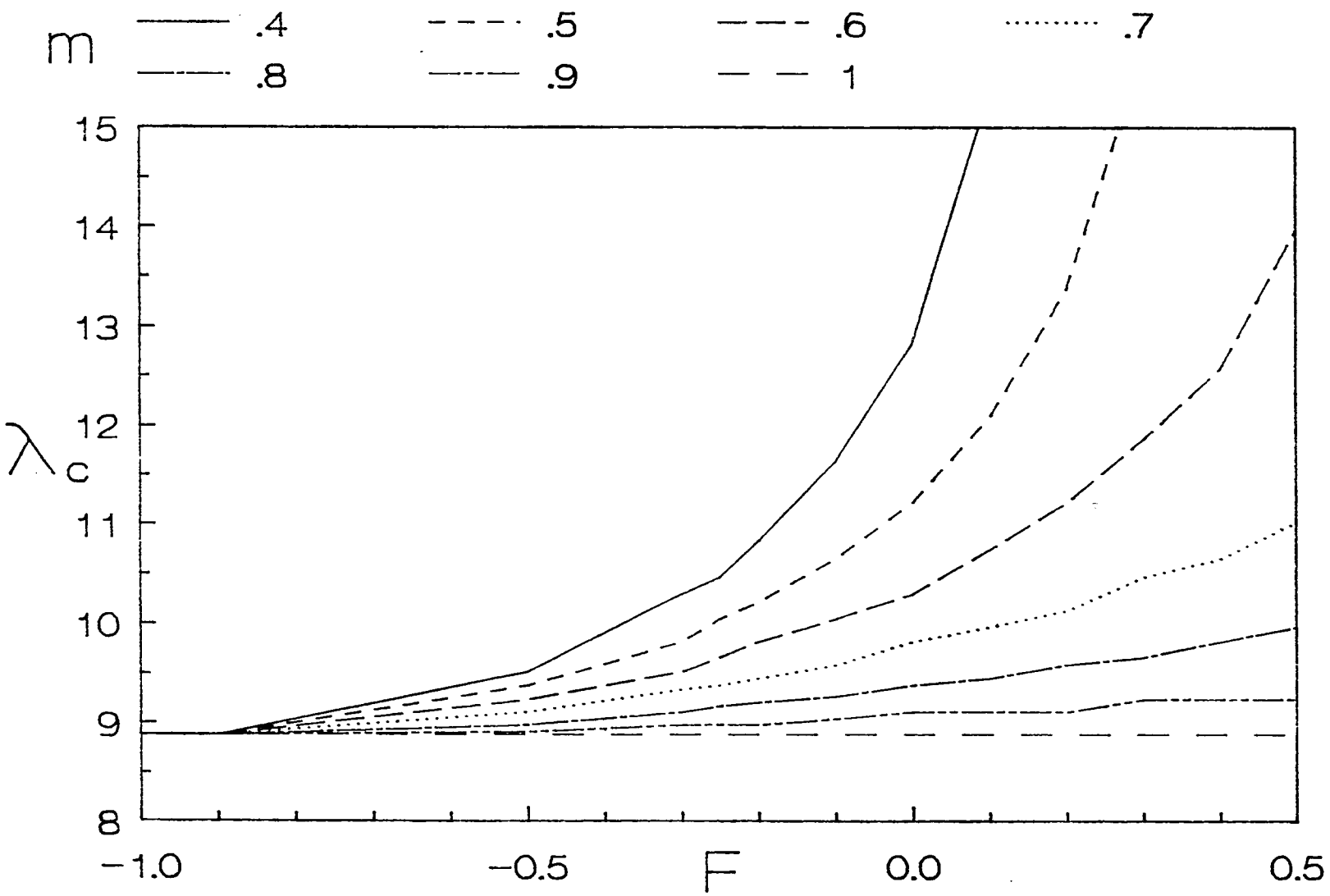

Figure 9 ε=0.1, J*=2000, Rg=10, l=1

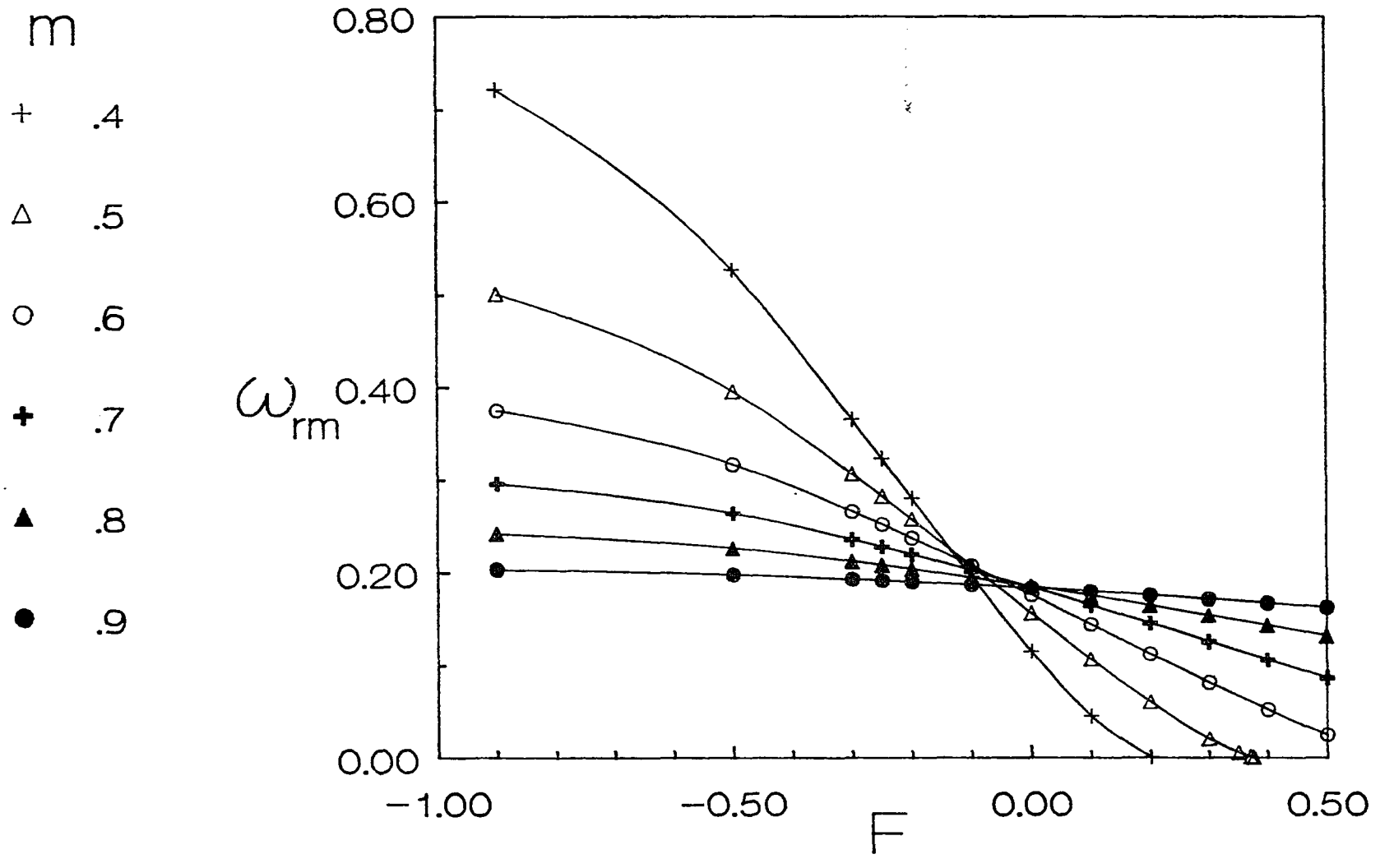

Figure 10 $\mathcal{E}$ =0.1, J*=2000, Rg=10, I=1

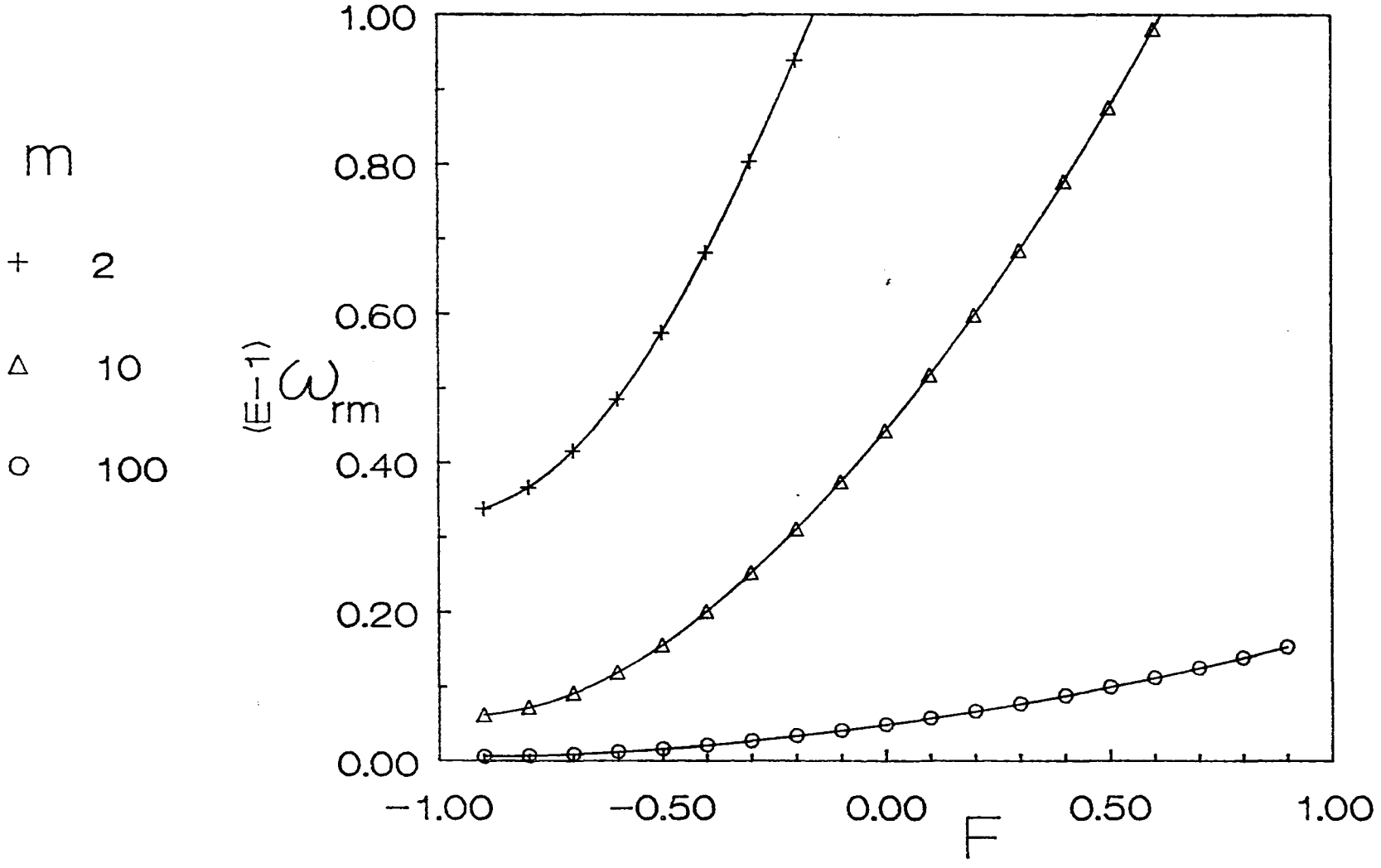

Figure 11 $\mathcal{E}$=0.05, J=2500, R^2g=150, I=1

References

ABRAMOWITZ, M. & STEGUN, I. A. 1972 *Handbook of Mathematical Physics*. Dover Publications, NY

AUL, R. W. & OLBRICHT, W. L. 1990 Stability of a thin annular film in pressure-driven, low-Reynolds-number flow through a capillary. *J. Fluid Mech.* **215**, 585-599

BAI, R., CHEN, K. & JOSEPH, D. D. 1990 Lubricated pipelining: stability of core-annular flow. Part V: experiments and comparison with theory. Submitted to *J. Fluid Mech.*

BENJAMIN, T. B. 1957 *J. Fluid Mech.* **2**, 554

BENNEY, D, J. 1966 Long waves on liquid films *J. Math. Phys.* **45**, 150-155.

BINNIE, A. M. 1957 Experiments on the onset of wave formation on a film of water flowing down a vertical plane. *J. Fluid Mech.* **2**, 551-553.

BLEYS, G. & JOOS, P. 1985 Adsorption Kinetics of Bolaform Surfactants at the Air/Water Interface. *J. Phys. Chem.* **89**, 1027-1032.

BRETHERTON, F. P. 1961 The motion of long bubbles in tubes. *J. Fluid Mech.* **10**, 166-188.

CHANDRASEKHAR, S. 1968 *Hydrodynamic and Hydromagnetic Stability*. Oxford, U. K.

CHEN, K., BAI, R. & JOSEPH, D. D. 1990 Lubricated pipelining. Part 3, Stability of core-annular flow in vertical pipes. *J. Fluid Mech.* **214**, 251-286.

CHEN, K. & JOSEPH, D. D. 1990 Lubrication theory and long waves. Private communications.

FELDERHOF, B. U. 1968 Dynamics of free liquid films. *J. Chem. Phys.* **49**, 44-51.

FRENKEL, A. L., BABCHIN, A. J., LEVICH, B. G., SHLANG, T. & SIVASHINSKY, G. I. 1987 Annular flows can keep unstable films from breakup: nonlinear saturation of capillary instability. *J. Colloid Interf. Sci.* **115**, 225-233.

GALLEZ, D. & COAKLY, G. 1986 Interfacial instability at cell membranes. *Prog. Biophys. molec. Biol.* **48**, 155-199.

GOREN, S. L. 1962 The instability of an annular thread of fluid. *J. Fluid Mech.* **27**, 309-319.

HAVENBERGH, J. V. & JOOS, P. 1983 The Dynamic Surface Tension in a Free Falling Film. *J. Colloid Interf. Sci.* **95**, 172-181.

HICKOX, C. E. 1971 Instability due to viscosity and density stratification in axisymmetric pipe flow. *Phys. Fluids*, **14**, 251-262.

HOOPER, A. 1985 *Phys. Fluids*, **28**, 1613.

HOOPER, A. & BOYD, W. G.1983 Shear-flow instability at the interface between two viscous fluids. *J. Fluid Mech.* **128**, 507-528.

HOOPER, A. & BOYD, W. G. 1987 Shear-flow instability due to wall and a viscosity discontinuity at the interface. *J. Fluid Mech.* **179**, 201-225

HU, H. H. & JOSEPH, D. D. 1989 Lubricated pipelines: stability of core-annular flow. Part 2. *J. Fluid Mech.* **205**, 359-396.

HU, H., LUNDGREN, T. & JOSEPH, D. D. 1990 Stability of core-annular flow with a small viscosity ratio. Submitted to *Phys. Fluids*, A.

JAIN, R. K. & MALDARELLI, M. 1988 *"The Hydrodynamic Stability of Thin Films"* in *Thin Films*. I. B. Ivanov (ed), Marcel Dekker, N.Y.

JOSEPH, D. D., RENARDY, Y. & RENARDY, M. 1984 Instability of the flow of immiscible liquids with different viscosities in a pipe. *J. Fluid Mech.* **141**, 309-317.

KAPITZA, P. L. *Zh. Eksperim. i Teor. Fiz.* ***18***, 3 (1948); **18**, 20 (1948); **19**, 105 (1949).

MELCHER, J. R. 1981 *Continuum Electromagnetics*. The MIT Press.

MELCHER, J. R. & TAYLOR, G. I. 1969 Electromechanics. In *Annual Review of Fluid Mechanics*. (Eds. W. R. Sears and M. D. Van Dyke.) Palo. Alto: Annual Reviews.

MILLER, C. A. & SCRIVEN, L. E. 1970 a Interfacial instability due to electrical forces in double layers. (I) General considerations. *J. Colloid Interf. Sci.* **33**, 360-370.

MILLER, C. A. & SCRIVEN, L. E. 1970 b Interfacial instability due to electrical forces in double layers. (II) Stability of interfaces with diffuse layers. *J. Colloid Interf. Sci.* **33**, 371-383.

PAPAGEORGIOU, D. T., MALDARELLI,C. & RUMSCHITZKI, D. S. (1990) Nonlinear interfacial stability of core-annular film flows. *Phys. Fluids*, A **2**, 340-352.

PAPAGEORGIOU, D. T. & SMITH F. T. (1988), *Proc. R. Soc. London Ser.* A **419**, 1

PARK, C. W. & HOMSY, G. M. 1984 Two-phase displacement in Hele Shaw cells: theory. *J. Fluid Mech.* **139**, 291-308.

PEKERIS, C. L. 1948 Stability of the laminar flow through a straight pipe of circular cross-section to infinitesimal disturbances which are symmetrical about the axis of the pipe. *P.N.A.S.* **34**, 285-295.

PREZIOSI, K., CHEN, K. & JOSEPH, D. D. 1989 Lubricated pipelines: stability of core-annular flow. *J. Fluid Mech.* **201**, 323-356.

SAEZ, A. E., LARBENIELL, K. G. & LEREC, J. 1986 The Hydrodynamics of Trickling Flow in Packed Beds I: Conduit Models. *J. AIChE* **32** (3), 353

RAYLEIGH, LORD 1879 On the capillary phenomena of jets. Appendix I. *Proc. Roy. Soc. A*, **29**, 71.

RAYLEIGH, LORD 1892 On the instability of a cylinder of viscous liquid under capillary force. *Phil. Mag.* **34**, 145.

RENARDY, Y. 1985 Instability at the interface between two shear fluids in a channel. *Phys. Fluids*, **28**, 3411-3443.

SAVILLE, D. A. 1970 Electrohydrodynamic stability: fluid cylinders in longitudinal electric fields. *Phys. Fluids*, **13**, 2987.

SAVILLE, D. A. 1971 Electrohydrodynamic stability: effects of charge relaxation at the interface of a liquid jet. *J. Fluid Mech.* **48**, 815-827.

SMITH, M. K. 1989 The axisymmetric long wave instability of a concentric two-phase pipe flow. *Phys. Fluids* A, **1**, 494-506.

TOMOTIKA, S. 1935 On the instability of a cylindrical thread of a viscous liquid surrounded by another viscous liquid. *Proc. Roy. Soc. A*, **150**, 322-337.

YIANTSIOS, S. G. & HIGGINS, B. G. 1988 Linear stability of plane Poiseuille flow of two superrposed fluids. *Phys. Fluids* A, **31**, 3225-3238.

YIH, C. S. 1957 Stability of parallel laminar flow with a free surface. *Proceedings of the Second U. S. National Congress of Applied Mechanics*. 623-628.

YIH, C. S. 1963 Stability of liquid flow down an inclined plane. *Phys. Fluids*, **6**, 321-334.

YIH, C. S. 1967 Instability due to viscosity stratification. *J. Fluid Mech.* **27**, 337-352.